UNIVERSITAT POLITÈCNICA DE VALÈNCIA

ESCUELA TÉCNICA SUPERIOR INGENIERÍA INDUSTRIAL VALENCIA

CHEMICAL ENGINEERING MASTER THESIS

STUDY AND SETTING-UP A THERMOCHEMICAL NANO-SPIKES OBTENTION SYSTEM ON ELECTROCHEMICALLY CHARACTERIZED TITANIUM ALLOYS

AUTHOR : Robin Vercruysse

SUPERVISOR : Javier José Navarro Laboulais

SUPERVISOR: Ángela Bermúdez Castañeda

Academic year: 2021-2022

THANKING'S

This thesis is the final step in the Industrial Engineering Chemistry programme at KULeuven University. The research and the writing of the thesis were done at the Universitat Politècnica de València. The subject of this research was very unique because this research was still in its early stages, which allowed me to be the first to discover anything. The electrochemistry of this thesis fitted nicely with the subjects that I am finishing in my final year at the KULeuven.

In this way, I would like to thank the lecturers at the KULeuven who have skilfully passed on their knowledge over the past few years. A special thanks also goes to the people of the international office of both KULeuven and UPV for making this exchange possible and assisting me with the questions and difficulties that arose before and during the exchange.

A special thanks goes to my parents. They were always there for me to listen to the difficulties and obstacles that arose during the research and during my stay. Thanks to their support and advice, I was able to overcome these obstacles more easily and smoothly.

The same goes for the friends I met during this exchange. In particular, Felix Hergert and Florian Kornmaier allowed me to let off steam after lab work and return to the lab the next day with a relaxed mind. My friends from Belgium also took a big task on their shoulders to support me with messages and video chats. They took away most of the desire to be at home, allowing me to focus entirely on the research and the writing of the thesis.

The biggest thanks go to the people in the lab, without whom this thesis would not have been possible. Thanks to their knowledge and time they gave me to train me in the metallurgy lab, I could finish my thesis in a beautiful way and return to Belgium with a richer knowledge of electrochemistry. For this I would like to thank Mrs. Elizaveta Klyatskina who assisted me in the microscopy lab and shared with me her knowledge on this special subject. A special thanks goes to Marta Navarro García who taught me how to polish and prepare the samples. But also for introducing me to the city and local culture of Valencia.

One person I certainly cannot forget and would like to thank is Ángela Bermúdez Castañeda. Ángela taught me everything about the electrochemical side of the research and was always ready to help me. During the meetings, she gave concrete and clear explanations. When I asked a question via message, I always got an immediate answer, which I really appreciate. So thank you Ángela!

The last and biggest thanks I offer to Mr Javier Navarro Laboulais. This man assisted me to the extent that he was available. It was amazing how he found the time to guide me through the research and writing of the thesis. And all this while Javier was watching his newborn daughter come into the world. Javier is a man with a very busy schedule and sometimes called himself Nivens McTwisp aka the rabbit of Alice in Wonderland because he was so busy and sometimes arrived late due to appointments that had previously run late. Yet Javier always managed to be there for me and provide information whenever I asked. Without Javier, I would not have been able to complete this research, so thank you very much.

I would also like to wish Javier and Ángela a bright future and much happiness with their daughter Gabriela.

With this thesis, I can conclude my career as a student and start a new adventure.

DANKWOORD

Dit eindwerk is de laatste stap in de opleiding Industrieel ingenieur Chemie aan de Universiteit KULeuven. Het uitvoeren van dit onderzoek en het schrijven van de thesis werd gedaan aan de Universitat Politècnica de València. Het onderwerp van dit onderzoek was heel uniek omdat dit onderzoek nog in het begin stadium zit waardoor ik als eerste alles kon ontdekken. De elektrochemie van deze thesis sloot mooi aan met de vakken die ik in mijn laatste jaar afrond aan de KULeuven.

Via deze weg wil ik de docenten aan de KULeuven bedanken die de afgelopen jaren vakkundig hun kennis hebben overgedragen. Een dankwoord gaat ook uit naar de mensen van het international office van zowel de KULeuven als de UPV om deze uitwisseling mogelijk te maken en mij bij te staan bij de vragen en moeilijkheden die optraden voor en tijdens de uitwisseling.

Een speciaal dankwoord gaat uit naar mijn ouders. Zij stonden altijd voor mij klaar om te luisteren naar de moeilijkheden en obstakels die optraden tijdens het onderzoek en in mijn verblijfperiode. Dankzij hun steun en advies kon ik deze obstakels soepeler en makkelijker overwinnen.

Dit geldt eveneens aan de vrienden die ik tijdens deze uitwisseling heb leren kennen. Met name Felix Hergert en Florian Kornmaier kon ik stoom af laten na het labowerk en de volgende dag met een ontspannend gevoel terug in het labo werken. Mijn vrienden uit België namen ook een grote taak op hun schouders om mij steeds te steunen met berichten en videochatten. Zij namen het verlangen naar het thuisfront voor een groot deel weg waardoor ik mij geheel kon focussen op het onderzoek en het schrijven van de thesis.

De grootste dankwoorden gaan uit naar de mensen in het labo want zonder hun was dit eindwerk niet mogelijk geweest. Dankzij hun kennis en tijd die ze mij gaven om me op te leiden in het labo mettalurgie heb ik mijn thesis op een mooie manier kunnen afronden en kan ik terug keren naar België met een rijkere kennis over de elektrochemie. Hiervoor wil ik graag mevr. Elizaveta Klyatskina bedanken die mij bijstond in het labo microscopie en me deelde in haar kennis over dit bijzondere onderwerp. Een speciaal dankwoord gaat uit naar Marta Navarro García die mij leerde de samples te polijsten en de voorbereiden ervan uit te voeren. Maar ook om mij de stad en de lokale cultuur van Valencia te leren kennen.

Wie ik zeker niet mag vergeten en wil bedanken is Ángela Bermúdez Castañeda. Ángela leerde mij alles over de elektrochemische kant van het onderzoek en stond altijd direct voor mij klaar. Tijdens de besprekingen gaf ze concrete en duidelijke uitleg. Toen ik iets vroeg via bericht kreeg ik altijd onmiddellijk antwoord wat ik enorm apprecieer. Dus dankuwel Ángela!

Het laatste en grootste dankwoord bied ik aan de heer Javier Navarro Laboulais. Deze man heeft mij bijgestaan in hoeverre hij beschikbaar was. Ik vind het geweldig hoe hij de tijd vond om mij te begeleiden tijdens het onderzoek en het schrijven van de thesis. En dit allemaal terwijl Javier zijn pasgeboren dochtertje in de wereld zag komen. Javier is iemand met een heel drukke agenda en noemde zich soms Nivens McTwisp aka the rabbit of Alice in Wonderland omdat hij het zo druk had en wel eens te laat kwam door eerder uitgelopen afspraken. Toch slaagde Javier er in om altijd voor mij klaar te staan en informatie te verschaffen wanneer ik het vroeg. Zonder Javier had ik dit onderzoek niet tot een goed einde kunnen brengen dus een welgemeende dankuwel.

Verder wil ik Javier en Ángela een mooie toekomst en nog veel geluk toe wensen met hun dochtertje Gabriela.

Met dit eindwerk kan ik mijn studente carrière afronden en beginnen aan een nieuw avontuur.

ABSTRACT

Due to the increasing ageing of the population and rising life expectancy, the demand for implants is rising. As a result, the corrosion resistance of these implants must be ensured. A suitable material for implants is titanium. Various alloys can be made with this metal to improve its characteristics. The most commonly used titanium alloy is Ti-6Al-4V. However, research shows that when this material undergoes corrosion and small particles of this alloy enter the body, the aluminium in the alloy can promote Alzheimer's disease. Therefore, it is important to increase the corrosion resistance of this alloy.

Another common problem are infections due to implants. Biofilms are a set of microbial cells that attach themselves to the implant surface. These can be responsible for the development of prosthetic infections. These infections can lead to the need for long-term antibiotic therapy and sometimes to implant removal.

A possible solution to combat these infections is the use of nanostructured active surfaces. These impede the adhesion of bacteria to the implant. These surface modifications reduce the irreversible adhesion of bacteria, thus reducing infections. This is considered a passive strategy that persists as long as the surface structure is present.

In this thesis, the aim will be to produce these nanostructured active surfaces on a titanium alloy. 3 different alloys will be used and investigated, namely: Ti-6Al-4V, TiCP and Ti-Sn. In order to understand the alloys, electrochemical behaviour will be investigated first.

In the second part of this thesis, the attempt is made to form the nanostructured active surfaces on these 3 titanium alloys based on thermal pyrolysis of acetone and further oxidation with air. After the heat treatment has been applied, various characterisation techniques will be carried out to analyse the properties of the obtained samples. Some of the techniques that will be used are: Scanning Electron Microscopy (SEM), Energy-Dispersive X-ray Spectroscopy microanalysis (EDS) and Transmission electron microscopy (TEM).

Key words: TiO_2 nanostructures, thermochemical processing, acetone pyrolysis, titanium alloys, medical implants.

RESUMEN

Debido al creciente envejecimiento de la población y al aumento de la esperanza de vida, la demanda de implantes está aumentando. Por ello, hay que garantizar la resistencia a la corrosión de estos implantes. Un material adecuado para los implantes es el titanio. Se pueden fabricar diferentes aleaciones con este metal para mejorar sus características. La aleación de titanio más utilizada es la Ti-6Al-4V. Sin embargo, las investigaciones muestran que cuando este material sufre corrosión y pequeñas partículas de esta aleación penetran en el organismo, el aluminio de la aleación puede favorecer la enfermedad de Alzheimer. Por ello, es importante aumentar la resistencia a la corrosión de esta aleación.

Otro problema común son las infecciones debidas a los implantes. Las biopelículas son un conjunto de células microbianas que se adhieren a la superficie del implante. Estas pueden ser responsables del desarrollo de infecciones protésicas. Estas infecciones pueden llevar a la necesidad de una terapia antibiótica a largo plazo y, en ocasiones, a la retirada del implante.

Una posible solución para combatir estas infecciones es el uso de superficies activas nanoestructuradas. Estas impiden la adhesión de las bacterias al implante. Estas modificaciones de la superficie reducen la adhesión irreversible de las bacterias, reduciendo así las infecciones. Esto se considera una estrategia pasiva que persiste mientras la estructura superficial esté presente.

En esta tesis, el objetivo será producir estas superficies activas nanoestructuradas sobre una aleación de titanio. Se utilizarán e investigarán tres aleaciones diferentes: Ti-6Al-4V, Ti-CP y Ti-Sn. Para entender las aleaciones, se investigará primero el comportamiento electroquímico.

En la segunda parte de esta tesis, se intenta formar las superficies activas nanoestructuradas en estas tres aleaciones de titanio a partir de la pirólisis térmica de la acetona y su posterior oxidación con aire. Una vez aplicado el tratamiento térmico, se llevarán a cabo diversas técnicas de caracterización para analizar las propiedades de las muestras obtenidas. Algunas de las técnicas que se utilizarán son: Microscopía Electrónica de Barrido (MEB), Microanálisis por Espectroscopía de Energía Dispersa de Rayos X (EDS) y Microscopía Electrónica de Transmisión (MET).

Palabras clave: Nanoestructuras de TiO_2, tratamiento termoquímico, pirólisis de acetona, aleaciones de titanio, implantes médicos.

RESUM

Degut al creixent envelliment de la població i l'augment de l'esperança de vida, la demanda d'implants està augmentant. Per això, s'ha de garantir la resistència a la corrosió d'aquests implants. Un material adequat en aquest sentit és el titani. Es poden fabricar diversos aliatges amb aquest material per a millorar les seues característiques. L'aliatge de Ti més utilitzat és el Ti-6Al-4V. Tanmateix, les investigacions mostren que quan aquest material experimenta corrosió i petites partícules d'aquest aliatge penetren a l'organisme, l'alumini pot afavorir la malaltia de l'Alzheimer. Per això, és important augmentar la resistència a la corrosió d'aquest aliatge.

Altre problema comú són les infeccions degudes als implants. Les biopel·lícules són un conjunt de cèl·lules microbianes que s'adhereixen a la superfície de l'implant. Aquestes poden ser responsables del desenvolupament d'infeccions protètiques. Aquestes infeccions poden conduir a la necessitat d'una teràpia antibiòtica a llarg termini i, en ocasions, a la retirada de l'implant.

Una possible solució per a combatre aquestes infeccions és utilitzar superfícies actives nanoestructurades. Aquestes impedeixen l'adhesió de bacteris, reduint aixina les infeccions. Açò es considera una estratègia passiva que persisteix mentre l'estructura superficial estiga present.

En aquesta tesi, l'objectiu serà produir aquestes superfícies actives nanoestructurades sobre un aliatge de titani. S'utilitzaran i investigaran tres aliatges diferents: Ti-6Al-4V, Ti-CP i Ti-Sn. Amb la finalitat d'entendre els aliatges, s'investigarà primer el comportament electroquímic.

En la segona part d'aquesta tesi, s'intenta formar les superfícies actives nanoestructurades en aquests tres aliatges de titani a partir de la piròlisi tèrmica de l'acetona i la seua posterior oxidació amb aire. Després de l'aplicació del tractament tèrmic, es duran a terme diverses tècniques de caracterització per a analitzar les propietats de les mostres obtingudes. Algunes de les tècniques que s'utilitzaran són: Microscòpia Electrònica D'Agranat, Microanàlisi per Espectroscòpia d'Energia Dispersa de Rajos-X (EDS) i Microscòpia Electrònica de Transmissió (MET).

Paraules clau: Nanoestructures de TiO_2, tractament termoquímic, piròlisi d'acetona, aliatges de titani, implants mèdics.

SAMENVATTING

Als gevolg van de toenemende vergrijzing van de bevolking en de stijgende levensverwachting neemt de vraag naar implantaten toe. Als gevolg daarvan moet de corrosiebestendigheid van deze implantaten worden verzekerd. Een geschikt materiaal voor implantaten is titanium. Met dit metaal kunnen verschillende legeringen worden gemaakt om de eigenschappen ervan te verbeteren. De meest gebruikte titaniumlegering is Ti-6Al-4V. Uit onderzoek blijkt echter dat wanneer dit materiaal corrosie ondergaat en kleine deeltjes van deze legering in het lichaam terechtkomen, het aluminium in de legering de ziekte van Alzheimer kan bevorderen. Daarom is het belangrijk de corrosiebestendigheid van deze legering te verhogen.

Een ander veel voorkomend probleem zijn infecties als gevolg van implantaten. Biofilms zijn een geheel van microbiële cellen die zich vasthechten aan het implantaatoppervlak. Deze kunnen verantwoordelijk zijn voor het ontstaan van prothese-infecties. Deze infecties kunnen leiden tot de noodzaak van langdurige antibioticatherapie en soms tot het verwijderen van het implantaat.

Een mogelijke oplossing om deze infecties te bestrijden is het gebruik van nanogestructureerde actieve oppervlakken. Deze verhinderen de hechting van bacteriën aan het implantaat. Deze oppervlaktemodificaties verminderen de onomkeerbare aanhechting van bacteriën, waardoor infecties afnemen. Dit wordt beschouwd als een passieve strategie die blijft bestaan zolang de oppervlaktestructuur aanwezig is.

In deze thesis zal het doel zijn om deze nanogestructureerde actieve oppervlakken te produceren op een titaniumlegering. 3 verschillende legeringen zullen worden gebruikt en onderzocht, nl: Ti-6Al-4V, TiCP en Ti-Sn. Om de legeringen te begrijpen, zal eerst het elektrochemisch gedrag worden onderzocht.

In het tweede deel van dit proefschrift wordt getracht de nanogestructureerde actieve oppervlakken te vormen op deze 3 titaanlegeringen op basis van thermische pyrolyse van aceton en verdere oxidatie met lucht. Na de warmtebehandeling zullen verschillende karakteriseringstechnieken worden uitgevoerd om de eigenschappen van de verkregen samples te analyseren. Enkele van de technieken die zullen worden gebruikt zijn: Scanning Electron Microscopy (SEM), Energy-Dispersive X-ray Spectroscopy microanalyse (EDS) en Transmission electron microscopy (TEM).

Trefwoorden: TiO_2 nanostructuren, thermochemische verwerking, aceton pyrolyse, titaanlegeringen, medische implantaten.

TABLE OF CONTENT

LIST OF FIGURES

LIST OF TABLES

Chapter 1: INTRODUCTION

Due to the increasingly innovative healthcare sector and better living conditions, the ageing of the population and life expectancy is increasing. This also increases the demand for implants, e.g. for hip or knee arthroplasty, dental implants and other regenerative procedures. Due to these increasing life expectancies, the implants must remain intact during this entire period and their structure and quality must be guaranteed.

Medical implants are foreign objects whose surface is ideal for bacterial attachment and the spread of microbial contamination, which can lead to the development of prosthetic infections. These infections may in turn lead to the need for long-term antibiotic therapy (which may take years) and ultimately to implant removal, resulting in a significant increase in hospitalisation time and costs, along with a stressful, painful and critical situation for the patient.

To avoid this situation, the implants can be modified in 2 different ways to improve the structure of the implant without changing its overall characteristics. The 2 possible ways are to create functionalised biocidal surfaces or structured antimicrobial surfaces. In this thesis, only the development of structured antimicrobial surfaces is investigated.

The most important metal used for implants is titanium. This metal is very interesting because of its low density and high rigidity, which makes it highly resistant to corrosion. Titanium is also very suitable for alloying with other metals to improve their properties. The metal possesses high biocompatibility, as it is non-toxic and not rejected by the human body, so Ti binds effectively to bone.

For the research in this thesis, 3 titanium alloys are investigated, namely Ti-6Al-4V, TiCP and Ti-Sn. In order to better understand these alloys, the electrochemical behaviour is first investigated using a conventional three-cell electrode in a sulphuric acid solution. This strong electrolyte was chosen to establish passivation and corrosion processes in Ti alloys, which are very stable under different solutions. The tests used to examine the alloys are: a corrosion test, a polarisation test and an impedance test.

The second part of this thesis focuses on the development of the structured antimicrobial surfaces. Here an attempt is made to develop a nanostructured surface by means of heat treatment in a high temperature vacuum tube furnace using acetone, argon and air. The samples to be examined undergo two different heat treatments with the aim of obtaining nanospikes. These nanospikes are ideal for inhibiting the biofilm of bacteria. The nanospikes are sharp and therefore pierce the bacterial cell wall on contact, killing the bacteria and preventing infection from establishing on the implant.

The creation of the nanospikes on the titanium alloys is performed at different flow rates to find the ideal parameters. Tests are then carried out on the electrochemical behaviour of these modified implants, and a comparison is made with the electrochemical behaviour before modification.

Chapter 2: LITERATURE REVIEW

2.1 History of titanium

Titanium was discovered by William Gregor at the end of the 18th century. Years later, Martin H. Klaproth named it titanium in honour of the titans of Greek mythology, but it was Matthew Hunter who obtained pure titanium by heating $TiCl_4$ with sodium in a steel reactor at 850ºC. In the mid-20th century, William J. Kroll developed a method to produce titanium commercially through a process of reducing $TiCl_4$ with magnesium in an argon atmosphere so as not to oxidize. The process is based on a crystallographic change where the alpha phase titanium changes to beta phase. Today, it is obtained by chlorination of rutile or ilmenite at 900°C to obtain $TiCl_4$ which is reduced to Ti by the Kroll process. [1]

Titanium is a non-magnetic transition metal, which symbol is Ti and its atomic number is 22. It is the ninth most abundant element in the earth's crust and because it is found at shallow depths below the earth's surface it is relatively easy to extract. It is not found in its pure state in nature, but in the form of oxides. Processing is what makes this metal expensive. The minerals from which titanium is extracted are rutile (TiO_2) and ilmenite ($FeO- TiO_2$) and once the metal is extracted, the titanium undergoes a metallurgical refining process to prevent it from reacting with N_2, O_2, and H_2. [2]

2.2 General information about titanium

Titanium (4.51 g/cm³) is an interesting metal due to its low density and high stiffness comparable to steel (7.8-8 g/cm³). As a result, it's useful as an alloying agent for a variety of metals, including aluminium, molybdenum, iron, as well as a metal base for many engineering and medical applications. Because of their low density and ability to tolerate high temperatures, these alloys are mostly used in airplanes, spacecraft, and missiles. Golf clubs, laptop computers, bicycles, and crutches all contain them. [3]

Titanium is a good material for aerospace applications due to its fatigue resistance, strength-to-weight ratio and relative formability. Especially for manufacturing jet engine components such as blades and as compressor discs because titanium has a high specific strength and stability when treated at high temperature. [3]

Titanium pipes are used in power plant condensers because of their corrosion resistance. This metal is also used in desalination plants and to preserve the hulls of ships, submarines, and other structures exposed to seawater due to its remarkable resistance to corrosion in seawater. [4]

The most important biological property of titanium is that it oxidizes when in contact with atmospheric air, and this oxide layer provides a corrosion resistant surface. This phenomenon is called passivation.

The corrosion resistance of titanium and its alloys is due to a thin layer of titanium oxide that forms in the presence of oxygen from the atmosphere or water — even salty. However, if titanium is exposed to an oxygen-free environment, such as a man-made vacuum or even outer space, the reaction will not occur. This implies that pure titanium is vulnerable to oxidation, acids, chemicals, corrosion, and rust under very special atmospheres or electrolytes. [5]

One of the most widely spread use of Ti and its alloys are medical devices, such as: surgical implements and orthopaedic implants, including those from dentistry. That have been attributed to its biocompatibility since it is non-toxic nor rejected by the human body and therefore Ti bonds effectively with bone. [4]

2.3 Titanium Oxides

Titanium dioxide (TiO_2), also called titanium(IV) oxide is the most stable oxidation form of titanium. The other oxidation forms are TiO and Ti_2O_3 but do not occur as often in a natural state. [6]

TiO_2 belongs to the family of transition metal oxides and occurs in different polymorphs. The polymorphs of TiO_2 found in nature are anatase (tetragonal), brookite (orthorhombic), rutile (tetragonal).

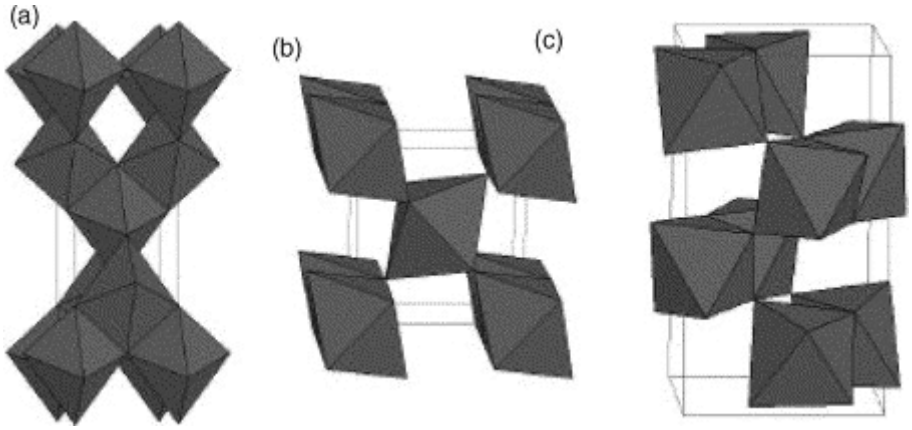

Figure 1: Crystal structures of anatase (a), rutile (b), and brookite (c)

Rutile (b), anatase (a), and brookite (c) all have (TiO_2^{6-}) octahedral structures that can be discussed. The distortion of each octahedral and the assembly patterns of the octahedral chains distinguish the three crystal structures. Anatase is made up of octahedral structures that are joined by their vertices, the edges are connected in rutile, and both vertices and edges are connected in brookite. This is shown in Figure 1.

Under all temperatures and pressures up to 60 kbar, thermodynamic simulations based on calorimetric data predict that rutile is the most stable phase, with TiO_2(II) becoming the thermodynamically favourable phase. [7]

2.4 Biomedical alloys

2.4.1 History

Until the 18th century the metallic materials used in surgical implants were gold and silver. In the 19th century steels began to be used, and already in this century stainless steels, chromium, cobalt and molybdenum alloys appeared. Titanium and its alloys were first used as an implant in the 1940s. [8] Today, 70-80% of the materials used in implants are made of a metal, and most of the metals used are made of titanium alloys.

2.4.2 General information

Titanium and its alloys have excellent biocompatibility and together with its mechanical properties, easy osseointegration and corrosion resistance make it the preferred metal for the manufacture of all types of implants. As a result, titanium and its alloys are probably the most widely used metal biomaterial in orthopaedic and dental medical implants. Titanium also has the advantage that it can be used with other elements to form alloys to improve mechanical properties. [9] The alloy Ti-6Al-4V is the most widely used alloy, as it meets the requirements of biocompatibility, osseointegration, mechanical properties, corrosion resistance and availability. [10] In addition, the properties of this alloy can be modified and improved by heat treatments, as it belongs to the α+β-type titanium alloys, this will be discussed further later. [9]

An important property that biomaterials must possess is corrosion resistance as they will be exposed to body fluids, such as interstitial fluid rich in electrolytes (Na^+, K^+, Cl^-, PO_4^-) and plasma proteins. The high affinity of titanium for oxygen means that the metal is permanently covered by a passive TiO_2 layer, i.e. a protective oxide layer forms on the surface of titanium, which helps protect the material from the environment. [11] This gives the metal a high corrosion resistance, reduces the leakage of ions and forms highly biocompatible materials. In addition to these properties, titaniums have been subjected to a wide variety of surface treatments to improve their properties in orthopaedic applications [12] such as increasing their wear resistance or improving their osseointegration.

The surface charge also has an important influence on biocompatibility. Titanium has a positively charged surface and will therefore form non-covalent bonds with negatively charged proteins, such as albumin and fibronectin. Albumin (a protein produced by the liver) has been shown to inhibit bacterial attachment, whereas fibronectin promotes bacterial attachment. Therefore, when applying surface modification techniques, some attention will have to be given to the surface load. [13] [14]

For a biomaterial to be considered ideal, it must not contain cytotoxic substances, i.e. compounds that damage or kill cells or tissues. Titanium has good biological compatibility compared to other popular biomaterials.

Titanium has excellent mechanical properties and has the highest strength-to-weight ratio of any pure metal. This property is very favourable for the realisation of an orthopaedic biomaterial that must withstand long-term joint cycles. [11] In addition, the mechanical properties of Ti and those of its β-structured alloys, e.g., Nb, Zr and Ta alloys, closely resemble the mechanical properties of cortical bone, which avoids mechanical shielding phenomena that lead to catastrophic implant failure. [15]

Finally, as mentioned above, osseointegration is one of the most important properties implants should possess. The topography of the material will influence this property.

2.4.3 Types of alloys

Titanium comes in three different forms α, β and α -β. The phase compositions might be changed by adding alloying elements, which would modify the bulk Ti-alloy characteristics. Aluminium, for example, can operate as α -phase stabilizers, increasing the alloy's strength while reducing its weight. Vanadium is a β -phase stabilizer improving ductility and formability. As a result of the addition of Al and V, the temperature for the α-phase transform to β-phase has been changed to a range, indicating that both α and β phases exist within the temperature range.

2.4.3.1 Ti-6Al-4V

Grade V Titanium (Ti–6Al–4V) is one of the most regularly used tertiary titanium alloys that can be used as a biomedical implant. The composition of Ti–6Al-4V is 6 wt% aluminium and 4 wt% vanadium, as shown by the symbol. The Ti–6Al–4V alloy, in example, has a higher strength and might be employed in a variety of applications, such as femoral component anchorage stems. Its poor wear resistance, high elastic modulus (still around 4–10 times that of human bone), and low shear strength are all disadvantages of Ti-6Al–4 V alloy, which could limit its use as an implant and as a screw. 'The stress shielding effect' is a phenomenon caused by a stiffness mismatch between the implant material and the surrounding bone. Long-term studies have indicated that if the load transfer from the artificial implant to the neighboring remodeling bone is insufficient, bone resorption can occur, causing the prosthetic device to loosen. As a result, it was determined that appropriate surface treatments were required to ameliorate the condition.

2.4.3.2 TiCP

According to the purity and processing oxygen content, commercially pure Ti (cp-Ti) is categorized into four Grades ranging from 1 to 4. The corrosion resistance, ductility, and strength of these distinct grades of cp-Ti vary. Grade 1 cp-Ti, for example, offers the highest purity, corrosion resistance, and formability because it is treated with the least oxygen content (about 0.18%). The overall mechanical strength, on the other hand, is the weakest. Grade 4 cp-Ti, on the other hand, has the maximum strength and moderate formability because it is processed with the most oxygen content (about 0.4%). Because of its great strength, Grade 4 cp-Ti is used for the most of Ti implants.

2.4.3.3 Ti-Sn

Ti–Sn has been determined to be nontoxic and allergen-free. As a result, tin (Sn) appears to be a safe alloying element for Ti. Furthermore, Sn has been shown to strengthen Ti alloys, resulting in binary Ti–Sn alloys with desirable mechanical properties that could be employed as a metal for dental casting. For example, experimental data showed that all Ti–Sn alloys having 1–30 wt% Sn had a hcp structure. The Vickers hardness (HV) of Ti–Sn alloys can be increased by increasing the Sn content; for example, 30 wt% Sn has a high hardness value of 357 HV. The grindability of the alloys was also investigated to demonstrate the CAD/CAM processability. Adding Sn to cp-Ti improves the grindability of Ti–Sn alloys, allowing for a larger Sn concentration to be ground more easily; for example, Ti–30 Sn had a 3.4 times higher grinding ratio than cp–Ti at a grinding rate of 1200 m/min. The grindability of each metal or alloy, on the other hand, was largely determined by the grinding conditions. As a result, careful analysis of the experimental data is required. [15]

2.4.4 Why is the integrity of the implant so important?

Microbiological infections in biomedical implants are a serious risk to modern medicine and a significant public health issue. The number of individuals getting hip and knee arthroplasty, dental implants, and other regenerative procedures has increased as a result of technological advancements, population ageing, and higher life expectancy. Medical implants are foreign bodies with a surface that is suitable for bacterial adhesion and microbial contamination, which can lead to prosthetic infections. These infections can lead to the necessity for long-term antibiotic treatment (which can last years) and, finally, the device's removal, resulting in a large rise in hospitalization periods and costs, as well as a stressful, unpleasant, and crucial condition for the patient. [16]

2.4.5 Problems with the implants

2.4.5.1 Corrosion

Although the titanium alloys used for the manufacture of joint replacements are biocompatible, once introduced into the body they have been shown to degrade over time. The mechanisms causing this deterioration are mechanical wear, corrosion and the combination of both (tribocorrosion). [17] This deterioration is undesirable both because of the release of metal particles that may cause adverse biological reactions in the patient, and because of a reduction in the structural integrity of the implants. [18]

Wear and corrosion cannot be explained separately, as the two terms are related. Tribocorrosion is a term that attempts to integrate wear (tribology) and corrosion. Tribology is the science that studies friction, wear and lubrication, whereas corrosion refers to the chemical aspects of material degradation in mechanical systems. Tribocorrosion usually occurs when two materials come into physical contact. There are several physical contacts that can cause this phenomenon, such as erosion, impact, abrasion, friction, displacement, etc. [19]

Degradation products in articulated prostheses are mainly due to friction. It has been shown that when a metal prosthesis is implanted, the level of metal ions in the patient's tissues can cause a number of health problems. [17]

On the one hand, mechanical wear is the loss of material from a solid surface when it moves in relation to another solid surface with which it is in contact. [20] There are different types of wear, such as frictional wear, abrasive wear and fatigue wear. Wear depends on the conditions of use of the prosthesis (applied load, type of movement, type of friction, working time, etc.) and the characteristics of the environment (corrosivity, presence of abrasive particles, etc.). Mechanical wear causes the release of metal particles into the body, which have been associated with tissue inflammation, loss of bone density and implant loosening. [18]

Corrosion, on the other hand, is the dissolution of a metal through an electrochemical reaction with its environment. Body fluids are electrolytic aqueous solutions containing chloride ions and dissolved oxygen. Table 1 shows the chemical composition of human blood plasma. [21]

This body fluid in combination with relative movement between modular parts, with the bone or cavity in which they are implanted, can promote conditions for the development of tribocorrosive phenomena. This means that it can lead to the release of metallic and oxidised particles, as well as metal ions, which are believed to cause infections, defects in distant organs and rejection of the medical device.

Table 1: Chemical composition of human blood plasma

Ion	Concentration (mmol/L)
Na^+	142,0
K^+	5,0
Mg^{2+}	1,5
Ca^{2+}	2,5
Cl^-	103,0
HCO_3^-	27,0
HPO_4^{2-}	1,0
SO_4^{2-}	0,5

Therefore, the following corrosion (redox) reaction occurs on the surface of the metal implant [21]:

$$M \leftrightharpoons M^{n+} + ne^-$$

$$O_2 + 2H_2O + 4e^- \leftrightharpoons 4OH^-$$

On the other hand, the body temperature is around 37°C, which can accelerate electrochemical reactions.

Another factor determining the corrosion behaviour of metal is the pH. Changes in pH of body fluids are usually minor, i.e. pH does not usually vary because they are buffered. Titanium and its alloys are the most resistant to corrosion. This is because the passive TiO_2 layer present on the surface of the material is very stable in the pH range between 2 and 12.

There are two fundamental characteristics that determine how and why a particular metal material corrodes. The first characteristic is the variation in the Gibbs energy that drives the corrosion process, i.e. the redox reaction, and the second has to do with the kinetics that limits the speed of this reaction. Titanium alloys resist corrosion due to the oxide layer present on the surface (metal passivation) which acts as a kinetic barrier against corrosion. [22] Therefore, the corrosion of implants is related to the implant material (chemical composition and nanostructure), the biological environment it is in (pH, temperature, ion concentration, oxygen content, presence of proteins), the chemistry of the released metal ions, the design (presence of cracks and irregularities) and the function of the implant. Variation in any of these parameters will have a direct influence on the metal ions released by corrosion. [18]

The main degradation mechanism identified in titanium implants is fretting corrosion, which assumes a contribution from electrochemical and mechanical mechanisms, as well as a contribution from accelerated wear due to corrosion. Fretting is a phenomenon that occurs between two materials in contact under load and relative motion which are also in contact with a liquid acting as an electrolyte. In passive materials, such as titanium, the wear caused by this mechanical action is influenced by the depassivation and re-passivation phenomena occurring on the surface.

The oxide layer present in titanium and its alloys is quite thin and can lead to the formation of wear particles. In recent studies, such particles have been found in the liver, spleen and lymphatic system.

Despite the fact that the Ti-6Al-4V alloy is widely used as an implant biomaterial, a study found that it can release aluminium and vanadium ions. Vanadium, in particular, has a significant cytotoxicity, and aluminium has been linked to senile dementia. As a result, these leachable metal ions may produce allergic reactions, cytotoxic effects, and even neurological diseases. Because the implant is only in the body for a brief time, various health issues such as Alzheimer's disease, osteomalacia, and peripheral neuropathy should not be overlooked, and alloys for implant application should be carefully chosen. When alloying with Titanium, more care should be used. [23]

2.4.5.2 Infection

Infectious diseases are the second leading cause of death after cardiovascular disease and cause twice as many deaths as cancer. [24]

These bacteria may originate from the environment in which the operation is performed, the patient's own skin or that of the nursing staff. In addition, micro-organisms may colonise the prosthesis during surgery, shortly after surgery (entering through the wound) or after surgery through the blood. [24]

When bacteria attach to an implant, several factors influence the development of a biofilm on the implant. The microorganisms must adhere to the implant surface for the time required for the adhesion to become irreversible. This adhesion depends on the flow of fluid to which the implant is exposed, the number of bacteria that adhere and the physicochemical characteristics of the implant. Once the bacteria have adhered to the implant and formed a biofilm, this biofilm acts as a source of infection, especially in immunocompromised patients undergoing disease and its treatments. [24]

Biofilms are a collection of microbial cells that attach to the surface of implants. They can be responsible for the development of prosthetic infections that can lead to the need for long-term antibiotic therapy and sometimes implant removal. [24]

Within the biofilm, bacteria are protected from any attack by antibodies, phagocytic cell attacks and antimicrobial treatments. The biofilm matrix is a complex formed by exopolysaccharides, water (in higher proportions) and bacterial cells. The formation of bacterial biofilms is a complex process involving a large number of factors, but three stages can be distinguished. The first stage is the initiation stage, where the bacteria have attached themselves to the surface, which can be an implant or tissue. The second stage is maturation, where the bacteria begin to divide and the daughter cells proliferate around the attachment site, forming a microcolony. In the final stage, called the dispersal stage, some bacteria are released from the biofilm matrix to colonise new surfaces. [24]

The treatment of prosthetic infections represents a challenge for the surgeon, a deterioration of the functional, physical and mental state of the patient and a very high economic impact for the healthcare institutions.

2.4.6 Potential solutions

In order to offer a solution against the colonisation and growth of bacterial biofilms on implants, an elaboration of antibacterial surfaces is being considered with 2 methodologies.

On the one hand, an attempt is made to create a functionalised biocidal surface, i.e. a substance with biocidal capacity or which alters the mechanism of biofilm formation is immobilised on the surface of the biomaterial, e.g. heavy metals (Cu, Ag, Zn, etc.), antibiotics, cation complexing agents, etc. [25] [26] All these substances are immobilised on the implant surface by adsorption, by functionalisation with silanes or by microencapsulation of the active substance. The controlled release of these inhibitory and/or biocidal substances guarantees their effect over long periods, but disappears as soon as the substance is depleted on the surface. The use of immobilised antibiotics is questioned, as it can cause long-term bacterial resistance, and preference is given to inhibitors of a different kind. This is beyond the scope of this thesis and will not be discussed further.

On the other hand, the development of structured antimicrobial surfaces is being considered. These surfaces undergo treatment that alters their structural properties or creates spatial patterns of

dimensions and frequencies that inhibit bacterial colonisation. [27] This modifies the desired topographical features on the surface of titanium without affecting the general properties of the titanium. It has been shown that mimicking the bone surface by creating a similar nanoscale roughness on the titanium surface will help promote osseointegration. [28]

While microstructures promote the formation of biofilms, nanostructured surfaces inhibit bacterial attachment. These surface modifications reduce the irreversible adhesion of bacteria, thus reducing the virulence of biofilm formation. In nature, surface topography has been studied to have an antimicrobial effect, such as in cicada wings. These have nanospike patterns that protect the insect from bacterial attack because they are sharp and therefore pierce the bacterial cell wall on contact, killing the bacteria. Nature-inspired nanotopography is gaining importance as a research avenue for the development of antimicrobial surfaces to combat bacteria that are resistant to multiple antibiotics. [12]

The formation of these nanostructured surfaces is considered to be a passive strategy (no biocides are released) that persists as long as the surface structure is present. The effectiveness of these surfaces can be limited by mechanical damage that may remove the nano-sized structures or by contamination of the surface with dead cells and their fragments.

Recently, titanium materials with filiform TiO_2 nanostructures grown by specific heat treatment have been developed with promising antibacterial properties. The preparation methods of these nanostructures are based on thermal and hydrothermal processes, which is an operational advantage compared to other methods that are more expensive or where the uniformity of the coating cannot be guaranteed for parts with non-uniform geometries. [29] The TiO_2 formed in this way can be functionalised to anchor substances with biocidal activity, thus providing a structured and functionalised active surface against biofilm formation. [30]

In order to optimise the corrosion resistance of the titanium implants, an attempt is made to increase the thickness of the passive oxide layer and to improve its quality. Several alternatives have been proposed to improve the wear resistance, osseointegration and prevent bacterial growth, such as: nano-structuring of the surface by forming nanotubes, nano-needles, nano-wires and others, and their respective functionalisation with materials and compounds or bactericidal proteins that inhibit the development of biofilms. [11]

In the case of the titanium alloy Ti-6Al-4V and similar alloys, they are modified with niobium, tandalum and zirconium are incorporated to limit the release of components such as aluminium and vanadium. The danger of the release of these metals was discussed in the section above. Although these added metals are more expensive, they offer a solution to these problems. [31]

Although most studies related to these developments have demonstrated the bactericidal effectiveness of the proposed structures, especially when functionalised, there are still several questions that remain unanswered at present.

Firstly, it is not clear how such formations affect mechanical contact and its evolution, and even more so their tribochemical behaviour. Secondly, the bactericidal effect of these nanostructured surfaces has been evaluated on materials that have not been subjected to tribological or tribochemical degradation. In this case, it is not known how particles removed from these formations by insertion processes or resulting from in-use degradation affect the growth of bacterial colonies.

This thesis will focus on the development of a structured antimicrobial surface. For this purpose, an attempt will be made to create and optimise a nanostructured surface under the influence of heat treatment for different titanium alloys to create implants and prevent infections. The goal is to create new Ti-based alloys with perfect qualities, such as no adverse effects, required to use the new materials successfully in dentistry.

Chapter 3: OBJECTIVES

The overall objective of the project is to set up a procedure to develop nanostructured titanium surfaces with potential antibacterial action for different titanium alloys.

This objective will be achieved through the following sub-objectives:

1. To determine the electrochemical characterization of the different titanium alloys (Ti-6Al-4V, Ti-CP and Ti-Sn). For this purpose, different tests such as cyclic voltammetry, linear sweep voltammetry and Electrochemical Impedance Spectroscopy are used.

2. To develop thermal oxidation processes for the various titanium alloys under different conditions, to observe their influence with nano-peak formation.

3. Surface characterization through scanning electron microscopy (SEM)

The results obtained in this work will serve as a basis for the development of dental and orthopaedic implants.

Chapter 4: MATERIALS AND METHODS

4.1 Materials

In this research 3 different alloys of titanium are used: Ti-6Al-4V, Ti4Sn and TiCP.

The alloy Ti-6Al-4V is a commercial metal and is supplied by a German company, namely "Deutsche Titan Gmbh". The quality control document given by the company with the alloy's aggregations is given in Table 2.

Table 2: Chemical composition of Ti-6Al-4V

Element	N	C	Fe	O	Al	V	Ti
%	0.05	0.08	0.25	0.13	5.5-6.5	3.5-4.5	89.49

The Ti-CP alloy used has a grade 3 oxygen content of approximately 0.24%. This metal is also commercially supplied to the university.

The last alloy used in this thesis is Ti-4Sn. This alloy is prepared at the university in the metallurgy lab. This metal has a tin content of about 4%.

4.2 Sample preparation

The samples must first undergo a preparation step before they can be used in the various tests.

First, polishing is performed using a roughening machine (Struers model LaboPol-21), as shown in Figure 2. Each sample is sanded through several types of SiC sandpaper from a low grain size to a higher one, namely from 80, 240, 500, 1000, 2500 and to 4000. The grainsizes of 80, 240 and 500 are only used when the sample has a very rough or heavily damaged surface. When the samples must be polished again after one of the tests in this thesis, only the grainsizes 1000, 2000 and 4000 are used, because the surface of the samples is not so badly damaged. The rotation speed during the roughening of the samples is 500 rpm.

Each time the grain size is changed, the samples must be rotated by 90° and polished again. Polishing is carried out until a homogeneous surface is present, without scratches or impurities. During the roughening process, a small stream of water is turned on to cool the surface of the grinder.

Figure 2: Struers roughing machine model LaboPol-21

As a second step, the samples are polished with a textile for final mirror finishing. This is a disc consisting of a porous neoprene. This disc is magnetic and is placed on the polishing machine (Struers model LaboPol-5) shown in Figure 3. Instead of water during polishing, a solution of OPS and hydrogen peroxide is used. This solution contains 10% H_2O_2. The rotation speed during the polishing of the samples is between 300 and 400 rpm.

Figure 3: Struers polishing machine model LaboPol-5

As a final step, the samples are rinsed and cleaned with soap and tap water to remove any remaining solution of the OPS. Then they were placed in an 50/50% ethanol/acetone solution for a few seconds for degreasing. Then the samples are dried using hot air. Once the samples have dried and the remains of the ethanol/acetone solution are no longer visible on the surface as well as dust or scratches, then the samples are ready for use.

4.3 Electrochemical evaluation

Several electrochemical tests were performed in 3 M sulphuric acid solution at room temperature using a conventional three-electrode cell (shown in Figure 4). A platinum (Pt) electrode and an Ag/AgCl electrode were used as counter and reference electrodes, respectively. All samples were working electrodes in an electrochemical test setup, whose surface area exposed to the solution was 0.785 cm^2.

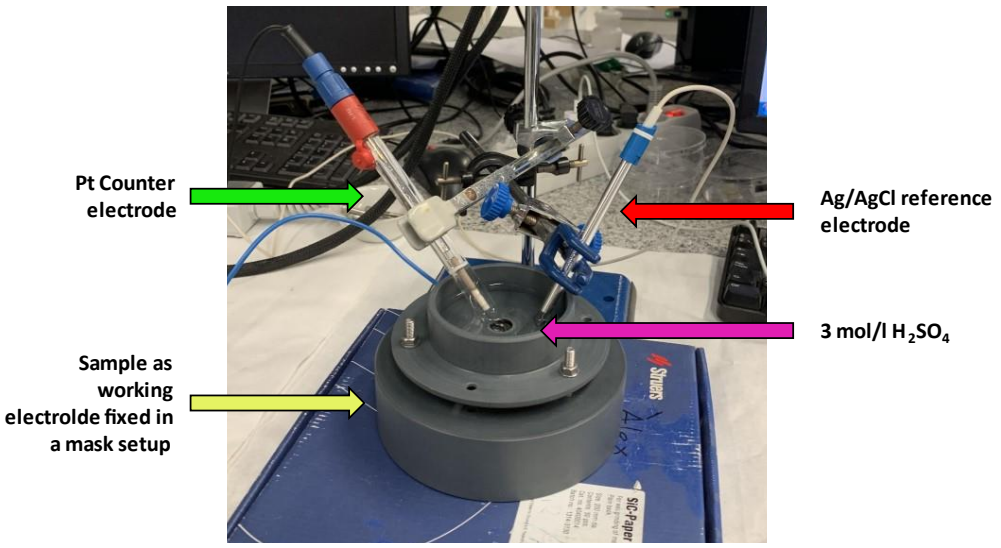

Figure 4:Cconventional three-electrode cell

A conventional three-cell electrode was connected to the AutoLab 302 potentiostat. The software used to measure and obtain electrochemical parameters was "Nova" version 2.1. This program was used to perform all tests and generate all data. The data was processed and analysed in "Origin" version 2021.

Sulfuric acid is the solution used as the medium in which the samplers are tested. At first a concentration of 0.5 M was used but this proved to be too low a concentration. The response of the tests was too low to make a concrete conclusion about this. Therefore, the concentration of sulfuric acid was increased to 3 M. This concentration proved to meet the requirements for a good response on the titanium test-samples. This strong electrolyte was chosen in order to be able to identify passivation and corrosion processes in Ti alloys, which are very stables under other solutions.

A note that must be made is that at the beginning of each experiment a new, well-polished sample is used to carry out the various tests. At the end of an experiment the sample is again roughened and polished according to the explanation in chapter 4.2 to remove the passivation layer. The purpose of the experiments described below is to investigate the behaviour of the passivation layer. Therefore, the surface of the test samples may only consist of the alloy substrate and no passivation layer may be present.

4.3.1 Polarisation test

To obtain a polarisation curve of the alloy, linear sweep voltammetry (LSV) is performed. At the start of this experiment, the OCP value is first calculated in the program "Nova 2.1". When the experiment is started over the range of -1.0 V to 2.0 V, the potential is set to V_{REF} and not V_{OCP}. During this experiment the potential is increased linearly with time while the current is recorded. The potential is measured with respect to the Ag/AgCl reference electrode, and the scan rate used for this test is 2 mV/s.

From the data obtained, a potential-log(I) graph is drawn up. Figure 5 is an example of such a graph. The setup used with the conventional three-electrode cell for the polarisation test is described as above and the "Linear polarisation" procedure is used in the "Nova 2.1" programme to carry out the tests. In this procedure, all parameters are entered (range of polarisation, scan rate).

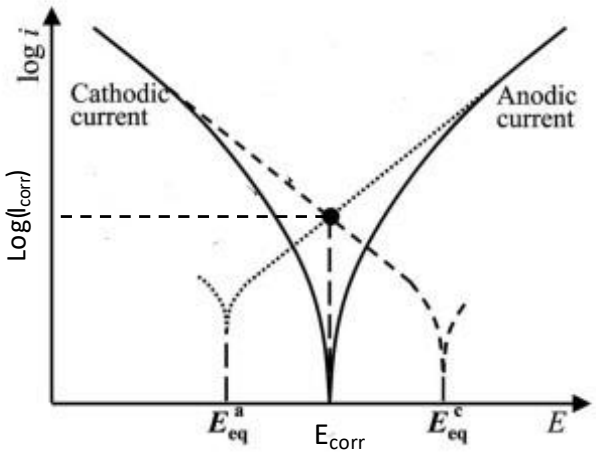

Figure 5: Schematic diagram of a polarisation curve

The reaction that occurs is:

$$Ti + 2H_2O \rightarrow TiO_2 + 4H^+ + 4e^- \qquad \text{(reaction 1)}$$

The reaction (1) in the polarisation test is in a passive equilibrium state because the scan rate (2 V/s) is very low.

From the analysis of these data, the following characteristic parameters of the curves can be obtained:

- Corrosion potential (E_{corr}), is the equilibrium potential between the reference electrode and the working electrode
- Corrosion current (I_{corr}), is the value of the current density at the E_{corr} potential
- Symmetry parameters (α_{anode}, $\alpha_{cathode}$) provide information on the symmetry of the performed fit. A good fit has a value of α_{anode} and $\alpha_{cathode}$ equal to 0,5
- Tafel slopes (β_{anode}, $\beta_{cathode}$) are the slopes of the tangents to the anode point and cathode point respectively.
- The polarization resistance (R_p) is defined as the slope of the potentiodynamic curve at potentials near the equilibrium potential.

$$i = i_0 \exp\left(\frac{\eta}{\beta_{anode}}\right) - i_0\left(-\frac{\eta}{\beta_{cathode}}\right) \qquad \text{(Eq. 1)}$$

The total current density is equal to the sum of the anode current density and the cathode current density. With the Butler-Volmer equation (Eq. 1) such a sum of currents can be represented as a function of the Tafel slopes (β_{anode}, $\beta_{cathode}$) and the polarisation η (difference between the open circuit potential and the corrosion potential). The Tafel slopes are determined by a linear approximation in a manner similar to that shown in Figure 5. On the other hand, i_{corr} is the cut-off point of the Tafel slopes. E_{corr} is obtained by substituting the already known values in one of the equations of the Tafel slopes. [32] [33]

4.3.2 Cyclic voltammetry

Cyclic voltammetry is used for the corrosion test of the various alloys. Here, the current is increased and then decreased over a range of -1.0 V to 2.0 V and this versus a Ag/AgCl reference electrode.

For this test, multiple-sweep cyclic voltammetry is used. In this method, the potential is repeatedly scanned in the forward and backward directions at various scan speeds, namely 6.25 mV/s; 25.0 mV/s; 56.3 mV/s; 100.0 mV/s; 156.3 mV/s. The setup used with the conventional three-electrode cell for cyclic voltammetry is described as above and the " Cyclic voltammetry potentiostatic " procedure is used in the "Nova 2.1" programme to carry out the tests. In this procedure, the parameters scan speed, the range of the potential and the number of scans the programme performs are set.

The reaction for cyclic voltammetry is not in a passive equilibrium state but in a kinetic controlled state. This is because the scan rate is too high.

The number of scans is set to 5. The surface of the test samples is polished as mentioned in chapter 4.2. No oxide layer is present on the test samples and the surface consists only of the composition of the material used. The first scan in the cyclic voltammetry causes the formation of the passive layer. When the potential is increased, a peak is obtained at the first cycle. This peak indicates the formation of the passive layer. The kinetics of this passive layer can only be seen in the first cycle of the cyclic voltammetry. In the following cycles, peaks also occur but at a higher potential then the first peak. This is because the passive layer has already been formed. Each time the number of new cycles increases, the current decreases because the passive layer increases. The different number of cycles are necessary to see how the passive layer develops. This can be seen in Figure 6.

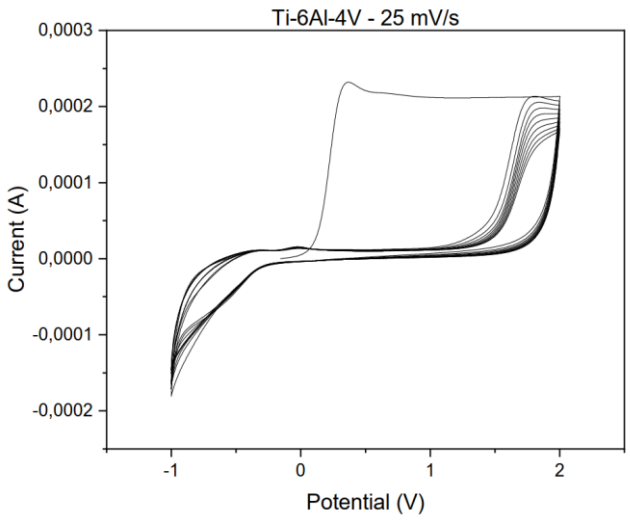

Figure 6: Example of a curve in cyclic voltammetry (Ti-6Al-4V with a scan rate of 25 mV/s)

It can also be noted that there is no peak in the negative current while there is a peak in the positive current. This indicates an irreversible process. The oxide layer formed in the first cycle remains intact and is not broken down again. There is oxidation but no reduction. Once the passive layer is formed, it cannot be reduced.

4.3.3 Electrochemical Impedance Spectroscopy (EIS) Test

The technique consists of applying a sinusoidal electric potential perturbation of varying frequency (shown in Figure 7) to the material under study and recording the current response within an electrochemical cell (shown in Figure 8). Impedance is defined as the ratio of the applied potential to the current measured at the output. In many electrochemical materials and systems, the impedance varies with the frequency of the applied potential in a way that is related to the properties of these materials. This is due to the physical structure of the material, the electrochemical processes taking place, or a combination of both. Therefore, if impedance measurements are made in a suitable frequency range and the results are plotted on axes according to the data obtained, it is possible to relate the results to the physical and chemical properties of the materials and electrochemical systems.

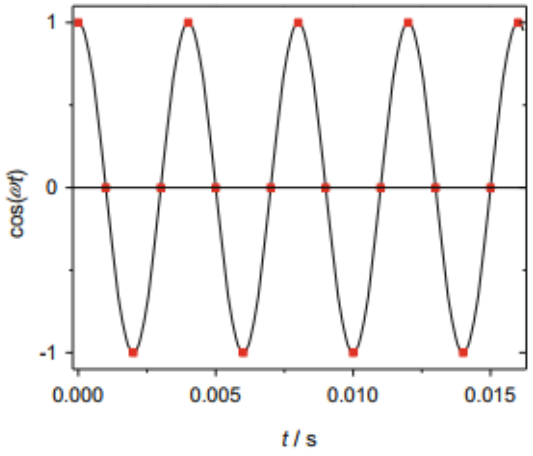

Figure 7: Example of a sinusoidal electric potential disturbance with varying frequency

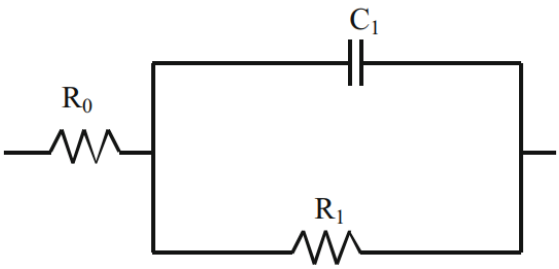

Figure 8: Example of the composition of an electrochemical cell

There are two ways to graphically represent the impedance results obtained from an EIS test:

1) Nyquist diagram, where the imaginary part multiplied by -1 (-Z'') is plotted against the real part (Z'). This is the most used representation system and the information obtained from it is based on the shape of the spectra.

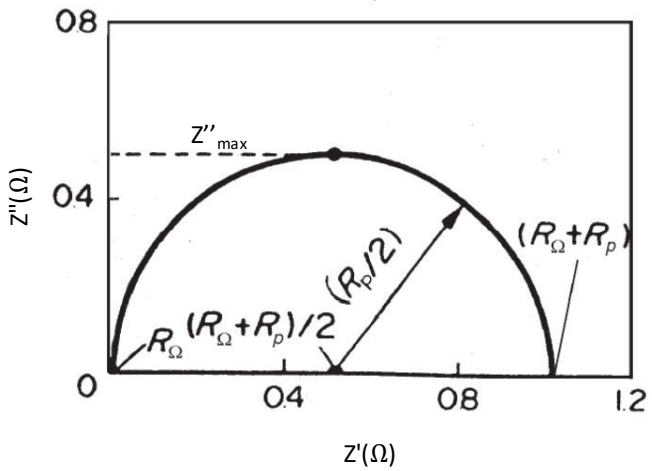

Figure 9:Nyquist diagram of a simple electrical circuit from Ref. [34]

Z(Ω) has a real and an imaginary component i.e. Z(Ω) = a + b - i. If the imaginary Z'' (Ω) with negative sign is represented as a function of the real Z'' (Ω), one obtains the Nyquist plot (see Figure 9). This is the most widely used representation system and the information it provides is based on the shape of the spectra. Each point on the Nyquist plot represents the impedance value at one frequency. Low frequency data is on the right side of the diagram, while high frequency data is on the left side of the diagram.

2) Bode diagrams, where the logarithm of the impedance modulus (log |Z|) and the phase shift (Φ) are plotted as a function of the logarithm of the frequency (logω). An example is shown Figure 10. The information obtained from this type of representation is mainly aimed at the behaviour as a function of frequency.

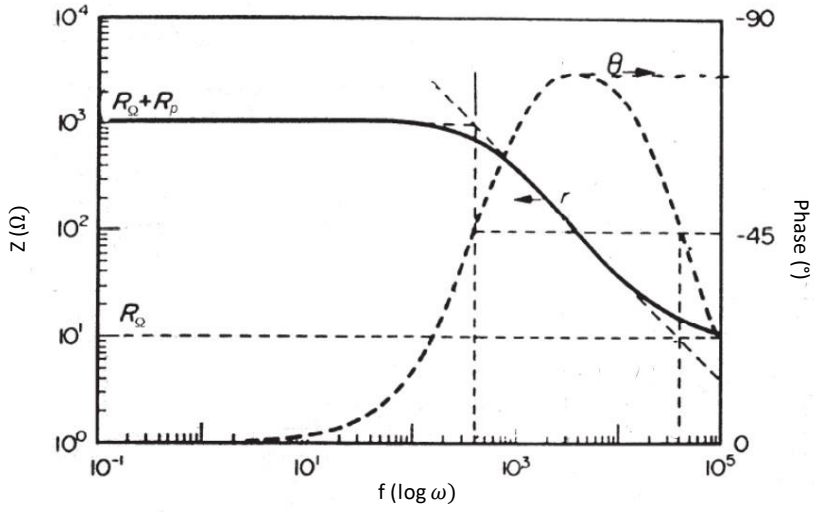

Figure 10: Bode diagram of a simple electrical circuit from Ref. [34]

For the impedance test, 4 points on the polarisation curve are chosen and these points will be examined in this section. More information on this will be given later in chapter 5.3. One of these 4 points, namely the OCP-value, is obtained by the program "Nova 2.1" during the test polarization. The other 3 points are calculated from the polarization curve obtained during the polarization test. These potential values are used in the settings in the "Nova 2.1" programme. The frequency range for the impedance test is set from 10 mHz to 10,000 Hz. The amplitude was set to 10 mV and the tests were performed with 5 points/dec.

The setup used with the conventional three-electrode cell for cyclic voltammetry is described as above and the "FRA impedance potentiostatic" procedure is used in the "Nova 2.1" programme to perform the tests. In this procedure, the applied potential, the range of frequency and the number of points per decade are set as parameters in the procedure. [34]

4.4 Thermal treatment of titanium alloys

This section describes the heat treatments carried out on the different alloys for the formation of nano-spikes. The process continues as a whole, but it will be carried out at two different temperatures, which are the first and second heat treatments respectively.

4.4.1 Setup of the process

For this experiment a high temperature tube furnace (MTI CORPORATION model OFT-1200X-S) is used, with dimensions of 2000 mm long, 44.5 mm inner diameter and 2.5 mm thick. A characteristic of the tube furnace or piston flow reactor is the variation of the gas flow composition depending on its position. If the argon flow rate is changed, the concentrations of the formed species also change.

The tube is connected to two glass gas washing bottles of 500 mL capacity. One is placed at the inlet and the other at the outlet. See Figure 11.

Figure 11: The furnace with the reactor and the 2 bottles (left acetone and right water)

The bottle at the inlet is filled with approximately 250 mL of acetone and the bottle at the outlet with 250 mL of water. A schematic representation of the experimental set-up is shown in Figure 13.

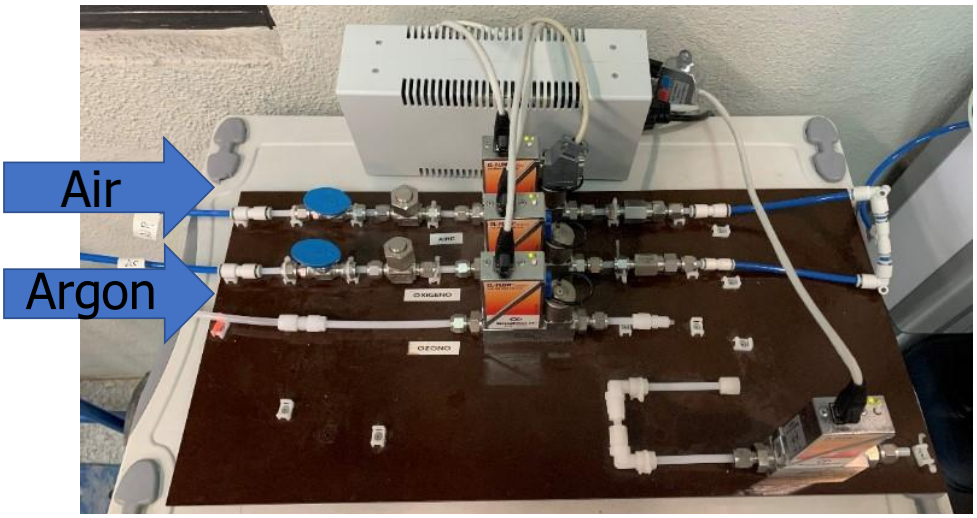

Figure 12: The circuit board to which the programme is connected with the inlet of the gases on the left and the outlet of the gases on the right

The Argon and air supply both enter the circuit board with two digital mass flow controllers (see Figure 12). The gas flow controllers are commanded by a home-made software written with "Labview 2016". The selected flow rates are 0.3; 0.5 and 1.0 L/min.

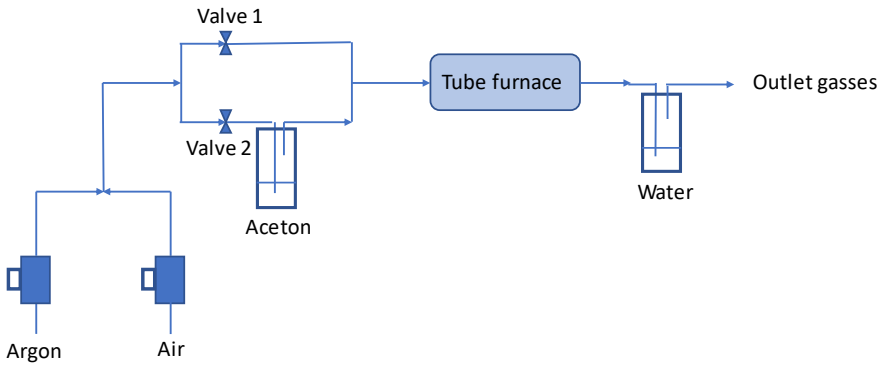

Figure 13: Sketch of the setup

The gas flows have two access routes to the reactor:

1) One is the direct connection between the circuit board and the reactor. For this purpose, valve 1 must be open and valve 2 closed.
2) The second way shall be used when it is desired to feed the argon/acetone vapour mixture to the reactor. In this case, valve 2 is open and valve 1 is closed.

This is shown in Figure 13.

The alloy samples are fed into the reactor using supports filled with a base of 2 mm Al_2O_3 particles. See Figure 14.

Figure 14: Support plate for the samples filled with Al_2O_3 particles

A piece of glass fibre and a porous zirconia plug are placed at each end of the glass cylinder of the reactor to serve as a filter. The furnace is closed and connected to the gas source.

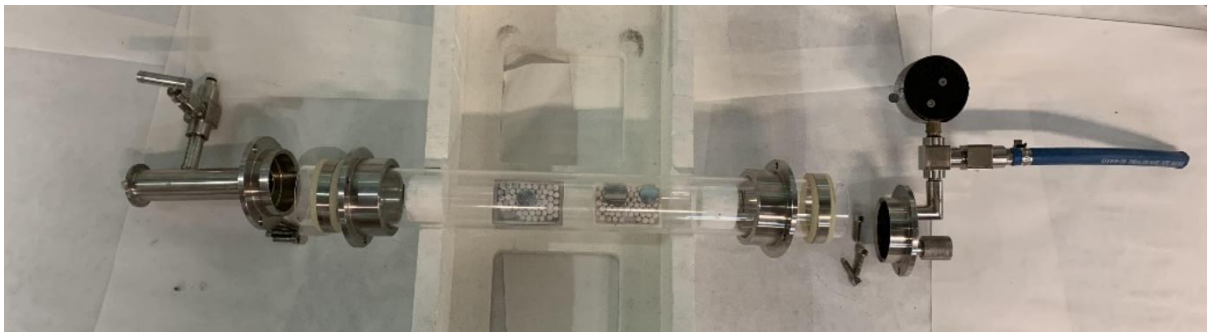

Figure 15: The composition of the tubular reactor with the titanium samples in it

Once the tube furnace is assembled, as can be seen in Figure 15, the reactor must be completely filled with argon before starting the reaction. Therefore, the amount of argon must be calculated as well as the time to ensure that all oxygen is expelled from the reactor.

With the dimensions of the reactor (2000 mm long, 44.5 mm inner diameter and 2.5 mm thick) the volume can be calculated, knowing that it is a cylindrical tube. Applying Eq. 2 we obtain a volume of 354.41 cm^3.

$$V_{reactor} = \pi * r^2 * L \qquad \text{(Eq. 2)}$$

The volume calculated then allows the retention time to be calculated using the following formula (Eq 3).

$$t_R = \frac{V_{reactor}}{Q} \qquad \text{(Eq. 3)}$$

The obtained retention time is about 22 s. To be sure that all oxygen has left the reactor, we choose a retention time of about 8 min. The smallest amount of oxygen present in the reactor can have a major impact on the formation of the TiC.

To ensure that the argon stream is circulating through the reactor, the bottle at the exit of the reactor should be checked for bubbling. The bubbling of the acetone bottle should also be checked to ensure that there are no leaks in the circuit. When the valves are closed, the flow rates shown in the programme should be 0.

As soon as the 8 minutes have elapsed, the flow is adjusted to the required flow rate and the first heat treatment cycle is started. The first heat treatment shall be performed at 850ºC for 45 minutes with an increment of 15ºC/min. These values for temperature, time and heating rate are chosen because they are the ideal parameters from a previous study carried out in the same laboratory and with the same material.

During the rise of the first heat treatment, only argon is allowed to pass through. When the desired temperature (850ºC) is reached, the argon flow is diverted to the bypass flow with acetone that is at room temperature. As soon as the flow of argon and acetone enters the reactor, the reaction starts. Once the 45 min of initial heat treatment have elapsed, the reactor switches back to the argon-only stream to remove any remaining acetone vapours. This is done during the temperature drop from 850 to 600 °C and takes approximately 17 min.

Once the temperature stabilises at 600 °C, the argon stream is switched to the air stream using the programme. This second heat treatment also takes 45 min. After this, the temperature drops back to room temperature and the samples are used for further research. Figure 16 and

Table 3 show the process.

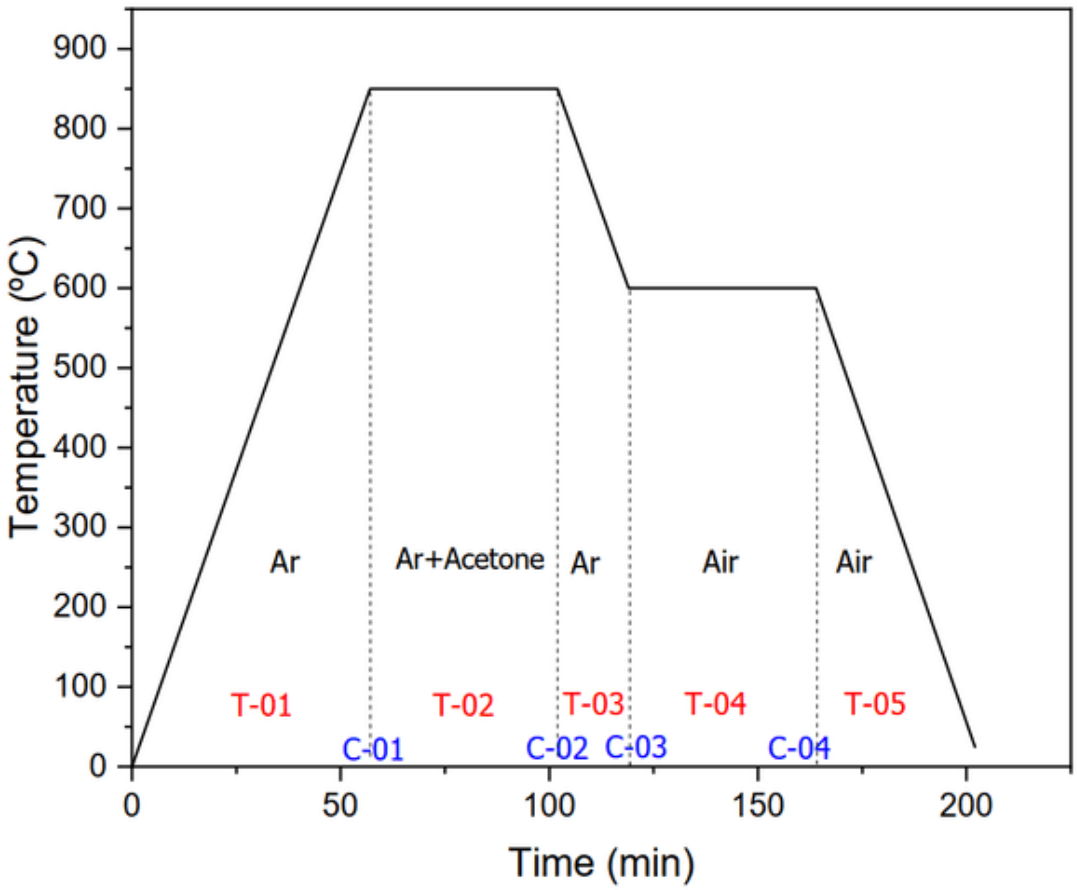

Figure 16: The process of the reactor in the furnace

Table 3: The process of the reactor in the furnace

Prompt	Input data	Comment
C-01	0 °C	Initial Temperature
T-01	57 min	During this time when the oven is heating up, only the Argon stream is flowing
C-02	800 °C	
T-02	17 min	In this time period the first heat treatment has started and there is now a flow of argon and acetone passing the reactor
C-03	800 °C	
T-03	17 min	The remaining vapours of the acetone are removed by passing the argon stream through the reactor.
C-04	600 °C	
T-04	45 min	The second heat treatment is started and switched to air flow
C-05	600°C	
T-05	-121	Program finished. Furnace is cooling down naturally

4.4.2 The formation of the nanospikes

The first heat treatment is carried out with an argon/acetone mixture in the absence of oxygen. The acetone vapour is exposed to a high temperature and then undergoes pyrolysis, i.e. thermal decomposition in the absence of oxygen whereby the acetone is broken down by heat without combustion reactions. As a result, a titanium (IV) carbide with a carbon layer is formed.

The second heat treatment is carried out with atmospheric air whereby the carbon is removed from the synthesised nanoparticles and titanium(IV) oxide is formed.

Figure 17 shows schematically what is formed on the surface of the Ti-6Al-4V alloy after application of the heat treatments.

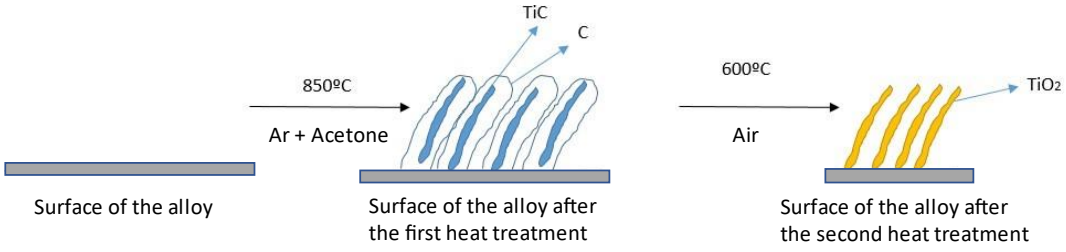

Figure 17: Overview of the process

The reactions that continue in this process are as follows:

$$Ti(s) + 2CH_3COCH_3(g) \rightarrow TiO_2(s) + 6C(g) + 6H_2(g) \quad \textit{(reaction 2)}$$

$$Ti(s) + 2CH_3COCH_3(g) \rightarrow TiC(s) + CO(g) + 6H_2(g) \quad \textit{(reaction 3)}$$

$$TiC(s) + 2\ O_2(g) \rightarrow TiO_2 + CO_2 \quad \textit{(reaction 4)}$$

The reactions (2) and (3) are caused during the first heat treatment. The second heat treatment undergoes an oxidation in which the formed TiC reacts with the oxygen from the air flow. This produces titanium (IV) oxide and carbon dioxide as shown in reaction (4).

4.4.3 Cleaning the reactor and components

At the end of the experimental procedure, the reactor, the porous zirconium filters and the glass fibre must be cleaned, since they look black due to the deposition of the pyrolysis products of the acetone. The cleaning is carried out by means of heat treatment.

The quartz and the porous zirconia tube shall be cleaned by heat treatment in the tube furnace at 850ºC for a period of about 30 min until the black colour has completely disappeared.

4.4.4 Techniques for examination of the nanospikes

4.4.4.1 SEM-test

The first technique used is Scanning Electron Microscopy (SEM). This is a topographical, structural, and compositional analysis technique.

With such a microscope an image of the sample can be made, but what is detected is the response of the material to the impact of an electron beam (electrons called primary electrons) rather than the recording of photons as is done in traditional optical microscopy.

The operation of SEM equipment is as follows: a high energy electron beam is generated and a system of lenses is used to focus the beam and cause it to strike a sample, which in turn will generate electrons (called secondary and scattered electrons) in response to the electronic strike, and these electrons leaving the sample are detected by devices that each record the number of electrons detected and convert them into a digital signal that is interpreted as colour intensity to build an image. [35] Figure 18 shows a schematic representation of an SEM device.

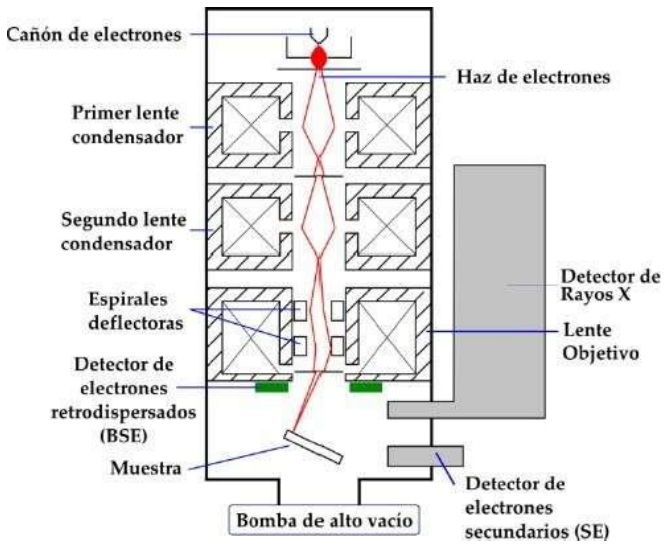

Figure 18: Schematic of SEM equipment Ref. from [35]

When the sample is hit by the high-energy electron beam, it produces a series of signals that are recorded on the different detectors of the equipment. Each of the signals independently provides information about the topography, composition, and electrical conductivity of the sample. To obtain the image, the electron beam is moved in the xy-plane so that it passes over the planned area. The resolution that can be achieved is up to 2 nm. [35]

The scanning electron microscope available for sample analysis (JEOL model JSM6300) is shown in Figure 19 and both the secondary electron detector and the X-ray detector will be used.

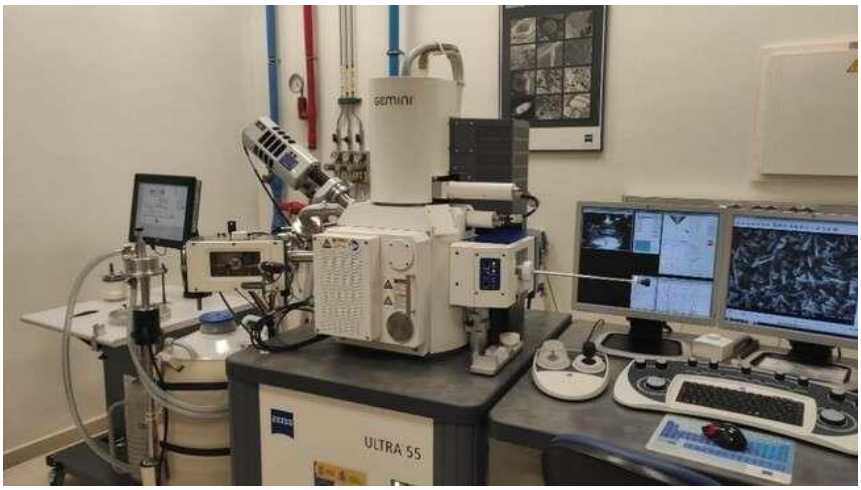

Figure 19: Scanning Electron Microscope (SEM) JEOL model JSM6300 [36]

On the one hand, the secondary electron detector is the one that provides the typical black and white image of the topography of the examined surface. It is the most suitable signal for the observation of nano-spikes because it has the highest resolution.

In order to introduce the samples into the equipment, they must fulfil two conditions: they must be dry and conductive. The samples obtained after the experimental procedure are dry but not very conductive and must therefore be covered on one side with conductive adhesive tape.

Once the samples are placed in the SEM microscope, several pictures will be taken at different resolutions (1K X, 5K X, 15K X, 30K X) to have different measurements of the same sample for further analysis. An example is shown in Figure 20. The size of the resolutions can sometimes vary depending on what is seen during the experiment.

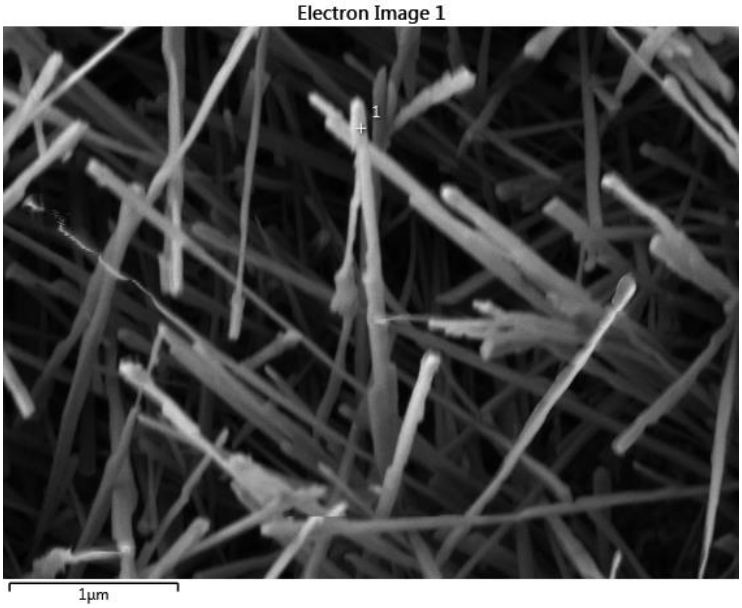

Figure 20: Nanospikes on a Ti-6Al-4V alloy with a flow rate of 1l/min

4.4.4.2 EDS-test

The Energy-Dispersive X-ray Spectroscopy microanalysis (EDS) test can be used to obtain a visual map of the distribution of elements in a given area and also determine the amount of each element in that specific area.

This technique uses the same apparatus as the SEM test in which an X-ray detector receives the X-rays from each of the points on the surface that the electron beam passes over. Since the energy of each X-ray beam is characteristic of each element, qualitative and quantitative analytical information can be obtained.

By applying this technique to a sample area, a graph is obtained showing the counts (cps/eV) at each energy value (keV) and a table showing the mass and atomic percentage of each element in the area.

During the SEM analysis in this study, the lowest possible electron acceleration voltage was used to discriminate between nanospike and substrate composition.

The nanospike composition was also confirmed by EDS on the TEM machine.

Figure 21 is the graph obtained by applying EDS microanalysis to the area corresponding to Figure 20.

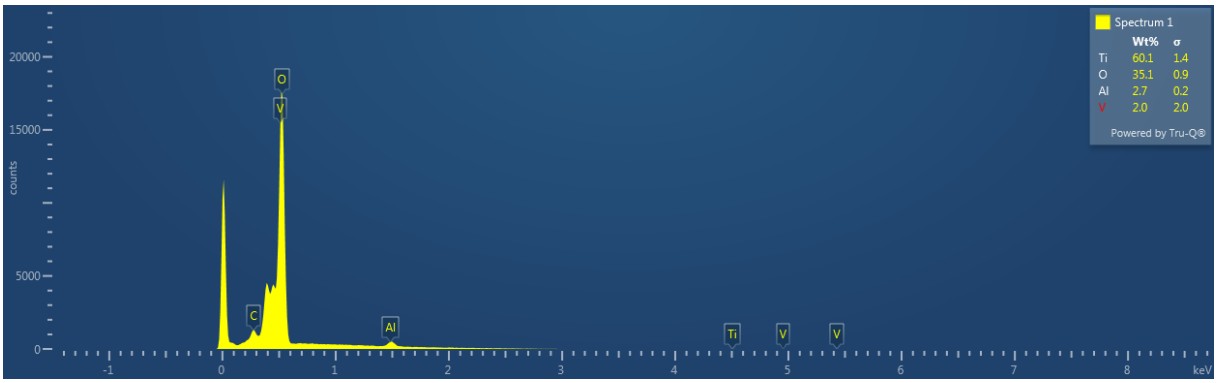

Figure 21: Composition spectrum of a Ti-6Al-4V alloy with a flow rate of 1 l/min

4.4.4.3 TEM-test

TEM (shown in Figure 22) is a microscopy technique capable of providing very high-resolution images down to a level of several Angstroms (~ 0.19nm). It images thin (100s nms) samples via the interaction of electrons as they pass through a specimen. Detecting a range of resultant secondary signals allows for the study of nano-scale morphological and chemical features of materials down to near atomic levels.

An electron source at the top of the microscope emits electrons that travel through a vacuum in the column of the microscope. It creates a vacuum to prevent the interaction between air particles and electrons. So that electron will not be scattered. Electromagnetic lenses are used to focus the electrons into a very thin beam and this is then directed through the specimen of interest. The electrons passing through the specimen then impact on a detector. Traditional bright field imaging relies on incident electrons being scattered and disappearing from the beam depending upon the compositional density and crystal orientation of the sample. The intensity of un-scattered electrons gives rise to a "shadow image" of the specimen, with different parts of a specimen displayed in varied darkness according to density. By rotating a sample, and taking multiple images at each rotation, it is also possible to build a 3D representation of the specimen (tomography). How this TEM is constructed is shown in Figure 23.

Figure 22: 120 kV Transmission Electron Microscope (TEM 120)

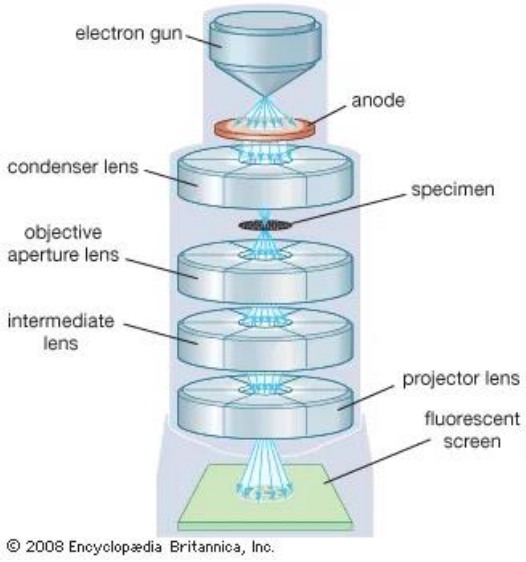

Figure 23: Construction of the TEM Ref. from [37]

The crystal structure of samples with regular atomic structure (crystalline material) may also be analysed via electron diffraction. Positive interference in the back focal plane leads to discreet spots of electron localisation, which can then be visualised by mapping the back focal plane to the imaging apparatus. The diffraction patterns can then be used to analyse to the crystal structure of the specimen.

X-ray emission consequent to the interaction of the primary electron beam with the sample, can also be detected by an energy-dispersive spectrometer (EDS) within the TEM. As the resulting X-ray energies are characteristic of the atomic structure of the element they originated from, the spectra generated can be used to identify the constituent elements. [38]

Chapter 5: RESULTS AND DISCUSSION

5.1 Electrochemical evaluation

5.1.1 Polarisation test

The results of the polarisation test are shown in Figure 24. The red curve shows the result of Ti-Sn, the green curve shows the result of Ti-6Al-4V, and the black curve shows the result of Ti-CP. These curves were checked for reproducibility and were carried out two times. The results of the various tests are shown in Appendix I.

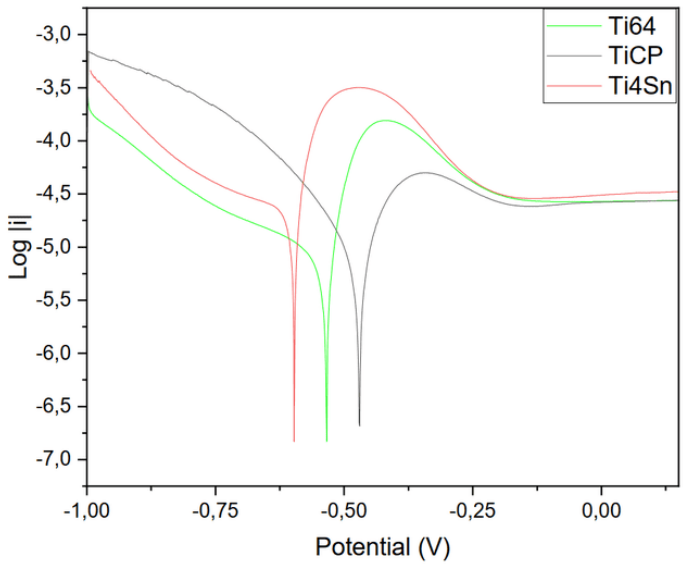

Figure 24: Results of the polarisation test

Figure 24 shows that the peak at log|i| of Ti-Sn is the largest and the peak of Ti-CP is the smallest. Tin is a more active element than titanium, which is why the Ti-Sn alloy has a larger peak on the polarisation curve than the alloy that only consist of titanium, Ti-CP. The intermediate curve is that of Ti-6Al-4V. Aluminium and vanadium are less reactive elements than tin but more active than titanium. Therefore, the peak of Ti-6Al-4V lies between the others.

Differences can also be seen in the potential. For example, Ti-Sn has a more negative potential than the other curves. This means that this alloy is less noble and therefore more vulnerable to corrosion. Ti-CP has the most positive potential, so this alloy is more noble and more resistant to corrosion. The nobler a metal is, the more resistant it is to corrosion.

5.1.1.1 Analysis of Polarization Curves

The polarization curves for the different substrates were analysed under Buttler-Volmer formalisms where its equation describes the electrokinetics phenomena on corrosion processes.

The Butler-Volmer equation (hereafter, BVE) is just valid around the corrosion potential because around this potential the electrochemical processes are controlled by the kinetics of the process, the chemical reaction rates. But far from this corrosion potential other processes such as the mass transfer of the passive layer formation could have a bigger importance. Then, from the experimental results a window of ± 50 mV around the corrosion potential (very close to the measured OCP) has been used from the polarization curve. The analysis is applied for each material and the results follow:

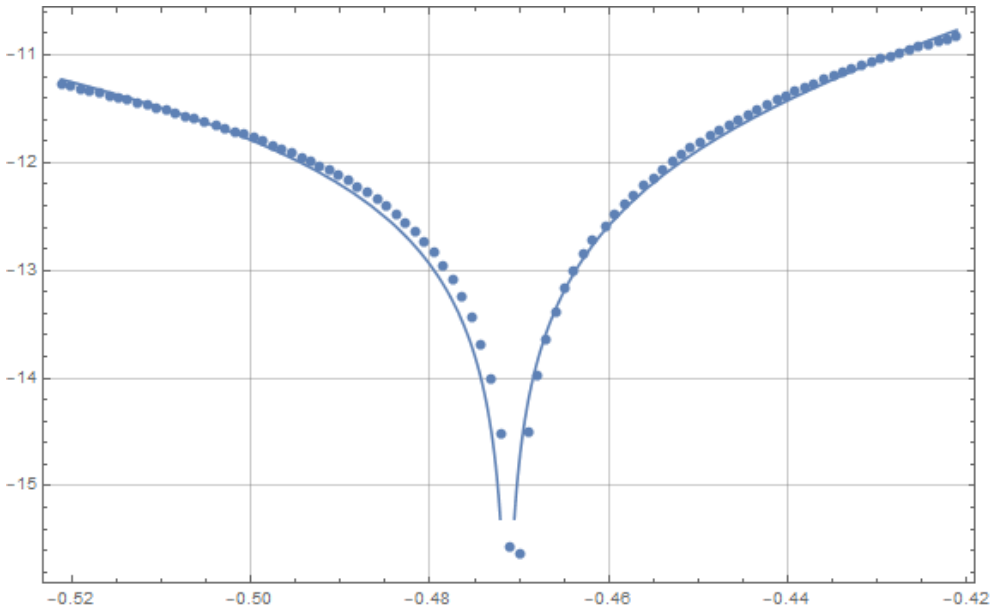

Figure 25: Polarization Curve for Ti-CP

Figure 25 is the fit of the BVE with the polarization curve of TiCP. The y-axe is the Ln of the absolute value of the current, and the x-axe are the applied potential vs Ag/AgCl.

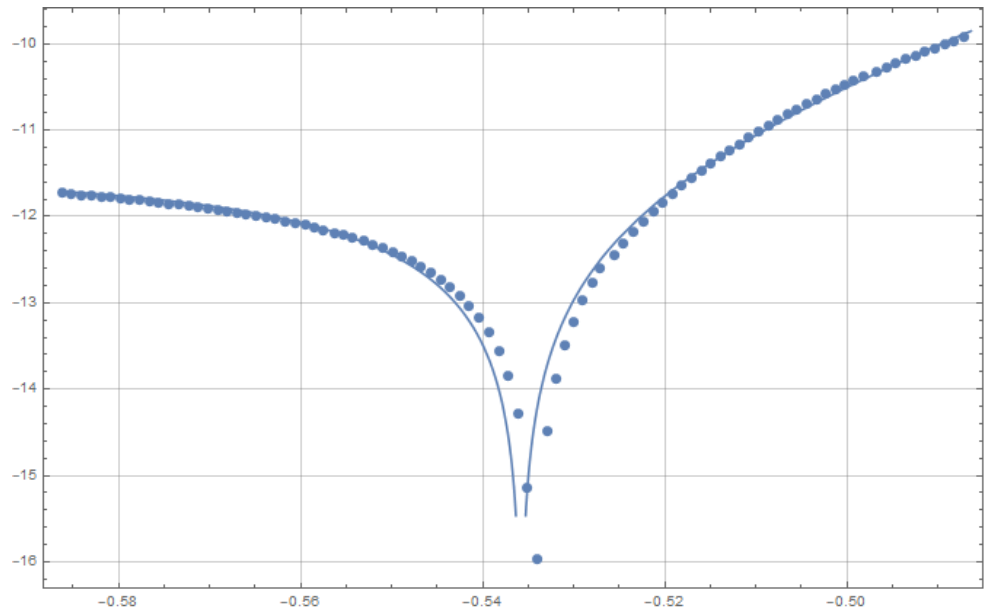

Figure 26: Polarization Curve for Ti-6Al-4V

Figure 26 is the fit of the BVE with the polarization curve of Ti-6Al-4V The y-axe is the Ln of the absolute value of the current, and the x-axe are the applied potential vs Ag/AgCl.

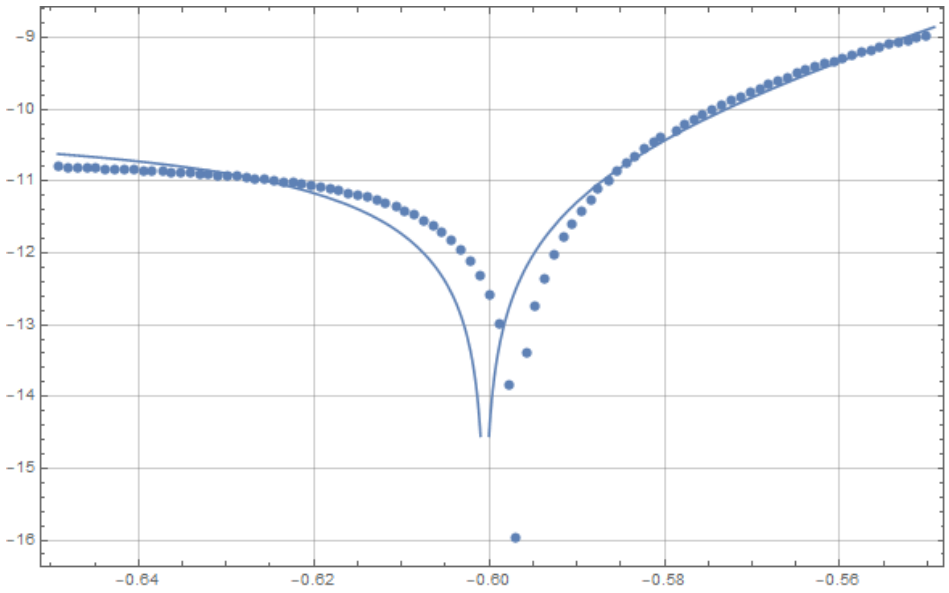

Figure 27: Polarization Curve for Ti4Sn

Figure 27 is the fit of the BVE with the polarization curve of Ti4Sn The y-axe is the Ln of the absolute value of the current, and the x-axe are the applied potential vs Ag/AgCl.

From Figure 25, Figure 26 and Figure 27 we can conclude that the Ti-CP and the Ti-6Al-4V behaves close to the BVE and then the redox formalism is applied for these alloys in the 3 M sulfuric media. The behavior of Ti4Sn alloy is far from BVE because there is a clear deviation on the fit in particular to the anodic branch. This anomalous electrochemical behavior is also confirmed in other electrochemical test as Impedance tests. This will be discussed later in section 5.1.3.

The analysis of the polarization curves provides the values of the corrosion current and potential, i_{corr} and E_{corr}, the transfer coefficients for the anodic and cathodic processes, $n\alpha_{an}$ and $n\alpha_{ct}$, the Tafel slopes anodic and cathodic, b_{an} and b_{ct}, and the polarization resistance, R_p. These values for all the materials are shown on Table 4.

Table 4: Results of the analysis of the polarisation curves

Material	i_{corr} ($\mu A/cm^2$)	E_{corr} (V)	$n\alpha_{an}$	$n\alpha_{ct}$	b_{an}(V/dec)	b_{ct}(V/dec)	R_p (Ω)
TiCP	9.20	-0.471	0.613	0.387	0.0949	0.1503	3499.1
Ti6Al4V	11.6	-0.536	0.976	0.024	0.0596	2.4532	2781.4
Ti4Sn	31.7	-0.600	0.929	0.070	0.06258	0.8243	1013.9

For the corrosion current i_{corr}, there is a lower value for Ti-CP and a higher value for Ti-Sn. This means that Ti-CP with the lowest value is difficult to corrode and Ti-Sn with the highest value is the easiest. Ti-6Al-4V is the intermediate value. In E_{corr}, we see a similar result. Ti-Sn has the most negative potential value. This indicates that this metal is the easiest to corrode as mentioned above because this metal is the least noble.

The table shows the symmetry factor $n\alpha_{an}$ and $n\alpha_{ct}$. The sum of these 2 values is relatively close to 1.0. In an ideal system, the sum of these should be close to 0.5, which is not the case here. The table slopes b_{an} and b_{ct} are not easy to interpret. Due to their complexity, these results are not discussed in this thesis.

An important value is the polarisation resistance R_p. TiCP has the highest value in this analysis. This means that this alloy is more resistant in comparison with Ti-Sn which has the lowest polarisation resistance. A lower polarisation resistance again indicates that the metal is easier to corrode.

5.1.2 Cyclic voltammetry

Figure 28 shows the result of the first cycle of the cyclic voltammetry of Ti-6Al-4V, Figure 29 shows the result of the first cycle of Ti-CP and Figure 30 shows an magnification of the result of the first cycle of Ti-CP because there is a strong negative value of the current which made the visual distinction of the peaks in the positive part of the potential no longer visible. Figure 31 show the result of the first cycle of Ti-Sn. All cyclic voltammetry tests were performed versus an Ag/AgCl reference electrode.

Each experiment in cyclic voltammetry was checked for reproducibility and was carried out two times. These results are presented for the Ti-6Al-4V alloy in Appendix II, for the Ti-CP alloy in Appendix III and for the Ti-Sn alloy in Appendix IV.

For each alloy, five different scan rates were carried out, namely 6.25 mV/s (shown on Figures 28, 29, 30 and 31 as magenta), 25 mV/s (shown on Figures 28, 29, 30 and 31 as blue), 56.3 mV/s (shown on Figures 28, 29, 30 and 31 as green), 100 mV/s (shown on Figures 28, 29, 30 and 31 as red) and 156.3 mV/s (shown on Figures 28, 29, 30 and 31 as black).

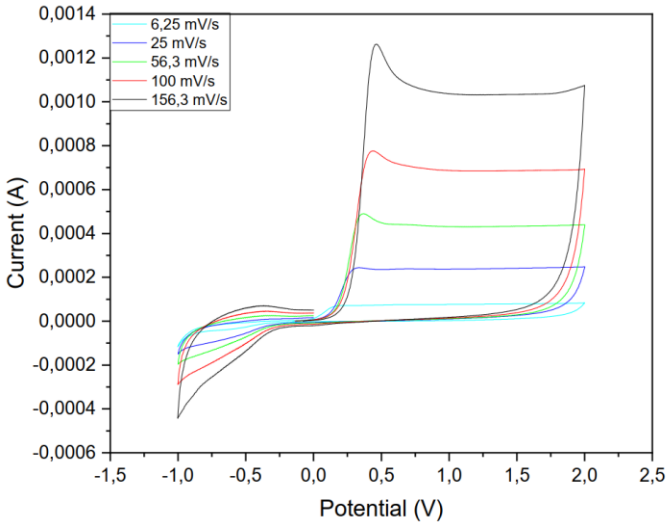

Figure 28: Results of cyclic voltammetry for the Ti-6Al-4V alloy

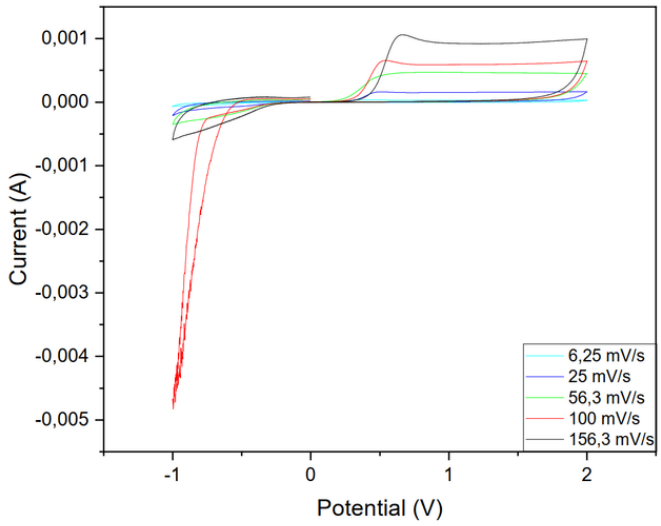

Figure 29: Results of cyclic voltammetry for the Ti-CP alloy

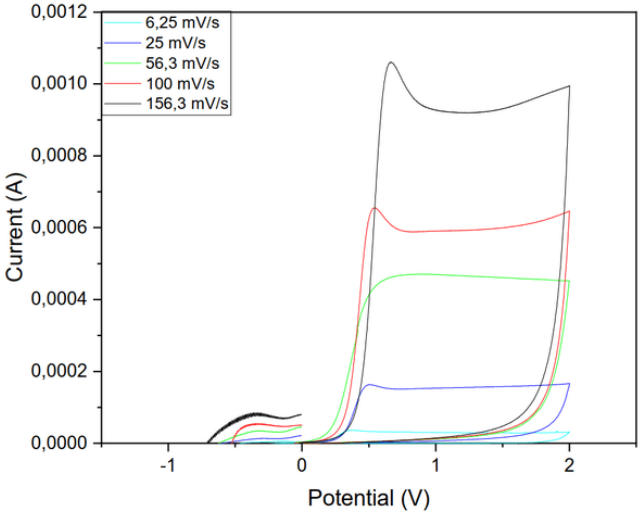

Figure 30: An magnification of the cyclic voltammetry results for the Ti-CP alloy

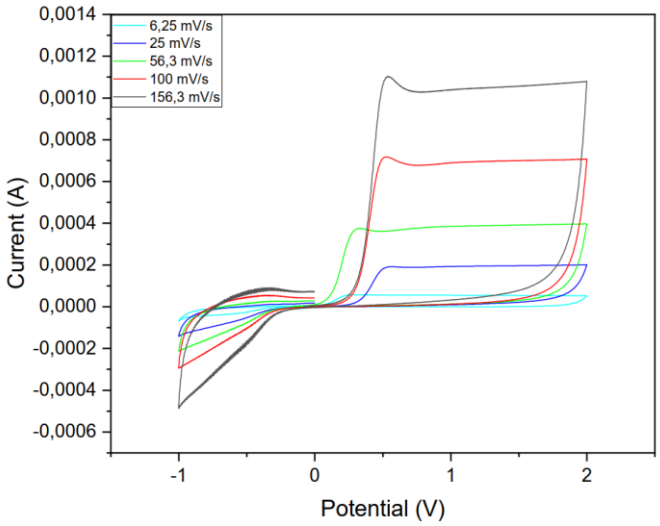

Figure 31: Results of cyclic voltammetry for the Ti-Sn alloy

For each first cycle of each alloy carried out, the potential peak E_{pk} was calculated with the corresponding current I_{pk}. This calculation was performed as illustrated in Figure 32.

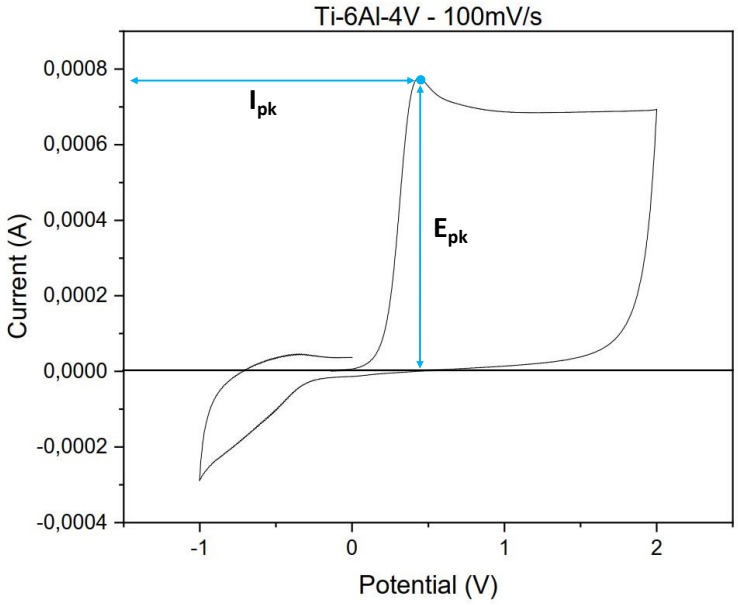

Figure 32: Example calculation E_{pk} and I_{pk} of a 1st cycle

The values of the peak potential (E_{pk}) and the current (I_{pk}) are then plotted in a graph versus the scan rate (v) and the square root of this scan rate ($\sqrt{v}$).

The values of the peak potential versus the scan rate are shown in Figure 33 and versus the square root of the scan rate are shown in Figure 34. In these figures the black squares represent the results for the Ti-6Al-4V alloy, the red spheres for Ti-Sn and the green triangles for Ti-CP.

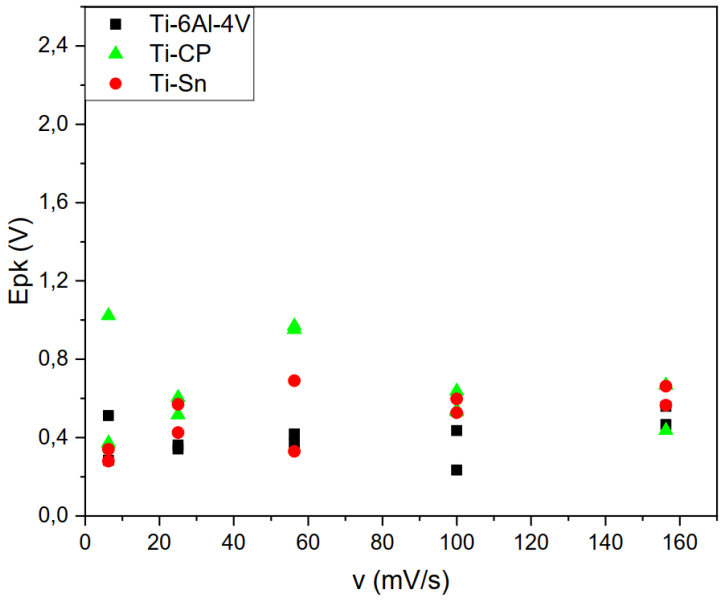

Figure 33: Results of peak potential vs the scan rates of the cyclic voltammetry experiments

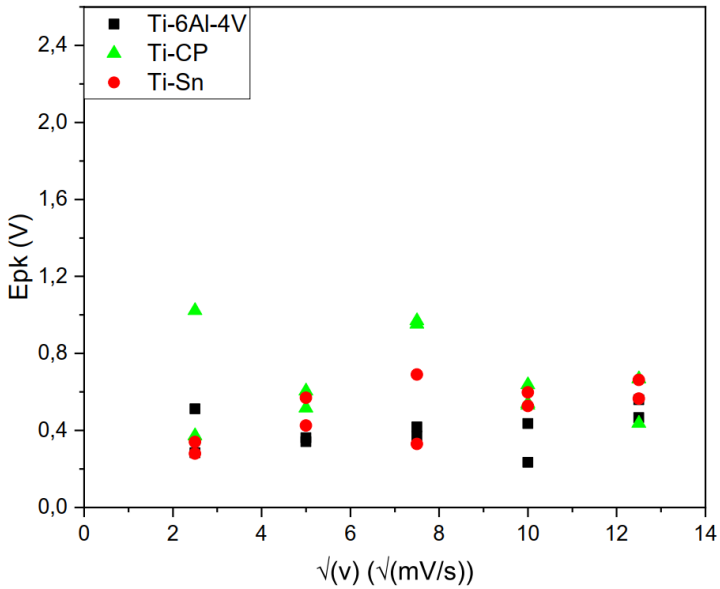

Figure 34: Results of the peak potential vs the square root of the scan rates of the cyclic voltammetry experiments

In Figures 33 and 34, it is shown that the values of the peak potential remain constant over the different scan rates. This indicates that the process which forms the passivation layer on the different alloys is determined by an electro-active field. If a shift in the peak potential were to occur at different scanning speeds, the passivation layer would be determined by diffusion. This is not the case here.

The values of the current versus the scan rate are shown in Figure 35 and versus the square root of the scan rate is shown in Figure 36. In these figures the black squares represent the results for the Ti-6Al-4V alloy, the red spheres for Ti-Sn and the green triangles for Ti-CP.

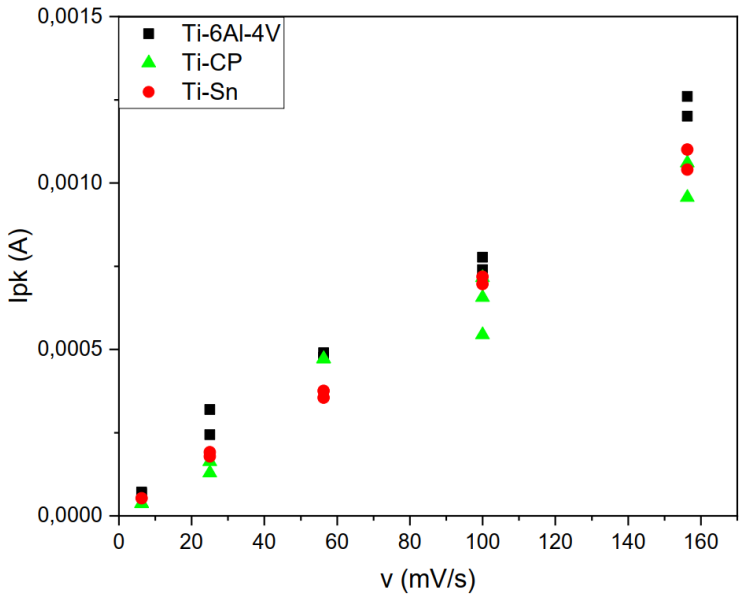

Figure 35: Results of the current vs the scan rates of the cyclic voltammetry experiments

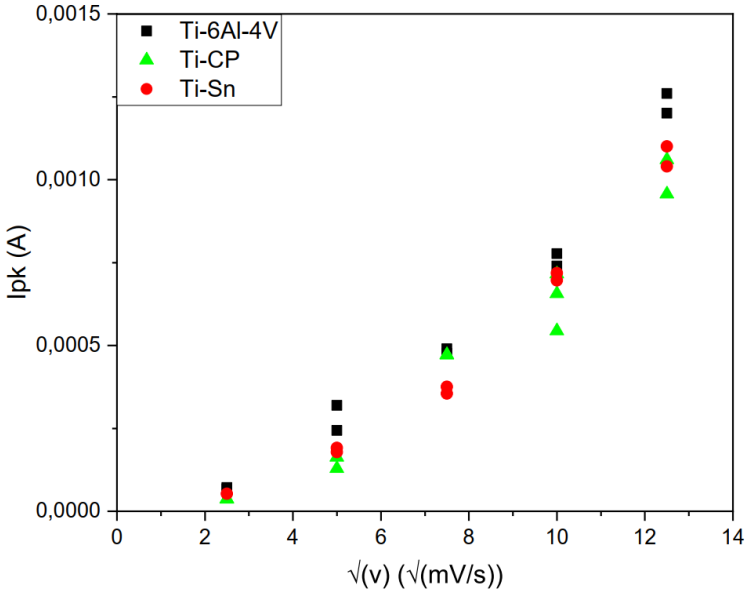

Figure 36: Results of the current vs the square root of the scan rates of the cyclic voltammetry experiments

In Figure 35 there is a line through the origin. Figure 36 does not show this trend, but a curve is present. This indication means that the process of the oxide layer is controlled by an electro-active field. If the process of the formation of the oxide layer were controlled, an inverse effect would occur. Then the graph of the current vs the scan rate would show a curve and the graph of the current vs the square root of the scan rate would show a straight line.

From these graphs we can conclude that the formation of the passivation layer is controlled by an electro-active field and not by diffusion. Electrochemistry is much slower than diffusion. This indicates that the electro-active field is the controlling factor for the formation of the passivation layer.

5.1.3 Impedance without the oxide-layer (before the thermal treatment)

To perform the impedance tests described in section 4.3.3, four different potential values are taken from the polarisation curve of each titanium alloy. The points chosen on the polarisation curve are shown below in Figure 38 for the Ti-6Al-4V alloy and in Figure 41 for the Ti-Sn alloy. The calculated values used to perform the impedance test are shown in Table 5. All these potential values were calculated versus an Ag/AgCl electrode.

Table 5: Potential values used when performing the impedance test

	OCP (V)	Potential peak (V)	Passivation potential (V)	$\frac{(OCP+Epeak)}{2}$ (V)
Ti-6Al-4V	-0,179	-0,416	-0,124	-0,297
TiCP	-0,016	-0,342	0,065	-0,179
Ti-Sn	-0,113	-0,472	-0,118	-0,293

The impedance test was not performed for the titanium alloy Ti-CP both with and without the oxide layer on the alloy. There were too few samples of this type of material, which would have required too much time. Therefore, performing the impedance test for Ti-CP would not be efficient. Priority was given to other tests in this thesis.

The reason why these different points on the polarisation curve were chosen is that all states of the passivation layer on this alloy are scanned. After these 4 potential points (shown in Table 5), it is possible to draw a picture of the behaviour of the passivation layer. An equilibrium state is present for the OCP value. This means that the potential on the surface is in a steady state. The potential peak is a potential where there is a lot of kinetic control over the passivation layer. This is not an equilibrium state. In this point there is a lot of electro-active chemistry. Another chosen point is the passivation potential, and this potential is a very stable value because it is chosen at a constant of the polarisation curve. The last chosen point, (OCP+Epeak)/2, is an intermediate point.

5.1.3.1 Ti-6Al-4V

Figure 37 shows the Nyquist diagram of the Ti-6Al-4V. The red curve shows the results of the OCP, the blue curve the peak potential, the green curve the passivation potential and the black curve the (OCP+peak)/2. Figure 38 shows the selected potential points on the polarisation curve.

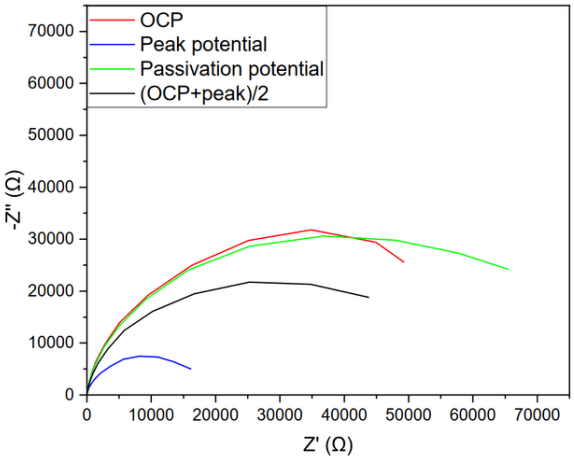

Figure 37: Nyquist diagram of Ti-6Al-4V without the oxide layer

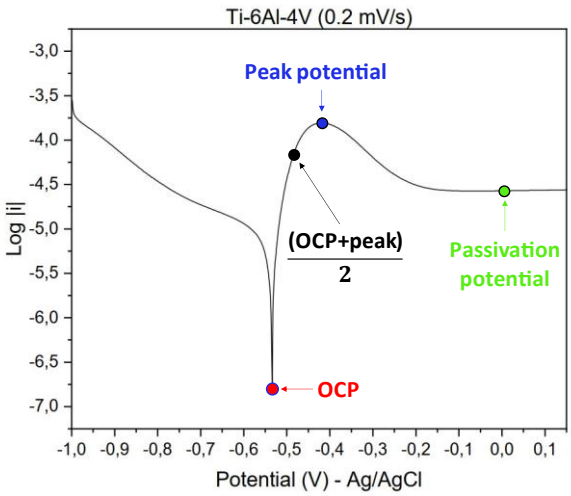

Figure 38: Polarisation curve of Ti-6Al-4V without the oxide layer with marked points used for the impedance test

Figure 39 shows the Bode diagrams of Ti-6Al-4V with on the left Z vs the frequency and on the right - Phase vs the frequency. The colour code for the different graphs is the same as mentioned above.

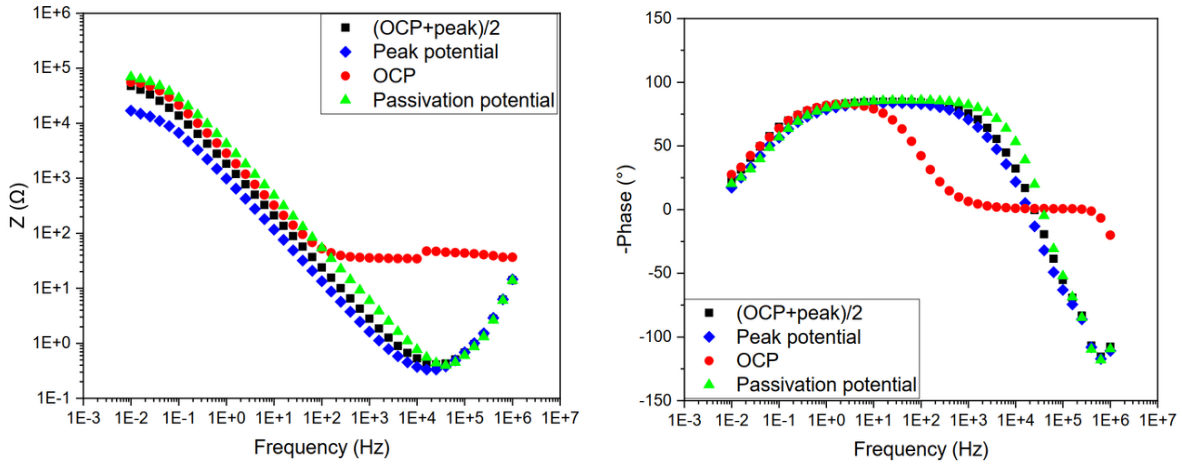

Figure 39: Bode diagrams of Ti-6Al-4V without the oxide layer with on the left Z vs frequency and on the right -Phase vs frequency

The graph of peak potential, passivation potential and (OCP+peak)/2 has a lower Z value as the frequency increases. This means that there is electrical transfer during this process. This is not the case for the value of the OCP. The graph shows a constant value, which means that no electron transfer takes place.

The Z-value of the peak potential, the passivation potential and the (OCP+peak)/2 increases again with increasing frequency after a decrease. This is dependent on the electrochemistry of the system. These Bode diagrams are shown in this thesis to provide additional information. Unfortunately, no concrete conclusion can be drawn from them. More experiments, information, and data are needed to give a clear analysis.

5.1.3.2 Ti-Sn

Figure 40 shows the Nyquist diagram of the Ti-Sn. The red curve shows the results of the OCP, the green curve the passivation potential and the black curve the (OCP+peak)/2. For the impedance test the experiments were not reproducible for the peak potential. That is why there are different experiments

Therefore, several experiments of the peak potential are shown in Figure 40 to show what the difference is and what it means in relation to each other and to the other selected potential points. So that this can be further investigated in later research. On Figure 40 the blue curve is the first experiment for the peak potential, the magenta curve the second experiment, the pink curve the third experiment and the yellow curve the fourth experiment. Figure 41 shows the selected potential points on the polarisation curve.

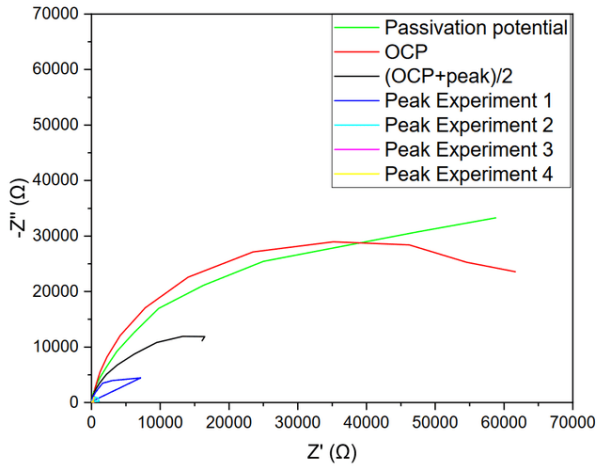

Figure 40: Nyquist diagram of Ti-Sn without the oxide layer

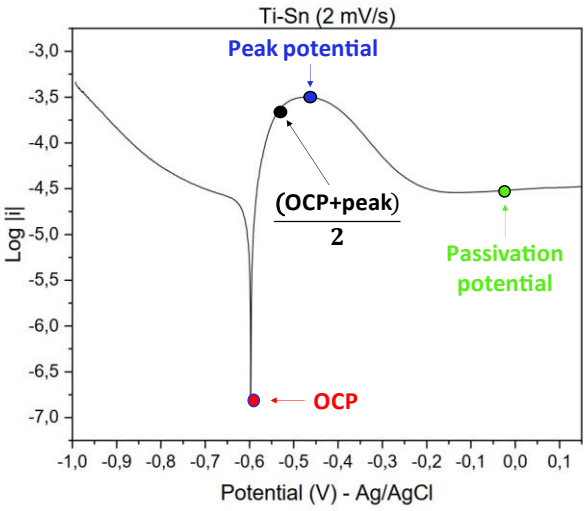

Figure 41: Polarisation curve of Ti-Sn without the oxide layer with marked points used for the impedance test

In Figure 40 the results of the peak potential are very small and almost not visible compared to the other 3 chosen potential points.

As the comparison of the different experiments is not possible with the Nyquist diagram, a switch is made to the Bode diagrams of Ti-Sn. Figure 42 shows the Bode diagrams of Ti-6Al-4V with on the left Z vs the frequency and on the right -Phase vs the frequency. The colour code for the different graphs is the same as mentioned above.

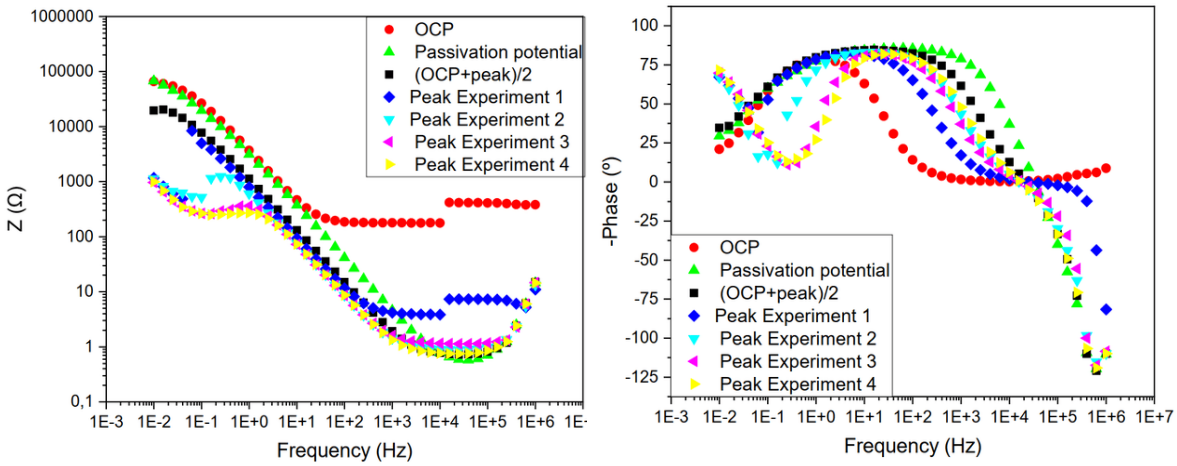

Figure 42: Bode diagrams of Ti-Sn without the oxide layer with on the left Z vs frequency and on the right -Phase vs frequency

Figure 42 shows all experiments that have been carried out. These results give a good overview of the whole process, but it is difficult to distinguish between the curves. Therefore, the different experiments are split up in the following figures: Figure 43 shows the curves of the OCP, passivation potential and (OCP+peak)/2 and Figure 44 the different experiments of the peak potential. The colour codes for the different curves remain the same as mentioned above.

Noteworthy in Figure 42 is that the curves converge at certain points, such as in the range 1E+4 Hz and 1E+5 Hz, 1E+0 Hz and 1E-1 Hz and 1E-2 Hz. The correct explanation for this is not clear. For this, more data and analysis should be done.

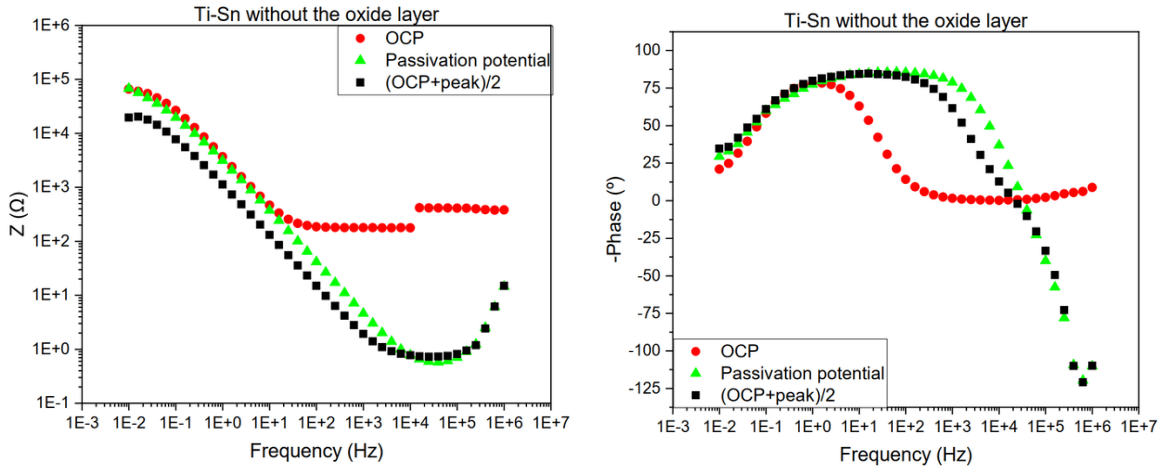

Figure 43: Bode diagrams of Ti-Sn without the oxide layer with on the left Z vs frequency and on the right -Phase vs frequency and consisting of the experiments for OCP, the passivation potential and (OCP+peak)/2

The curves in Figure 43 show a similar correlation to the results of Ti-6Al-4V. These curves are reproducible and are in a stable zone. Again, it can be seen that the OCP value shows a constant as in the results for Ti-6Al-4V. This indicates that there is little electron transfer at this chosen point.

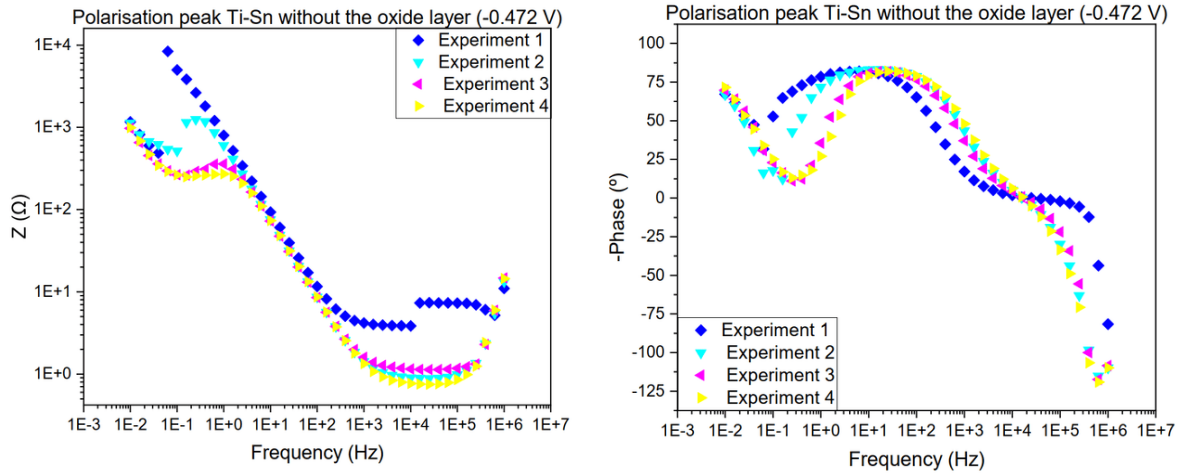

Figure 44: Bode diagrams of Ti-Sn without the oxide layer with on the left Z vs frequency and on the right -Phase vs frequency and consisting of the various experiments for the peak potential

Figure 44 shows the results of the peak potential at a value of -0.472 V. The results vary a lot, which is why no clear result can be given. This is because the peak potential is in a meta-stable range. In contrast to the OCP value and the passivation potential, the point of the peak potential can vary greatly. It is not in an equilibrium state. Various analysis techniques are required to investigate this point further. Due to the lack of time, this was not possible in this thesis. Besides the other analysis techniques, more experiments and data are also required.

5.2 Thermal treatment of the titanium alloys

5.2.1 Condition of thermal treatment

For the thermal treatment of the titanium alloys, Ti-6Al-4V, Ti-Sn and Ti-CP, experiments are performed at different flow rates. The different experiments that were done are summarised in Table 6. The flow rates that were chosen are 0.3; 0.5 and 1.0 l/min based on previous research done at the university. Also, attention was paid to where the samples were placed in the reactor. Per series that was performed, 3 samples were placed in the reactor. This can be seen in Figure 45.

Table 6: Experimental data from the thermal treatment for the formation of the nanospikes

	Flowrate (l/min)	Position in the reactor	Reproduced	Appendix
Ti-6Al-4V	0.3	End	Yes	V
	0.5	Begin	Yes	VI
	0.5	End	Yes	VII
	1.0	Begin	No	VIII
	1.0	Middle	No	IX
	1.0	End	No	X
Ti-Sn	0.3	Begin	Yes	XI
	0.5	Middle	Yes	XII
Ti-CP	0.3	Middle	Yes	XIII

Figure 45: Example of how the samples were placed in the reactor (0.3 l/min with Ti-Sn on the left, Ti-CP in the middle and Ti-6Al-4V on the right)

The experiments were checked for reproducibility. Only the series of 1 l/min of Ti-6Al-4V alloy was not performed a second time due to time constraints.

Ti-CP was only performed at a flow rate of 0.3 l/min and Ti-Sn only at 0.3 and 0.5 l/min for the simple reason that only 1 sample was available from Ti-CP and 2 samples from Ti-Sn.

5.2.2 Morphology study by SEM of treated alloys

For the SEM test, the intention was to use the same magnifications to examine the nanospikes, namely 1k, 5k, 15k and 30k. However, this will not always be the case and sometimes other magnifications will be used or one magnification will be missing. At the beginning of the study, it was not yet clear which magnifications could best be chosen. Unfortunately, the tests could not be resumed because there was no time left to do so. All the results of the SEM test are given in Appendix V to XIII. Which series of experiments belongs to which alloy with the corresponding parameter is listed in Table 6.

5.2.2.1 Reproducibility of the oxide layer

For the reproducibility of the experiments, attention is paid to the density of the nanospikes and how the nanospikes look, the morphology. In Figure 46 we see nanospikes of the Ti-6Al-4V alloy at a flow rate of 0.5 l/min. For both the first and the second test we see the same sharp nanospikes. In the first test, the density seems to be a bit less than in the second test, but this is not significant enough. It can therefore be concluded that this test is reproducible.

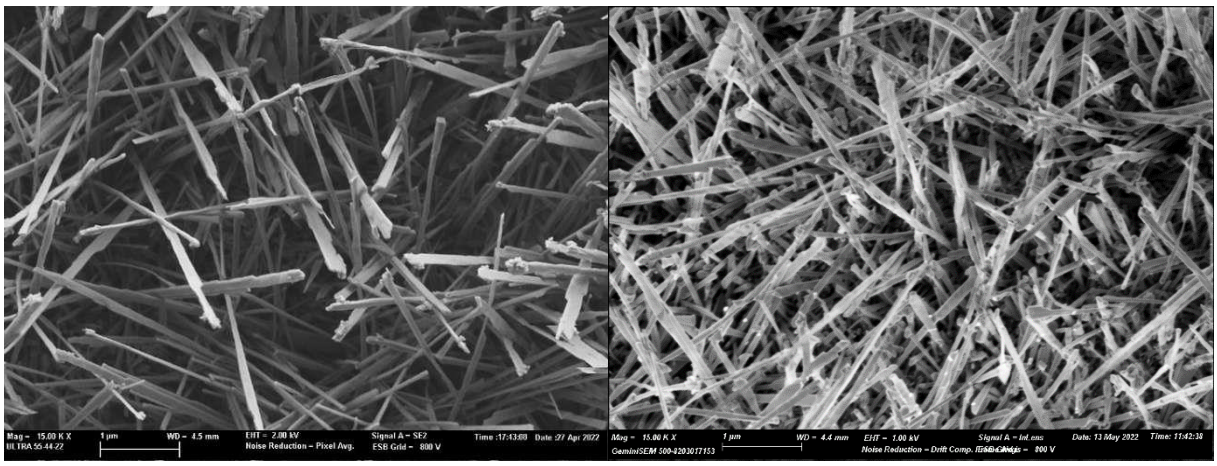

Figure 46: SEM results of Ti-6Al-4V of flow rate 0.5 l/min, position beginning with both a magnification of 15k x with left series 1 and right series 2

This is one example of the many others that are listed in Appendix V to XIII. It is concluded that the remaining experiments performed have a proper reproducibility.

The 2 exceptions are the results of series 2 with flow rate 0.3 l/min of Ti-Sn and Ti-CP. Figure 47 shows the comparison of series 1 (with 25k x magnification) and series 2 (with 15k x magnification) of Ti-Sn alloy. The figure shows that the density of the nanospikes in series 2 is very low compared to series 1. However, the morphology is similar between the two series.

Figure 48 shows the comparison between series 1 and 2 for the Ti-CP alloy with a flow rate of 0.3 l/min and both have a magnification of 15k x. The density is very low and the substrate of the alloy can be seen. The morphology has the same shape but in series 2 some differences can be noticed like the formation of plates and more bar-shaped peaks.

These two exceptions to reproducibility come from the same batch. A possible explanation is that something went wrong during the formation of the nanospikes in the reactor. More tests and data are needed to clarify this.

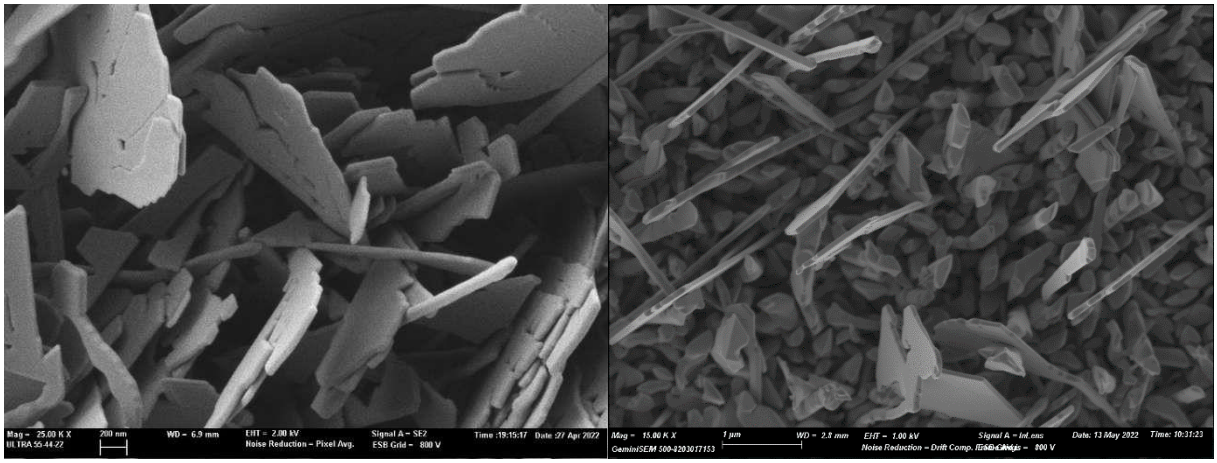

Figure 47: SEM results of Ti-Sn of flow rate 0.3 l/min with on the left series 1 and a magnification of 25k x and on the right series 2 with a magnification of 15k x

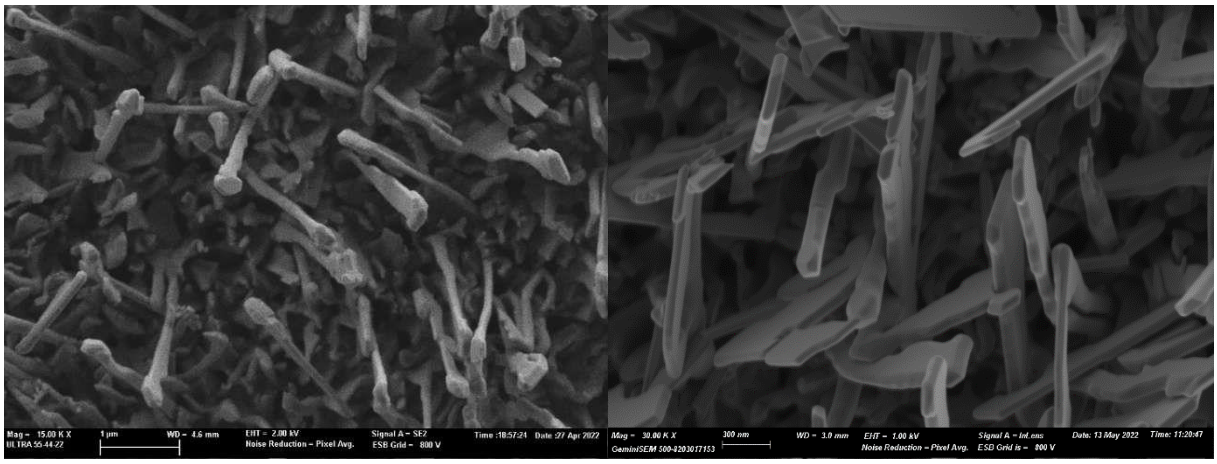

Figure 48: SEM results of Ti-CP with flow rate 0.3 l/min both with 15k x magnification and on the left series 1 and on the right series 2

5.2.2.2 The shape of nanospikes in different alloys

The difference in shape of nanospikes of the alloys is discussed in this section. Figure 49 shows the nanospikes of the Ti-6Al-4V alloy at a flow rate of 0.3 l/min. The top figure has a general view at 5k x magnification and the bottom figure a detail view at 30k x magnification. The figure shows needle-shaped nanospikes. The direction of the nanospikes is homogeneous in different zones. There is no uniform surface where all the nanospikes are oriented in exactly the same direction. The density of these nanospikes is high. In the figure, the alloy substrate is hardly visible. This is certainly desirable as the purpose of these nanospikes is to prevent bacterial growth on the alloy.

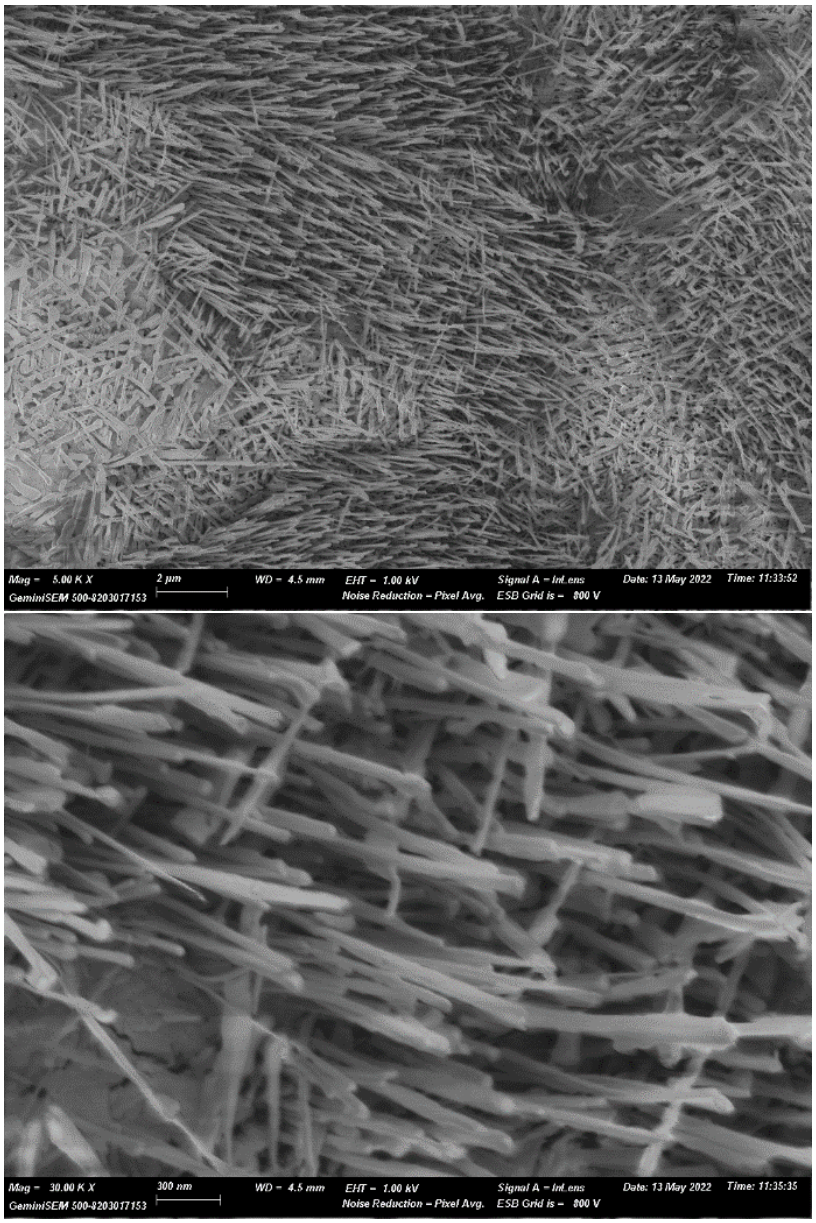

Figure 49: SEM results of Ti-6Al-4V from series 2 with a flow rate of 0.3 l/min: at the top a magnification of 5k x and a magnification of 30k x at the bottom (Appendix V)

Figure 50 shows the SEM result of the Ti-Sn alloy at a flow rate of 0.3 l/min with the top figure at 5k x magnification and the bottom figure at 25k x magnification. The figures show triangular shaped plates. In some zones, these plates are oriented in the same direction, but there is no general direction of the growth of these nano-flakes. Sometimes there are also nanospikes between the flakes but these nanospikes occur very infrequently so the nanoflakes are the predominant form in the morphology of the oxide layer. The density of these flakes is also very high, so that the surface of the alloy cannot be seen. If one compares the morphology with that of Ti-6Al-4V, there is a big difference. There, only needle-shaped nanospikes are visible, whereas in the case of Ti-Sn, only nanoflakes are visible. More research is needed to explain this observation furthermore.

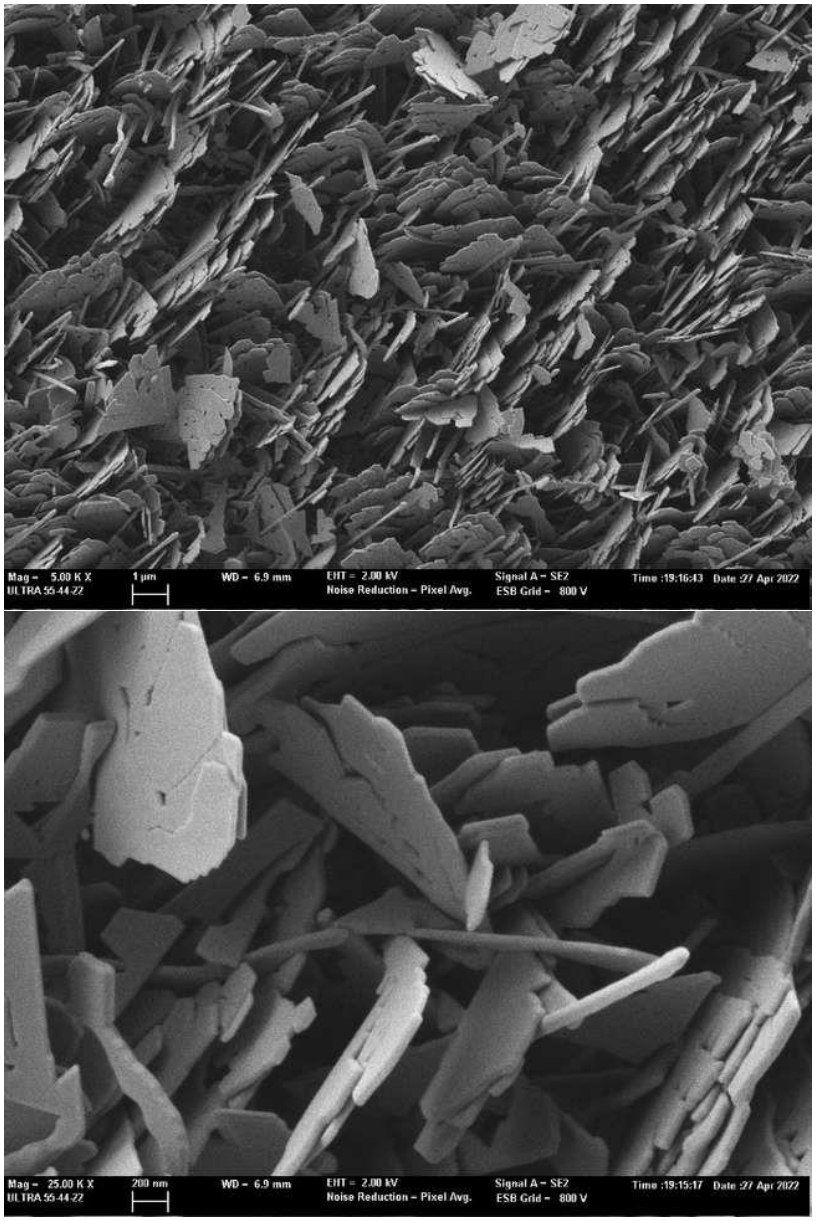

Figure 50: SEM results of Ti-Sn from series 1 with a flow rate of 0.3 l/min: at the top a magnification of 5k x and a magnification of 25k x at the bottom (Appendix XI)

Figure 51 shows the SEM result of the Ti-CP alloy at a flow rate of 0.3 l/min with the top figure at 3.5k x magnification and the bottom figure at 30k x magnification. As with the Ti-6Al-4V alloy, the figures show elongated nanospikes. The difference with Ti-6Al-4V is that here there is no needle-shaped structure. A crystal like structure is present at the end of the nanospike. The density is less than in Ti-6Al-4V. In some areas of the figure the surface of the alloy can be seen.

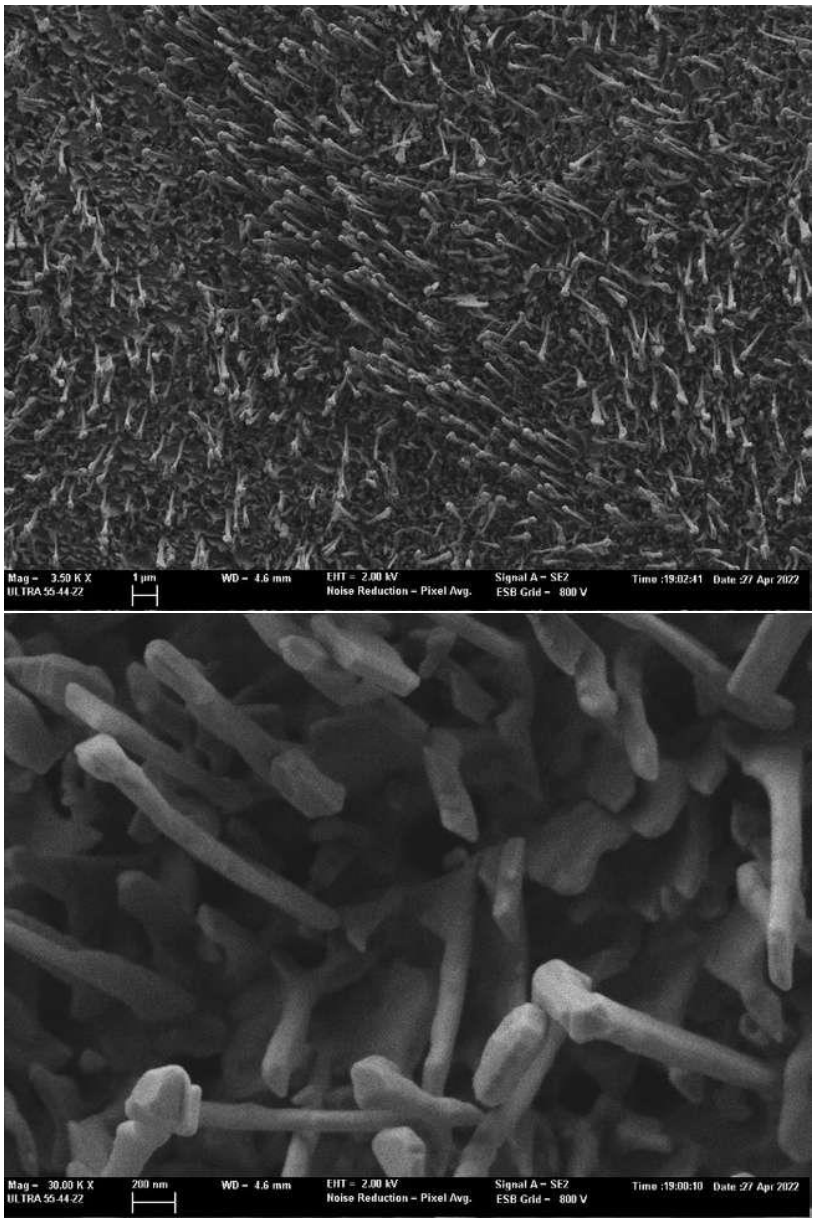

Figure 51: SEM results of Ti-CP from series 1 with a flow rate of 0.3 l/min: at the top a magnification of 3.5k x and a magnification of 30k x at the bottom (Appendix XIII)

5.2.2.3 The different flow rates

In this thesis there are different flow rates used, namely 0.3 l/min; 0.5 l/min and 1.0 l/min. The results of the Ti-6Al-4V alloy are used to investigate this comparison of flow rates. Because there were not enough samples of the other alloys present in the lab, the different flow rates could not be performed for Ti-Sn and Ti-CP.

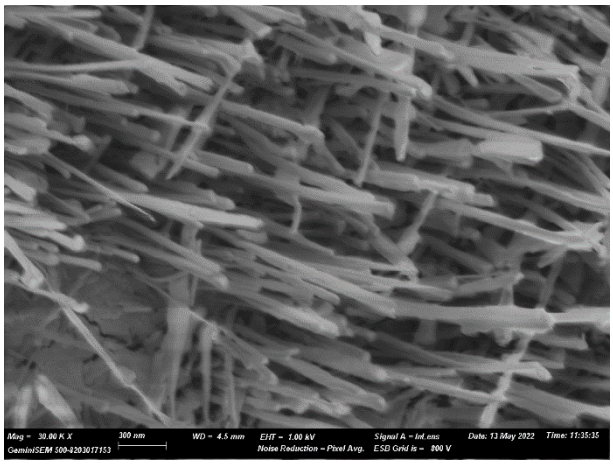

Figure 52: SEM results of Ti-6Al-4V from series 2 with a flow rate of 0.3 l/min and a magnification of 30k x (Appendix V)

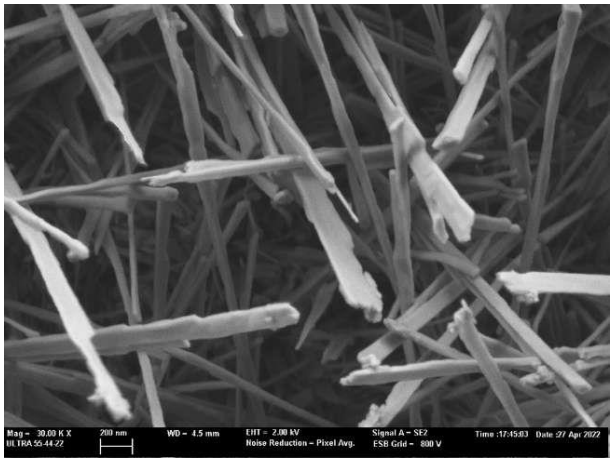

Figure 53: SEM results of Ti-6Al-4V from series 1 (position: beginning) with a flow rate of 0.5 l/min and a magnification of 30k x (Appendix VI)

Figure 52 shows the SEM result with flow rate 0.3 l/min, Figure 53 the SEM result with flow rate 0.5 l/min and Figure 54 the SEM result of 0.1 l/min. All figures belong to the alloy Ti-6Al-4V.

By using the legend and the scale on the figures, an attempt was made to calculate the width of the nanospikes. The results were as follows: the nanospikes on Figure 52 have a width of approximately 112 nm, the nanospikes on Figure 53 have a width of 148 nm and the nanospikes on Figure 54 have a width of 130 nm.

Based on these data, it can be concluded that the flow rate does not have a major influence on the size of the nanospikes in Ti-6Al-4V. This is contradictory to the conclusion of the research done earlier on this subject. More research is needed to give a more definitive answer on the influence of the flow rate.

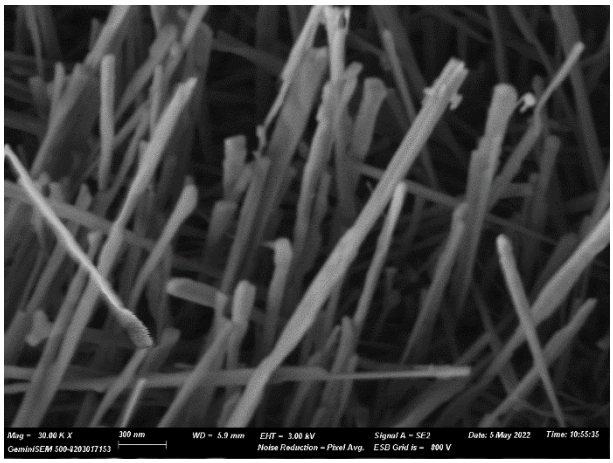

Figure 54: SEM results of Ti-6Al-4V (position: middle) with a flow rate of 1.0 l/min and a magnification of 30k x (Appendix IX)

5.2.2.4 The position in the reactor

The position in the reactor can also be an important factor, as can be seen in Figure 55. If the samples are placed too close to the beginning of the reactor, the nanospikes are not formed properly. This can be seen by the black colour that the sample still has after the experiment. A possible explanation for this could be that the oxidation process does not continue sufficiently. Since the black colour originates from the Ti-C. From the visual observations in the figure below, it is therefore important that the samples are not placed too close to the ends of the reactor and especially not too close to the beginning in order to allow the oxidation process to proceed sufficiently.

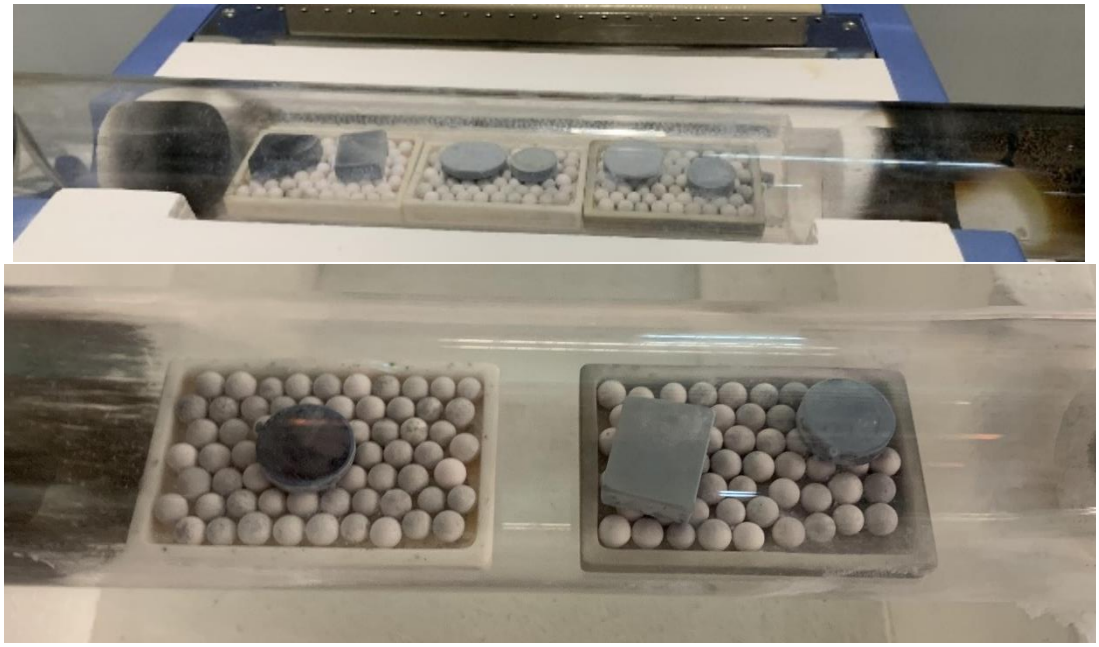

Figure 55: Results of Ti-6Al-4V alloys after heat treatment

In figures 56 to 58, are the SEM results for Ti-6Al-4V with a flow rate of 1.0 l/min. All three figures have a magnification of 15k x. This series was chosen because it is the only series with 3 identical materials in the reactor. The densities of the samples in the middle and at the end of the reactor are similar but the density of the sample at the beginning of the reactor is not so high. Here the surface of the substrate is still visible. The morphology of the sample placed at the beginning of the reactor is also different from the other two samples. The nanospikes in this sample are much finer than in the samples in the middle or at the end of the reactor.

From this it can be concluded that the result of the formation of the nanospikes at the beginning of the reactor is different than in the middle or at the end. The formation of the nanospikes in the middle or at the end of the reactor are very similar. From this it can be assumed that it is better to place the samples more in the direction of the middle and the end than in the beginning.

However, this conclusion is taken from one series and is therefore not very concrete. More research is needed to establish a certain conclusion.

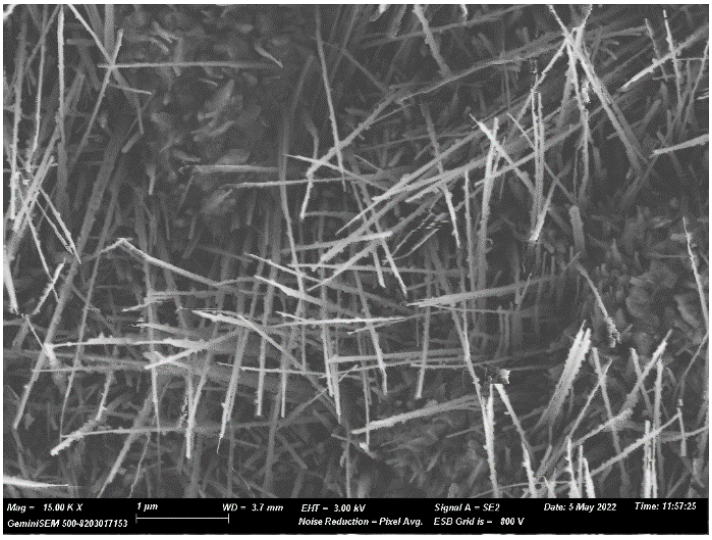

Figure 56: SEM results of Ti-6Al-4V (position: beginning) with a flow rate of 1.0 l/min and a magnification of 15k x (Appendix VIII)

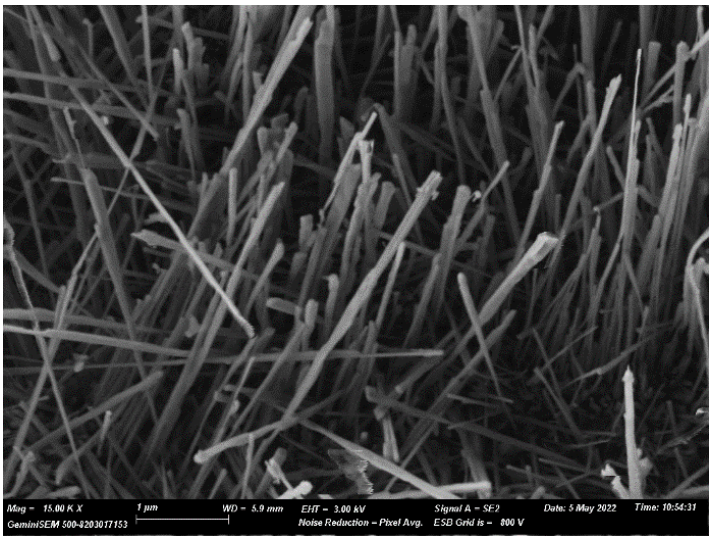

Figure 57: SEM results of Ti-6Al-4V (position: middle) with a flow rate of 1.0 l/min and a magnification of 15k x (Appendix IX)

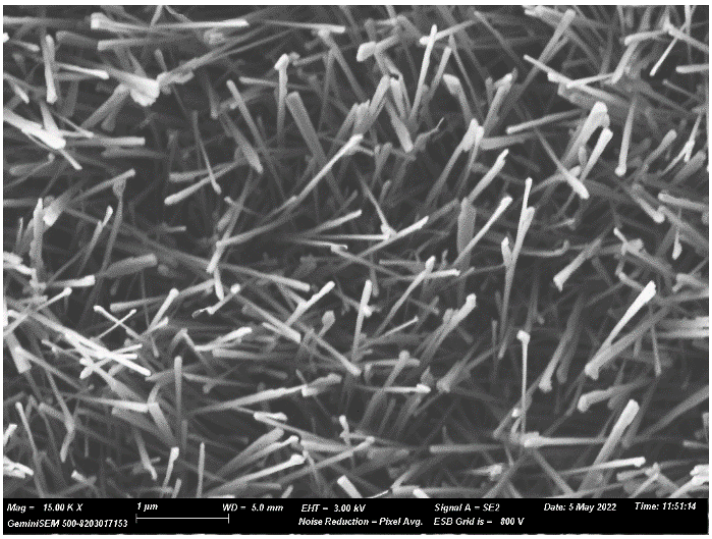

Figure 58: SEM results of Ti-6Al-4V (position: end) with a flow rate of 1.0 l/min and a magnification of 15k x (Appendix X)

5.2.3 EDS-test

Figure 59 shows the result of the EDS result for the alloy Ti-6Al-4V with flow rate 0.5 l/min. The legend on the figure shows that the percentage of the measured zone consists of 57.4% Ti; 37.2% O; Al 3.5% and 1.9% V. This result is in line with expectations, since the alloy under investigation initially has 6% Aluminium and 4% Vanadium in its composition. The measured larger amount of oxygen originates from the oxide layer. The question that arises here is whether the measurement of Aluminium and Vanadium originates from the substrate of the alloy or is also present in the formed nanospikes. To answer this question, the composition of a single nanospike must be examined. This is possible with the TEM test.

The spectrum shows that the peak of oxygen is twice as large as the peak of titanium immediately to the left of the oxygen peak. This is in line with expectations, since these 2 peaks belong to the generated nanospikes consisting of TiO_2. This also indicates that the thermal oxidation was carried out successfully.

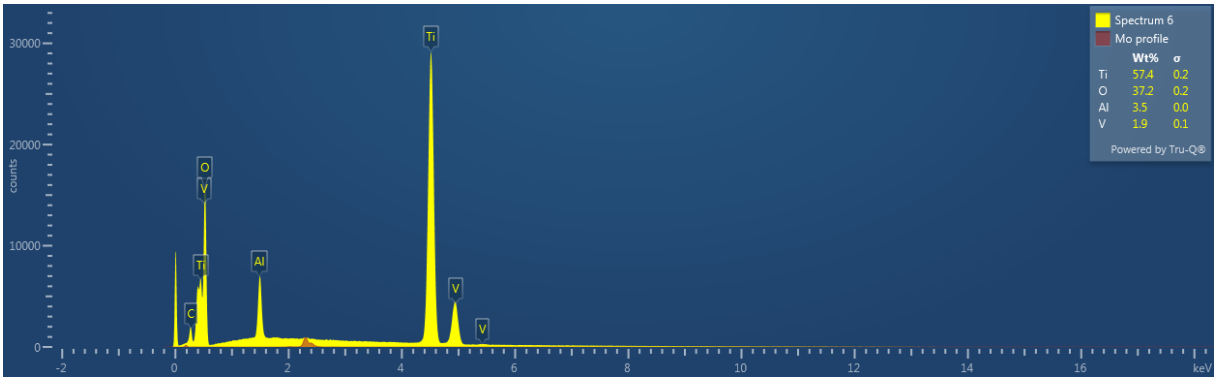

Figure 59: Test result EDS test: spectrum for Ti-6Al-4V with flow rate 0.5 l/min

Figure 60 shows the result of the EDS result for the alloy Ti-Sn with flow rate 0.5 l/min. The legend on the figure shows that the percentage of the measured zone consists of 60.6% Ti; 39.0% O and 0.4% Sn. The amount of tin that was calculated is so small that it can be considered negligible. Thus, the investigated zone consists mainly of titanium and oxygen. The same observations are made for TiSn as for Ti-6A-4V. Again, the peak of oxygen is twice as large as the peak of titanium immediately to the left of that of oxygen. This indicates that nanospike with TiO_2 were successfully performed.

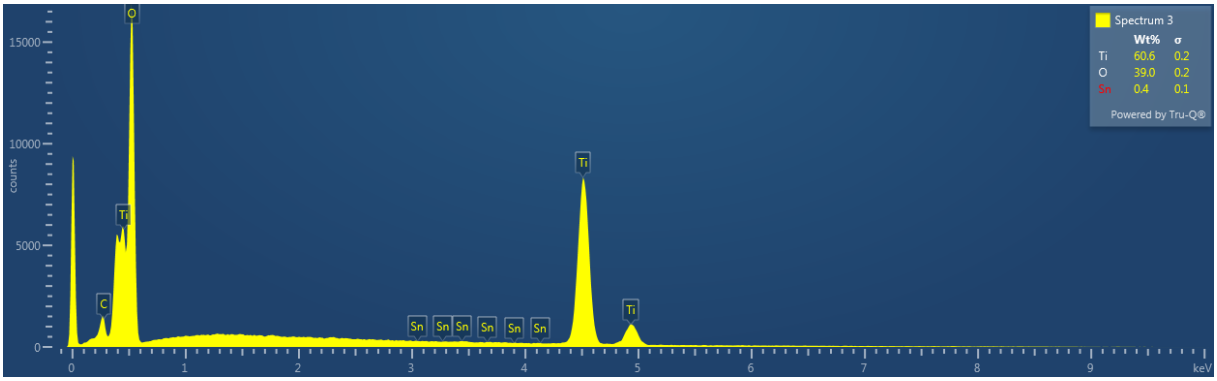

Figure 60: Test result EDS-test: spectrum for Ti-Sn with flow rate 0.5 l/min

For the Ti-CP alloy no spectrum of the EDS test was prepared due to lack of time. Since this alloy consists only of titanium it is assumed that no other elements other than titanium and oxygen would occur. Therefore, priority was given to other analyses.

5.2.4 TEM-rest

Figure 61 shows the result of the TEM test of the Ti-6Al-4V alloy with a flow rate of 1.0 l/min. In this figure a nanospike can be seen. Based on the scale on the figure, an attempt was made to measure the width of the nanospike. The possible width is 105 nm.

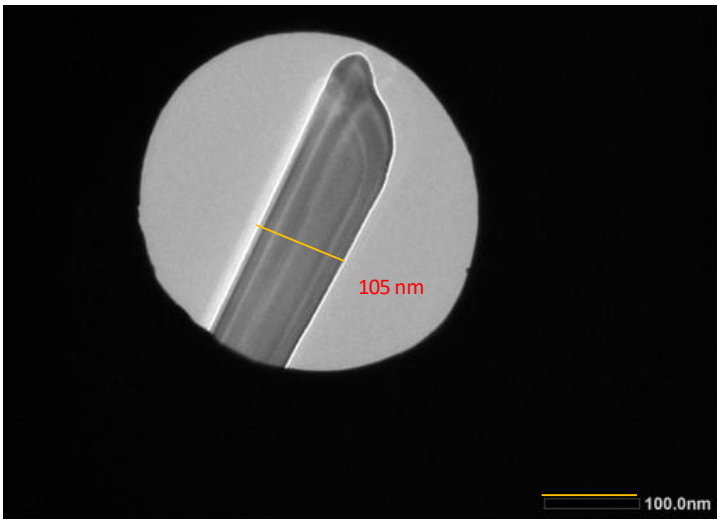

Figure 61: TEM test result of Ti-6Al-4V with flow rate 1.0 l/min position middle

Figure 62 shows the corresponding spectrum of the TEM test of Figure 61. The spectrum shows that, when measuring the nanospike, 37.0% Cu, 31.8% Ti, 28.6% O, 2.0% C and 0.6% Al are found. It is notable that a percentage of copper is measured. This can be explained by the analysis technique that was used. The surface of the alloy was scraped off and placed in a small mask. This mask is made up of a copper grid. During the analysis, this copper grid is also measured, which causes a measurement error. The two other elements that also stand out are aluminium and carbon. The aluminium may originate from the substrate of the Ti-6Al-4V because this alloy initially contains 6% Al. The carbon may explain that part of the Ti-C is not oxidised and thus carbon is measured.

These possible explanations need to be investigated further to make sure that this is indeed the case.

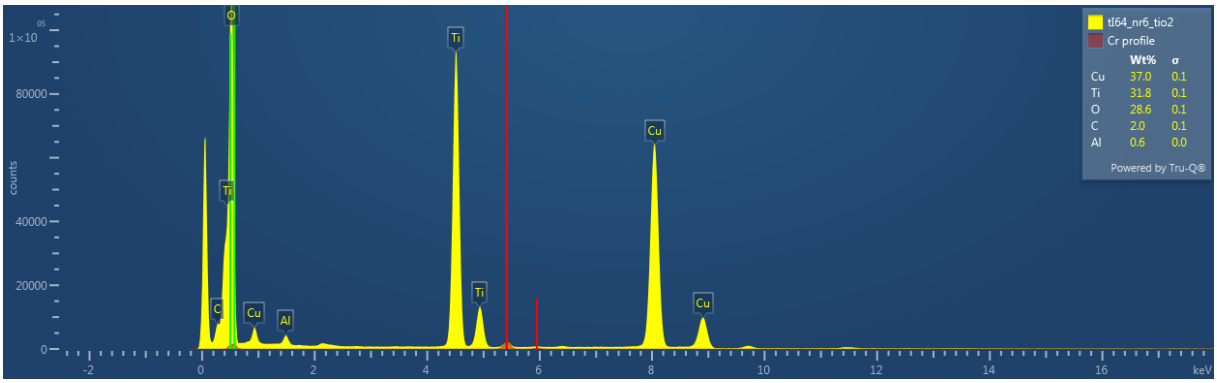

Figure 62: Test result TEM-test: spectrum for Ti-6Al-4V with flow rate 1.0 l/min

Figure 63 shows the result of the TEM test of the Ti-Sn alloy with a flow rate of 0.3 l/min. This figure shows several frame segments that were scraped off the sample. In the figure, an attempt was made to measure the width of a nanospike and a nanoflake using the scale. The possible width of the nanospike is 105 nm and of the nanoflake 397 nm.

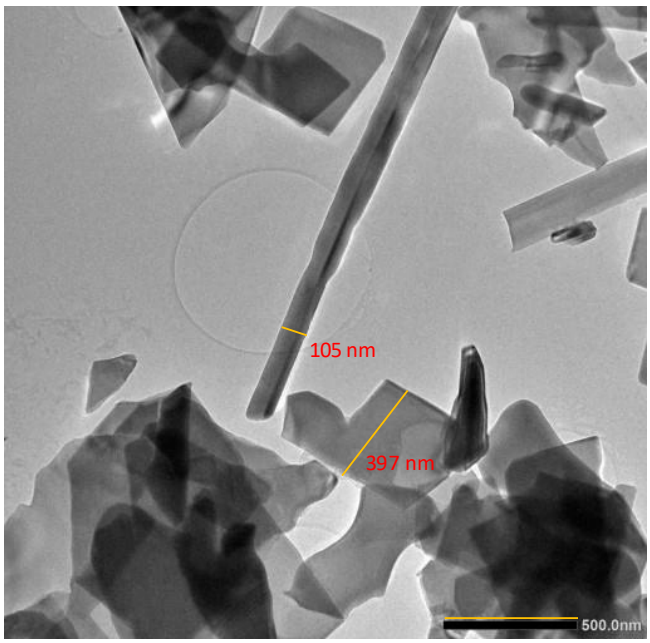

Figure 63: TEM test result of Ti-Sn with flow rate 0.3 l/min position beginning

Figure 64 shows the corresponding spectrum of the TEM test of Figure 63. The spectrum indicates that at the measurement of the nanospike 68.3% Ti, 32.2% O, 1.6% Na and 0.9% Cl are found. It is notable that the TEM gives a measurement of a small amount of sodium and chloride. These components are classified as contamination. However, the quantities are very small, so that they can be considered negligible.

The quantities of titanium and oxygen are in line with the expected values.

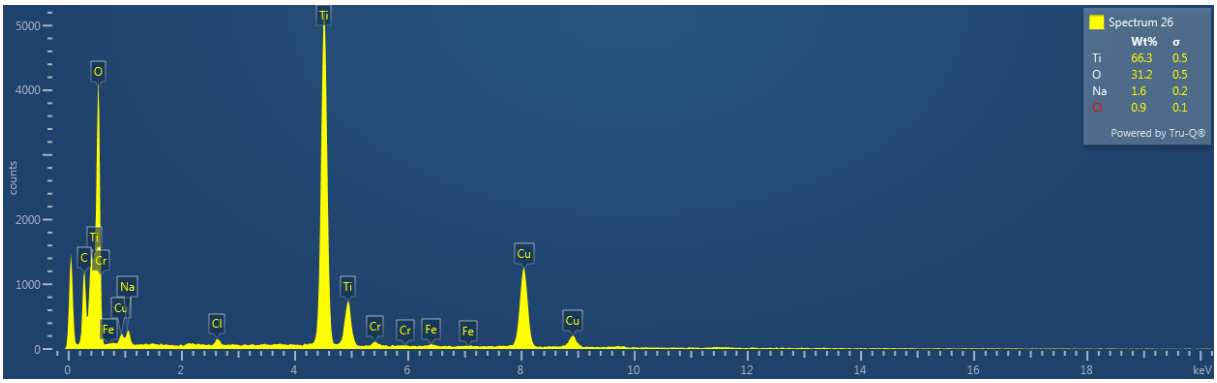

Figure 64: Test result TEM-test: spectrum for Ti-Sn with flow rate 0.3 l/min

Figure 65 shows the result of the TEM test of the Ti-CP alloy with a flow rate of 0.3 l/min. In this figure a nanospike can be seen. An attempt was made to measure the width of the nanospike using the scale. The possible width of the nanospike is 97 nm.

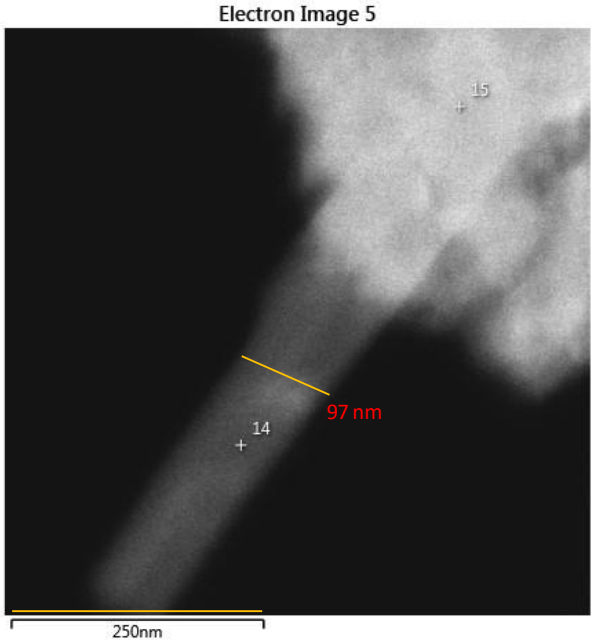

Figure 65: TEM test result of Ti-CP with flow rate 0.3 l/min position middle

Figure 66 shows the corresponding spectrum of the TEM test of Figure 65. The spectrum shows that only titanium is found in the measurement of the nanospike, namely 100X. On the spectrum there are again some peaks present of copper as previously seen with Ti-6Al-4V. The result of the 100% Ti is in line with expectations because the Ti-CP consists only of titanium.

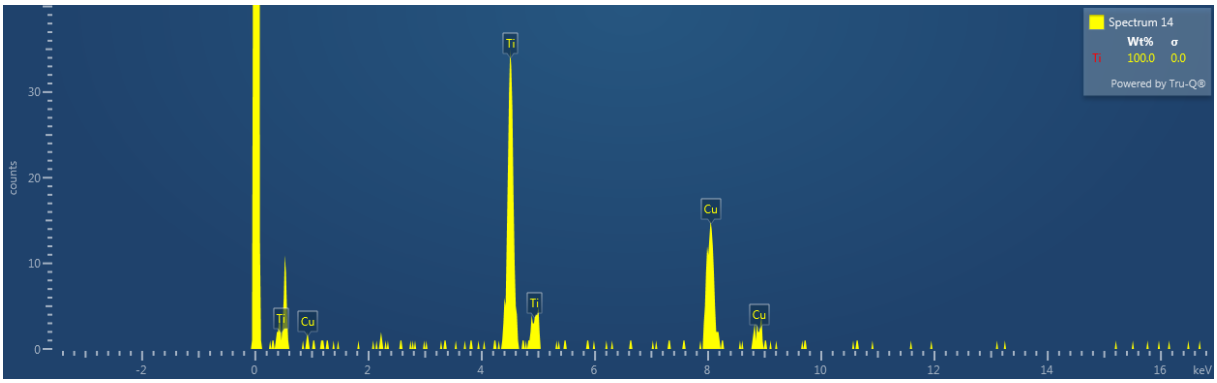

Figure 66: Test result TEM-test: spectrum for Ti-CP with flow rate 0.3 l/min

5.2.5 Impedance with the oxide-layer and the comparison with the impedance without the oxide layer

These experiments for the impedance with the oxide layer were performed with the same potential values of the polarisation curve that were used in the experiments for the impedance without the oxide layer. These values are listed in Table 7.

Table 7: Potential values used when performing the impedance test

	OCP (V)	Potential peak (V)	Passivation potential (V)	$\frac{(OCP+Epeak)}{2}$ (V)
Ti-6Al-4V	-0,179	-0,416	-0,124	-0,297
TiCP	-0,016	-0,342	0,065	-0,179
Ti-Sn	-0,113	-0,472	-0,118	-0,293

In an ideal scenario, the experiments would first be carried out to produce the polarisation curves for the alloys with the oxide layer, as was done for the alloys without the oxide layer. Unfortunately, this was not possible due to lack of time.

5.2.5.1 Ti-6Al-4V

Figure 67 shows the Nyquist diagram of the Ti-6Al-4V. The red curve shows the results of the OCP and the green curve shows the passivation potential. For the peak potential, 2 experiments were performed, experiment 1 depicted as the blue curve and experiment 2 depicted as the magenta curve.

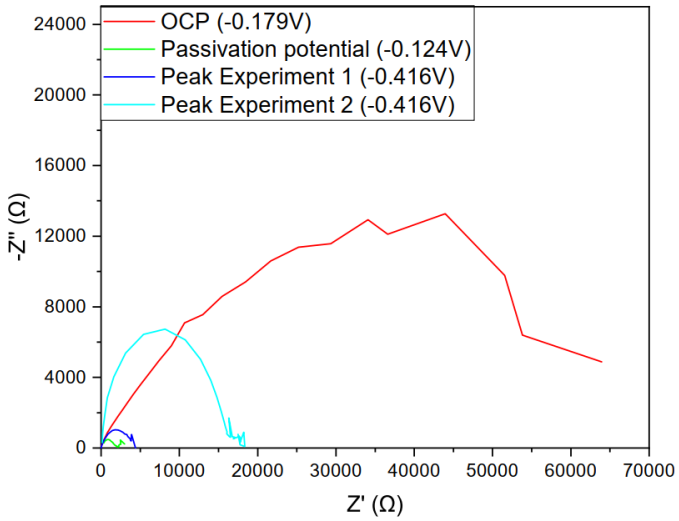

Figure 67: Nyquist diagram of Ti-6Al-4V with the oxide layer

Figure 68 shows the Bode diagrams of Ti-6Al-4V with the oxide layer: the graph on the left shows Z vs the frequency and on the right -Phase vs the frequency. The colour code for the different graphs is the same as mentioned above.

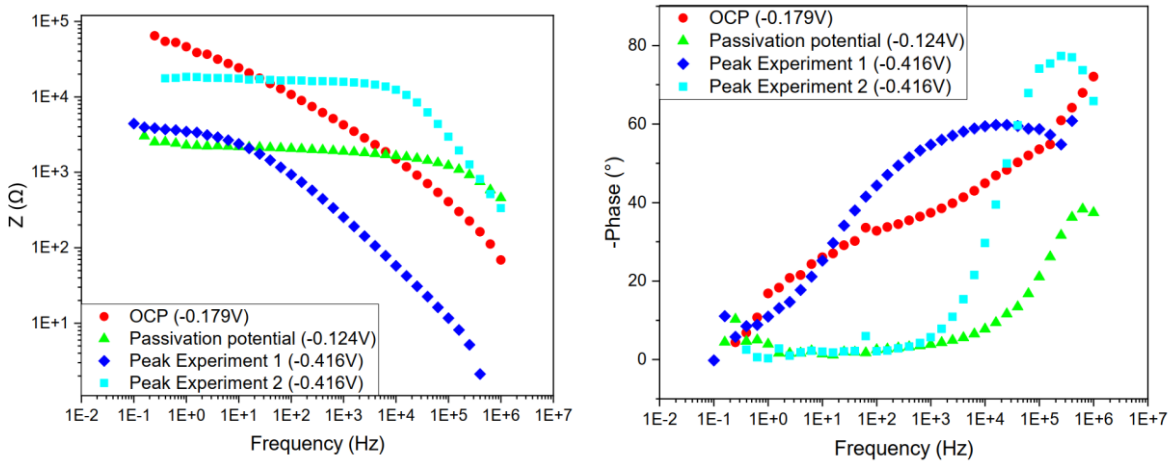

Figure 68: Bode diagrams of Ti-6Al-4V with the oxide layer with on the left Z vs frequency and on the right -Phase vs frequency

Figure 69 shows the curves of the results of the impedance test of the alloy Ti-6Al-4V without the oxide layer (black squares) against the results of the test with the oxide layer (red circles). The results are plotted individually to give a better overview. Top left are the results of the passivation potential, top right are the results of the peak potential and bottom right are the results of the OCP.

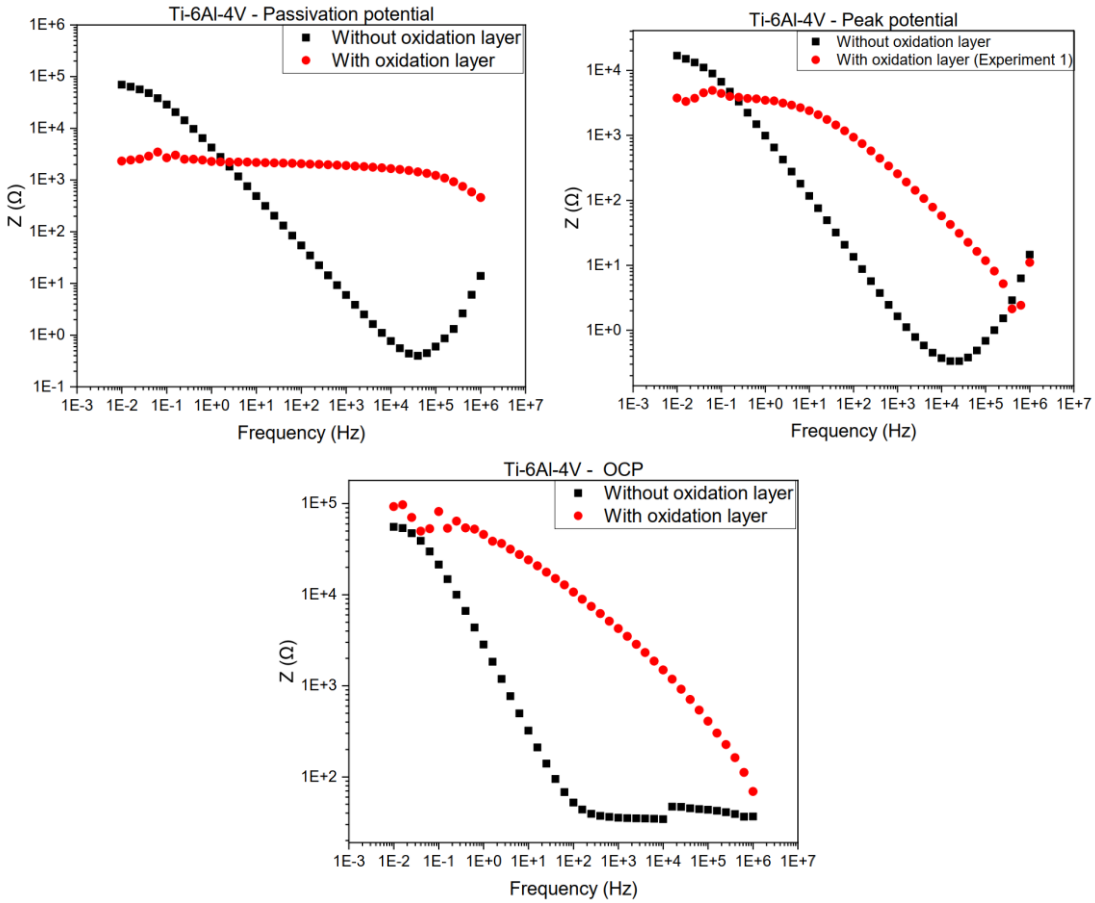

Figure 69: Bode diagrams with Z vs frequency for all results of Ti-6Al-4V with and without the oxide layer

For the point (OCP+peak)/2 no experiment was performed for the alloy with the oxide layer. An additional experiment was chosen for the peak potential.

In the different graphs it can be seen that the curves of the experiments with the oxide layer have a higher Z value over the frequency range than the curves of the experiments without the oxide layer. This means that the alloys with the oxide layer are better protected against corrosion. To provide more information on these curves and the difference between the samples with and without the oxide film, other analytical techniques and more data are required.

5.2.5.2 Ti-Sn

For the Nyquist diagram, the values were very inconclusive for Ti-Sn so it was decided not to show them here and to continue with the Bode diagrams. These are shown in Figure 70. These figures show the results of the impedance test for the Ti-Sn alloy with the oxide layer with on the left the Z vs the frequency and on the right the -Phase vs the frequency. The black squares are the results of the (OCP+peak)/2, the red circles of the OCP, the green triangles of the passivation potential and the blue diamonds of the peak potential.

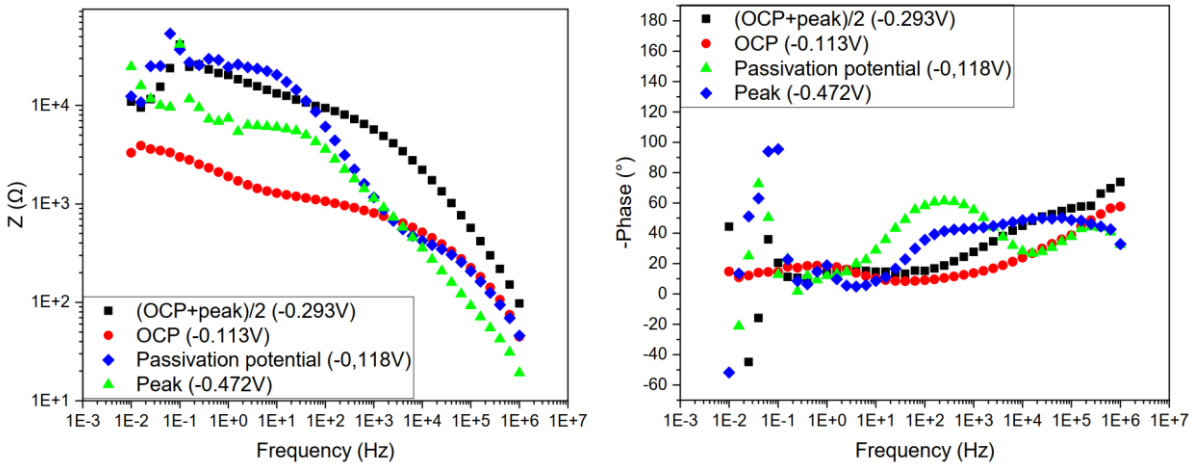

Figure 70: Bode diagrams of Ti-Sn with the oxide layer with on the left Z vs frequency and on the right -Phase vs frequency

In Figure 70, the values are very fluctuating at low frequency. This can be clearly seen in the graph on the right. The right graph also shows that the passivation potential and peak potential in the middle of the graph show an optimum, while the other graphs maintain a relatively constant behaviour. To further explain these observations, more research is needed with other analysis techniques and above all more data.

Figure 71 shows the curves of the results of the impedance test of the alloy Ti-Sn without the oxide layer (red circles) against the results of the test with the oxide layer (black squares). The results are plotted individually to give a better overview. Top left are the results of peak potential, top right are the results of the (OCP+peak)/2, bottom left are the results of the OCP and bottom right are the results of the passivation potential.

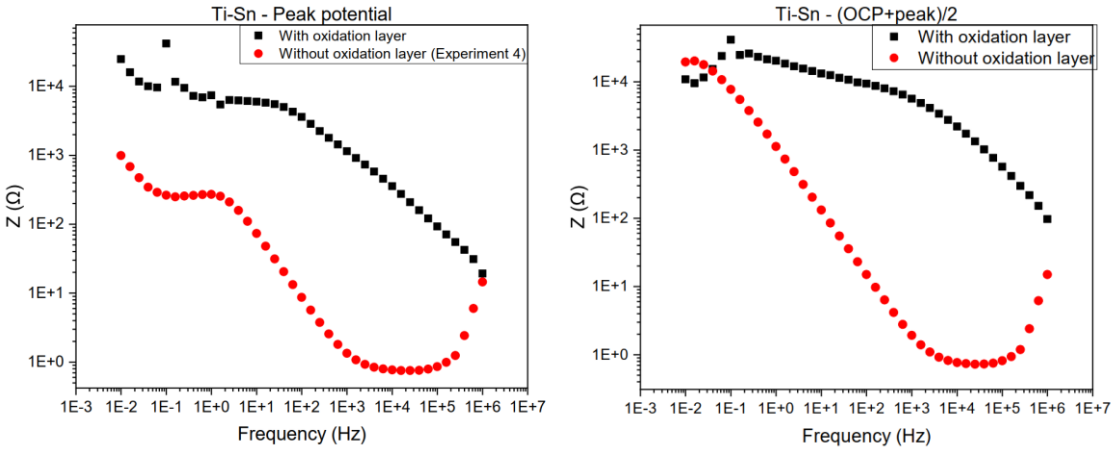

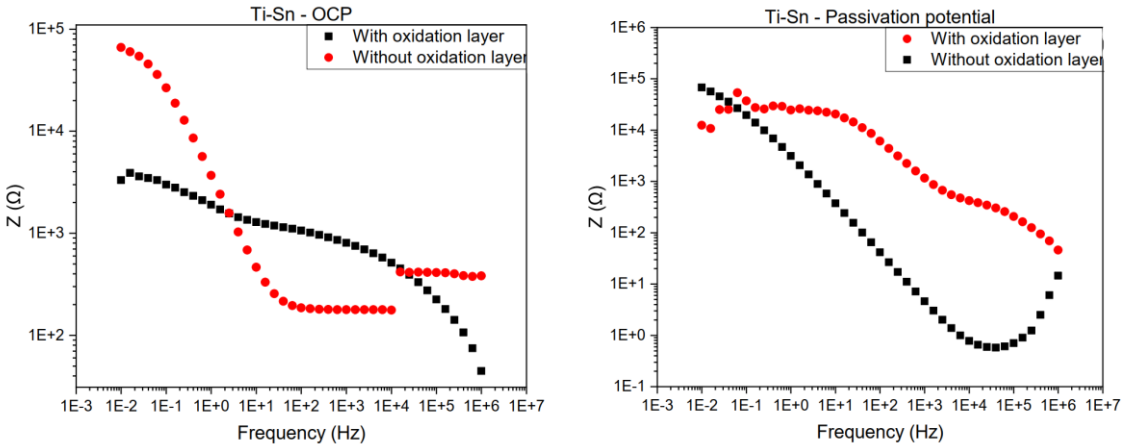

Figure 71: Bode diagrams with Z vs frequency for all results of Ti-Sn with and without the oxide layer

In the comparison of the series of experiments on Ti-Sn shown in Figure 71, the results are similar to those for the alloy of Ti-6Al-4V. The curves of the experiments with the oxide layer have a higher Z value over the frequency range than the curves of the experiments without the oxide layer. This means that the alloys with the oxide film are better protected against corrosion.

Chapter 6: CONCLUSION

Concerning the study and setting up a thermochemical nano-spikes obtention system on electrochemically characterized titanium alloys the following conclusions can be drawn for the first part of the electrochemical evaluation of the 3 investigated titanium alloys:

For the experiments of the polarization curve, it can be concluded that Ti-CP is the most corrosion-resistant alloy. This metal has the most noble character, possessing the highest potential and the lowest I_{corr}. The alloy most vulnerable to corrosion is Ti-Sn. This alloy possesses the highest Icorr and lowest E_{corr}. Tin is the least noble metal found in the investigated alloys so this metal can corrode the most easily. The characteristics of the alloy Ti-6Al-4V are between the other two alloys making it the intermediate.

The results of the cyclic voltammetry show that the formation of the passivation layer for all three alloys is determined by an electro-active field and not by diffusion.

The results of the impedance test are very abstract and difficult to interpret with the limited data and analysis techniques used in this thesis. Also no impedance tests were performed on the Ti-CP alloy due to the lack of available material and time. For Ti-6Al-4V and Ti-Sn we can conclude that for the selected points: peak potential, the passivation potential and the (OCP+peak)/2 electron transfer does occur at the passivation layer. For the OCP value this also happens but not if the frequency is measured at higher values. Then the OCP has a constant value. What this exactly means cannot be determined with the information given in this thesis. For this, more data and other research analyses are required. Another observation that was made during these experiments is that the chosen potential points of the polarization curve: the OCP, the passivation potential and (OCP+peak)/2 are reproducible. These chosen points are in an equilibrium state. This is not the case for the peak potential. This point is not reproducible and is located in a meta-stable zone because this zone of the system is controlled by the kinetics of the passivation layer.

In the second part of this thesis, an attempt was made to form nanospikes on the various alloys via thermal pyrolysis of acetone and further oxidation with air. The experiments carried out were checked for reproducibility and the results were positive. With two exceptions, nanospikes were obtained with the same morphology and density. In order to further explain these 2 exceptions, it is necessary to repeat these tests.

For the comparison between the alloys that were investigated, it can be seen that for the formed oxidation layers, small zones are present with a homogeneous growth direction of the nanospikes but no large uniform growth direction. The densities for the Ti-6Al-4V and Ti-Sn alloys are very similar. With these alloys it is not possible to see the substrate. In the case of Ti-CP, the density is low and the substrate is still visible. The greatest differences can be seen when comparing the morphology of the alloys. For Ti-6Al-4V needle-like structures can be seen, for Ti-Sn mainly nano-flakes can be seen on the oxide layer and for Ti-CP tube-like nanospikes with a spherical crystal at the end. These morphological phenomena cannot be explained by the limited results and analysis methods.

For the formation of the nanospikes, different flow rates were also used, namely 0.3; 0.5 and 1.0 l/min. It was expected based on previous research that the width of the nanospikes would be thinner as the flow rate increased. This observation was not the case in this study. More data and experiments are required to confirm or disprove this hypothesis.

Attention was also paid to where the samples were placed in the reactor. The results showed that the samples were best placed in the direction of the middle and the end of the reactor. In the beginning or at the edges of the reactor the conditions are not ideal for the formation of the nanospikes. Judging

from the visual aspect, the oxidation of the Ti-C may not be optimal in these zones. Further research is required to confirm this hypothesis.

From the EDS and TEM test it can be concluded that the nanospikes consist of TiO_2. For the alloys of Ti-6Al-4V and Ti-Sn it was found that the metals Al, V and Sn do not occur in a significant amount in the nanospikes themselves. The research in this analysis technique was rather limited due to time constraints. It is important to test these experiments for reproducibility in order to find out whether the metals are present in the nanospikes or not.

The comparison of the impedance tests for both Ti-6Al-4V and Ti-Sn between the samples with and without the oxide layer shows that the samples with the oxide layer are better protected against corrosion than the samples without the oxide layer. A part of this comparison is to investigate in the future the polarisation curve of the alloys with the oxide layer. Due to lack of time these experiments could not be performed. The polarisation curves provide important information on the behaviour of the passivation layer which can be essential in the decisions made.

Most of the conclusions have shown that a lot of research is still needed to answer many questions. This research is the first phase to create nanospikes in one smooth process using mass flow controllers to regulate the different flow rates. This new method of forming nanospikes opens up a new avenue of research. There is a lot of potential in this area but it will take time and patience. The preparation and formation of the nanospikes on a sample is a time-consuming process. Still, the research was successful and is a good first step towards the future.

References

[1] "A Brief History Of Titanium," Titek titanium specialists, [Online]. Available: https://titek.co.uk/brief-history-titanium/. [Accessed 24 March 2022].

[2] "Titanium Element Facts," chemicool, [Online]. Available: https://www.chemicool.com/elements/titanium.html. [Accessed 24 March 2022].

[3] C. Cavallo, "Thomas for industry," [Online]. Available: https://www.thomasnet.com/articles/metals-metal-products/steel-vs-titanium-strength-properties-and-uses/. [Accessed 5 April 2022].

[4] "Royal Society of Chemistry," [Online]. Available: https://www.rsc.org/periodic-table/element/22/titanium. [Accessed 5 April 2022].

[5] T. Scalisi, "Bob Villa," 19 May 2021. [Online]. Available: https://www.bobvila.com/articles/does-titanium-rust/#:~:text=The%20pure%20titanium%20material%20is,key%20to%20its%20corrosion%20resistance.. [Accessed 5 April 2022].

[6] A. Augustyn, "Britannica," [Online]. Available: https://www.britannica.com/science/titanium/Compounds. [Accessed 5 April 2020].

[7] O. Carp, C. Huisman and A. Reller, "sciencedirect," 2004. [Online]. Available: https://www.sciencedirect.com/science/article/pii/S0079678604000123. [Accessed 5 April 2022].

[8] C. M. Abraham, "National Library of Medicine," 16 May 2014. [Online]. Available: https://www.ncbi.nlm.nih.gov/pmc/articles/PMC4040928/. [Accessed 11 April 2022].

[9] R. Bisbal, Pedro Dávila, Franklin Gomez, Sonia Camero, Marcial Pérez and Gema González, "Journal of the Faculty of Engineering Central University of Venezuela," December 2012. [Online]. Available: http://ve.scielo.org/scielo.php?script=sci_arttext&pid=S0798-40652012000400010. [Accessed 11 April 2022].

[10] Joan Lario-Femenía, Angélica Amigó-Mata, Ángel Vicente-Escuder, Francisco Segovia-López and Vicente Amigó-Borrás, "Revista de Metalurgia," 30 December 2016. [Online]. Available: https://revistademetalurgia.revistas.csic.es/index.php/revistademetalurgia/article/view/1397. [Accessed 11 April 2022].

[11] J. Quinn, "sciencedirect," 20 November 2020. [Online]. Available: https://www.sciencedirect.com/science/article/pii/S2589004220309421. [Accessed 11 April 2022].

[12] T. Diu, "nature," 20 November 2014. [Online]. Available: https://www.nature.com/articles/srep07122. [Accessed 11 April 2022].

[13] M. Jäger, "National Library of Medicine," 13 November 2017. [Online]. Available: https://pubmed.ncbi.nlm.nih.gov/29137166/. [Accessed 11 April 2022].

[14] R. M. d. Nascimento, "National Library of Medicine," 28 Frebruary 2017. [Online]. Available: https://pubmed.ncbi.nlm.nih.gov/28108961/. [Accessed 11 April 2022].

[1 L. Xiaotian and C. Shuyang , “National Library of Medicine,” 23 September 2017. [Online].
5] Available: https://www.ncbi.nlm.nih.gov/pmc/articles/PMC5633690/. [Accessed 11 April 2022].

[1 L.-C. Zhang, “Wiley Online Library,” 2 March 2019. [Online]. Available:
6] https://onlinelibrary.wiley.com/doi/10.1002/adem.201801215. [Accessed 02 May 2022].

[1 M. K. Dimah, “researchgate,” July 2012. [Online]. Available:
7] https://www.researchgate.net/publication/256913617_Study_of_the_biotribocorrosion_behaviour_of_titanium_biomedical_alloys_in_simulated_body_fluids_by_electrochemical_techniques. [Accessed 11 April 2022].

[1 N. Eliaz, “National Library of Medicine,” 28 January 2019. [Online]. Available:
8] https://www.ncbi.nlm.nih.gov/pmc/articles/PMC6384782/. [Accessed 11 April 2022].

[1 M. T. Mathew, “Hindawi XML Corpus,” 6 January 2010. [Online]. Available:
9] https://www.hindawi.com/journals/at/2009/250986/. [Accessed 11 April 2022].

[2 M. P. Gispert, “sciencedirect,” January 2006. [Online]. Available:
0] https://www.sciencedirect.com/science/article/abs/pii/S0043164805000554. [Accessed 11 April 2022].

[2 S. Virtanen, “National Library of Medicine,” May 2008. [Online]. Available:
1] https://pubmed.ncbi.nlm.nih.gov/18226986/. [Accessed 11 April 2022].

[2 T. Hanawa, “sciencedirect,” December 2004. [Online]. Available:
2] https://www.sciencedirect.com/science/article/pii/S0928493104000906. [Accessed 11 April 2022].

[2 M. Kawahara, “National Library of Medicine,” 8 March 2011. [Online]. Available:
3] https://pubmed.ncbi.nlm.nih.gov/21423554/. [Accessed 2022 April 2022].

[2 J. L. d. P. J. R. P. J. L. I. Lasa, “ SciELO,” August 2005. [Online]. Available:
4] https://scielo.isciii.es/scielo.php?script=sci_arttext&pid=S1137-66272005000300002. [Accessed 2 May 2022].

[2 D. R. Monteiro, “National Library of Medicine,” 31 March 2009. [Online]. Available:
5] https://pubmed.ncbi.nlm.nih.gov/19339161/. [Accessed 6 May 2022].

[2 R. N.Palchesko, “sciencedirect,” 8 April 2011. [Online]. Available:
6] https://www.sciencedirect.com/science/article/pii/S0928493110003437?via%3Dihub. [Accessed 6 May 2022].

[2 R. Helbig, 27 May 2016. [Online]. Available:
7] https://pubs.rsc.org/en/content/articlelanding/2016/BM/C6BM00078A. [Accessed 02 May 2022].

[2 R. Kane, “sciencedirect,” November 2013. [Online]. Available:
8] https://www.sciencedirect.com/science/article/pii/S1369702113003775. [Accessed 11 April 2022].

[2 H. Hu, “Applied Physics Letters,” 21 December 2017. [Online]. Available:
9] https://aip.scitation.org/doi/10.1063/1.5003817. [Accessed 02 May 2022].

[30] H.Chouirfa, “sciencedirect,” 1 January 2019. [Online]. Available: https://www.sciencedirect.com/science/article/pii/S1742706118306354?via%3Dihub. [Accessed 05 May 2022].

[31] J. Liu, “sciencedirect,” 1 February 2017. [Online]. Available: https://www.sciencedirect.com/science/article/pii/S0928493116318239. [Accessed 11 April 2022].

[32] Masahiko Tachibana, Kazushige Ishida and Yoichi Wad, “tandfonline,” 24 April 2012. [Online]. Available: https://www.tandfonline.com/doi/pdf/10.1080/00223131.2012.676880. [Accessed 9 April 2022].

[33] D. Landolt, Corrosion and surface chemistry, Lausanne, Switserland: EPFL Press, 2006.

[34] J. L. V. Gutiérrez, “UNIVERSIDAD POLITÉCNICA DE VALENCIA,” December 2007. [Online]. Available: https://riunet.upv.es/bitstream/handle/10251/12346/TesisMaster_LuisVazquez.pdf?sequence. [Accessed 26 April 2022].

[35] J. W. C. MAMANI, 2018. [Online]. Available: https://repositorio.umsa.bo/bitstream/handle/123456789/19199/TM-2163.pdf?sequence=1&isAllowed=y. [Accessed 2022 May 16].

[36] “Universitat pollitecnica de Valencia,” [Online]. Available: http://www.upv.es/entidades/SME/info/1145949normalc.html. [Accessed 17 May 2022].

[37] M. Editors, “microbiologynote,” 09 July 2020. [Online]. Available: https://microbiologynote.com/transmission-electron-microscope/. [Accessed 16 May 2022].

[38] “University of Nottingham,” [Online]. Available: https://www.nottingham.ac.uk/isac/facilities/tem.aspx#:~:text=How%20does%20TEM%20work%3F,through%20the%20specimen%20of%20interest.. [Accessed 20 May 2022].

[39] M. Niinomi, “sciencedirect,” 15 March 1998. [Online]. Available: https://www.sciencedirect.com/science/article/pii/S092150939700806X. [Accessed 02 May 2022].

APPENDIX I: RESULTS POLARISATION TEST

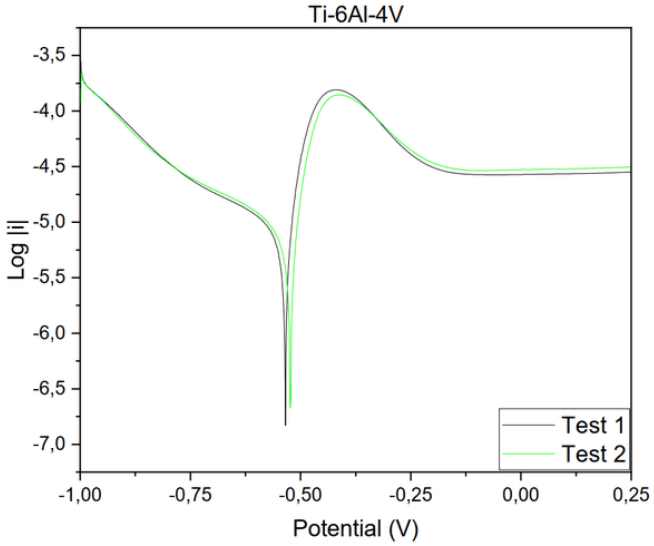

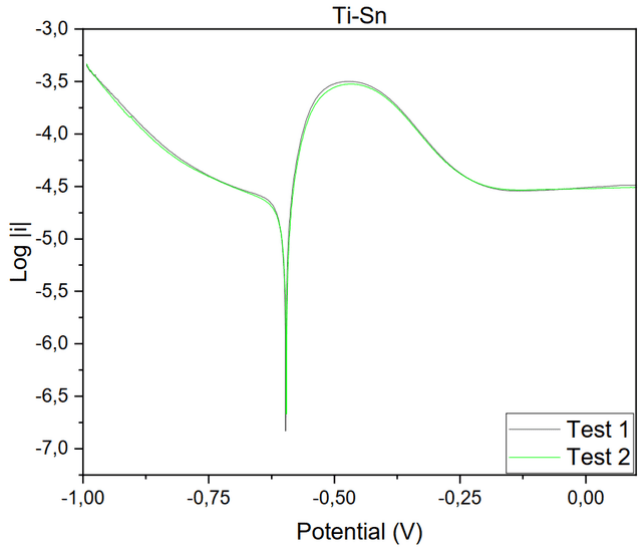

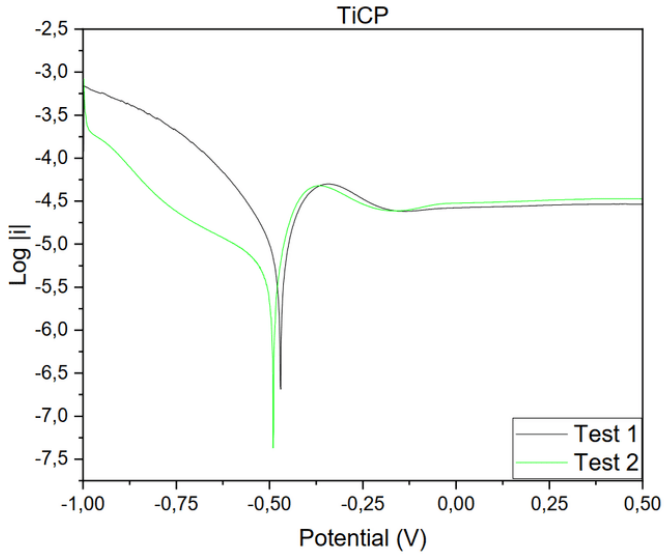

APPENDIX II: RESULTS CORROSION TEST OF TI-6AL-4V

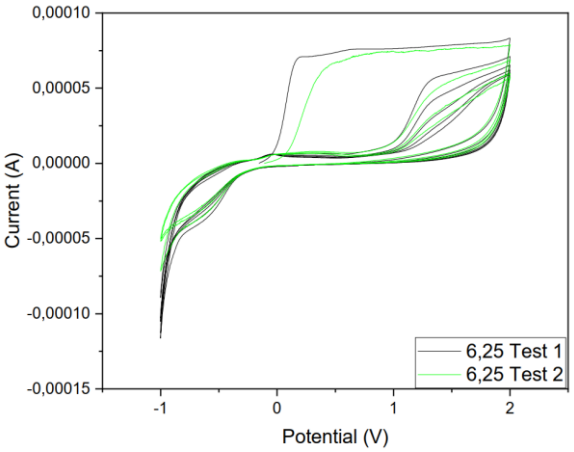

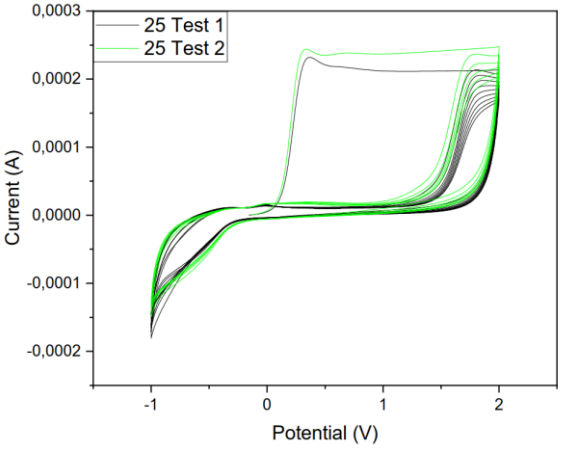

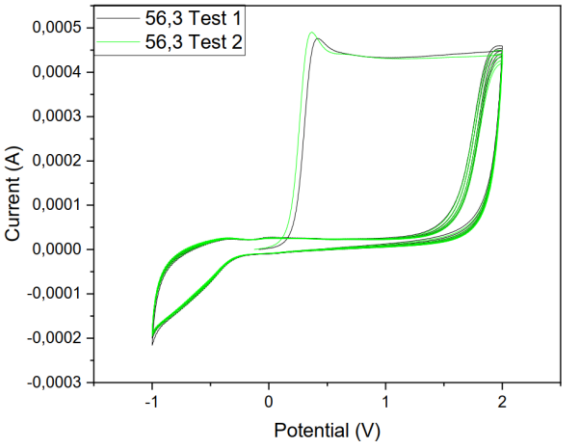

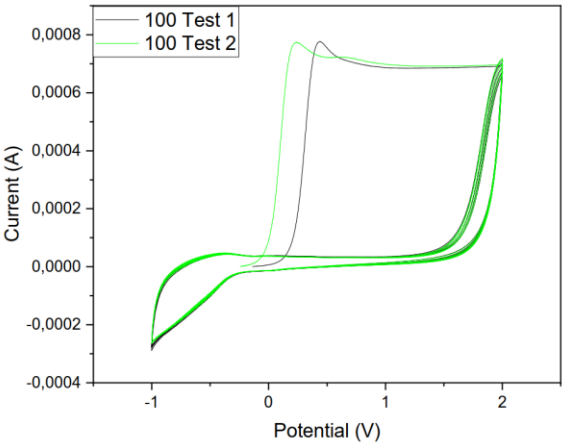

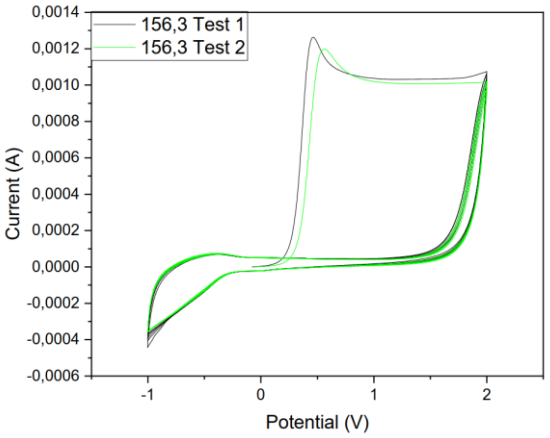

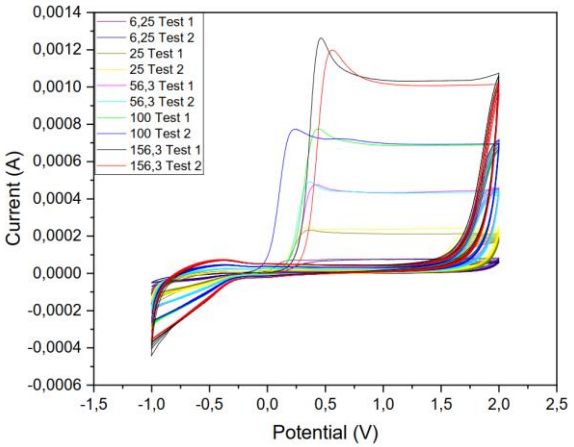

APPENDIX III: RESULTS CORROSION TEST OF TI-CP

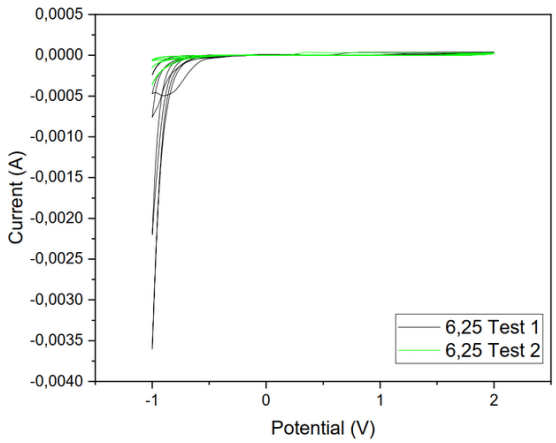

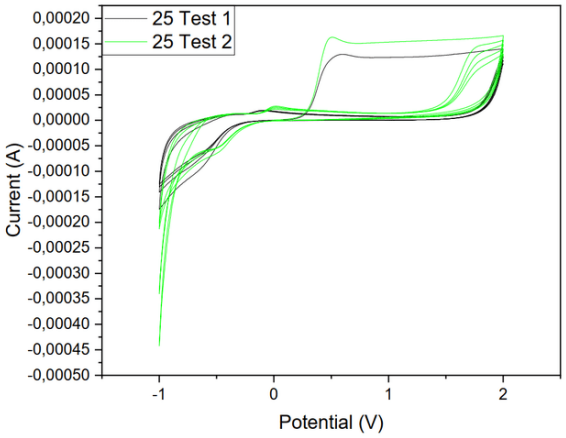

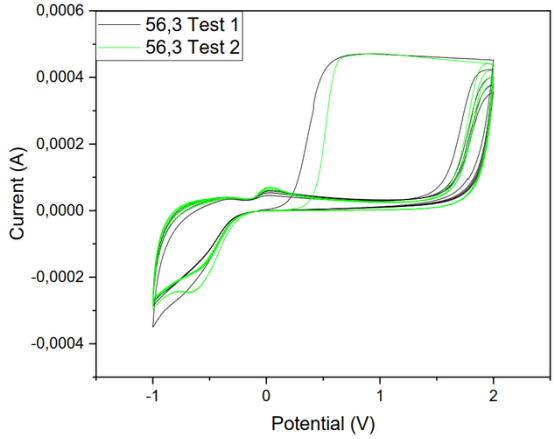

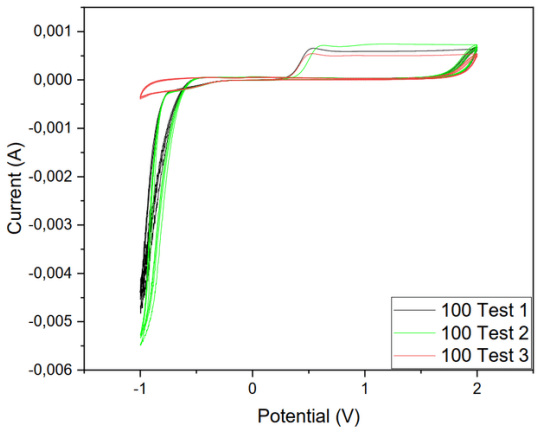

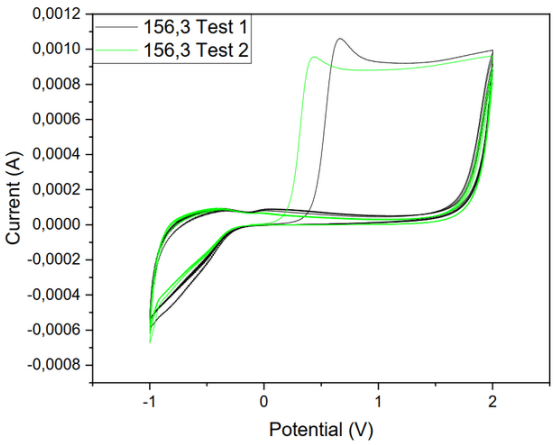

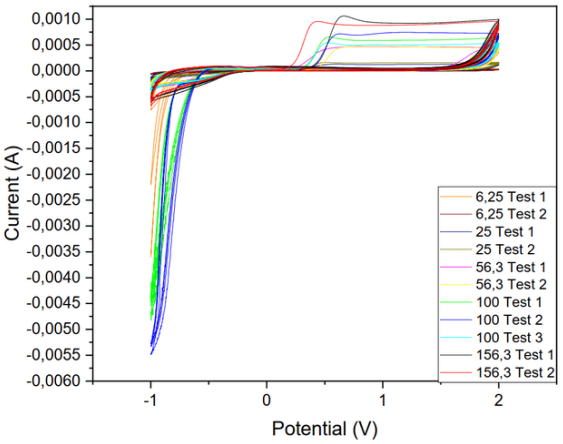

APPENDIX IV: RESULTS CORROSION TEST OF TI-SN

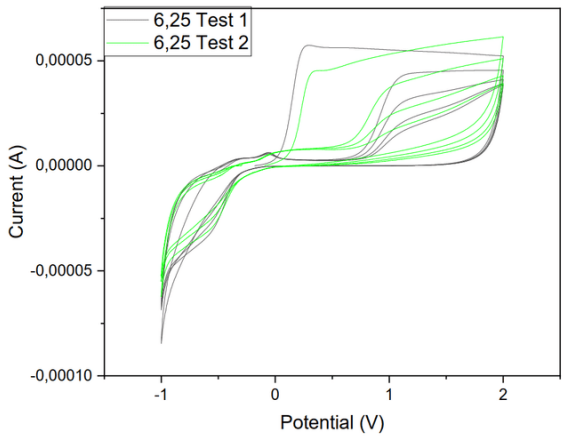

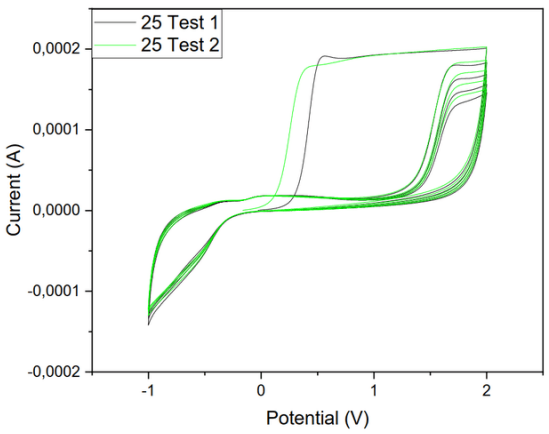

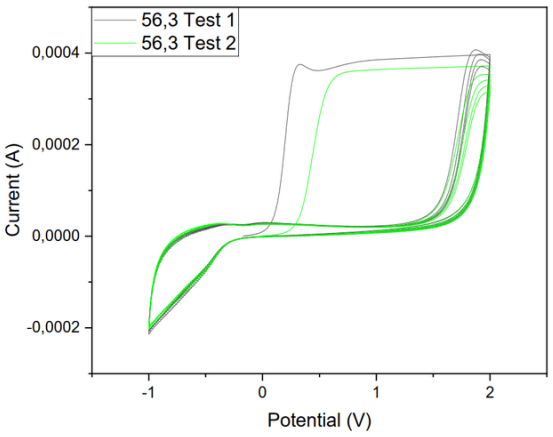

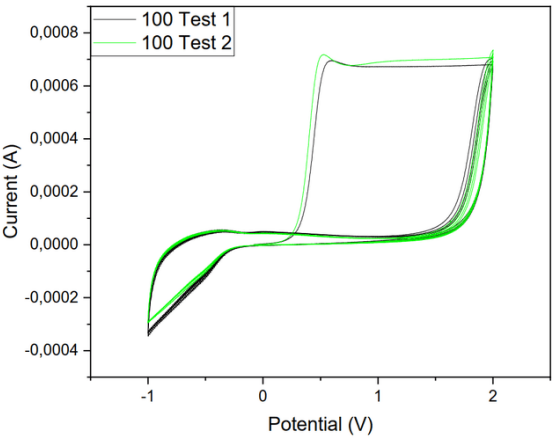

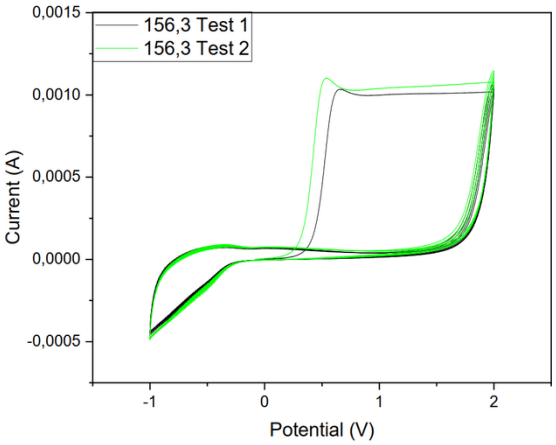

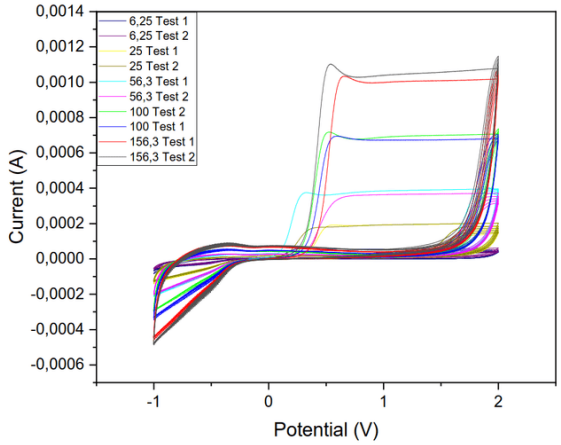

APPENDIX V: RESULTS SEM OF TI-6AL-4V 0.3 L/MIN

Serie 1

A - 2k

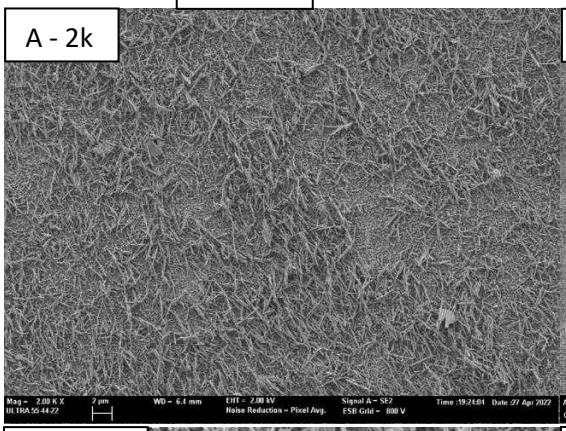

Serie 2

B - 1k x

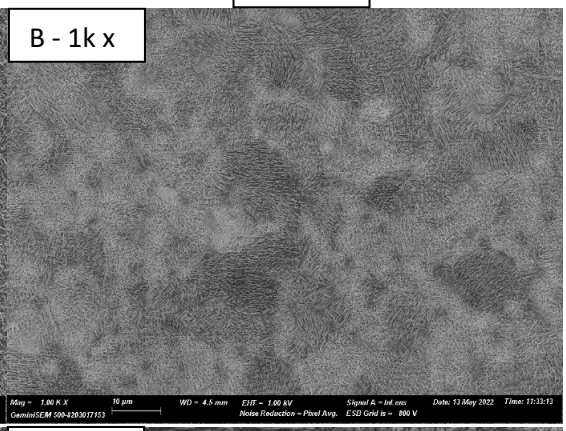

C - 10k x

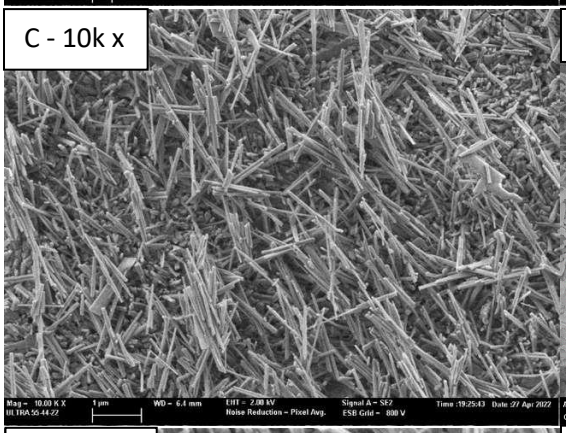

D - 5k x

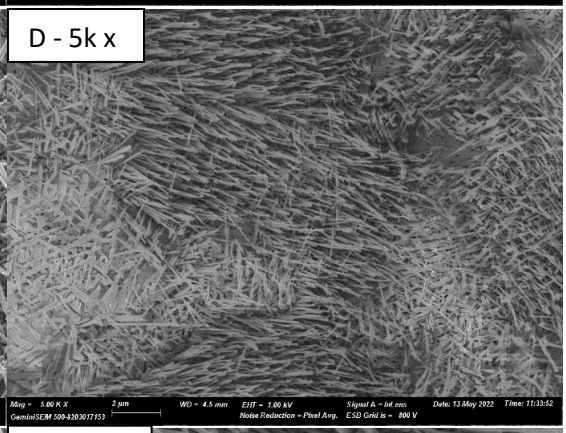

E – 25k x

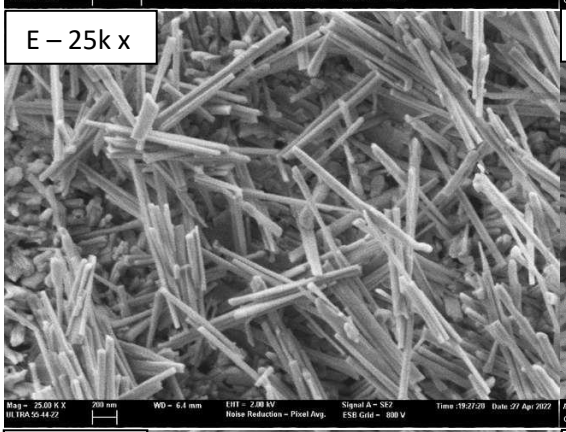

F - 15k x

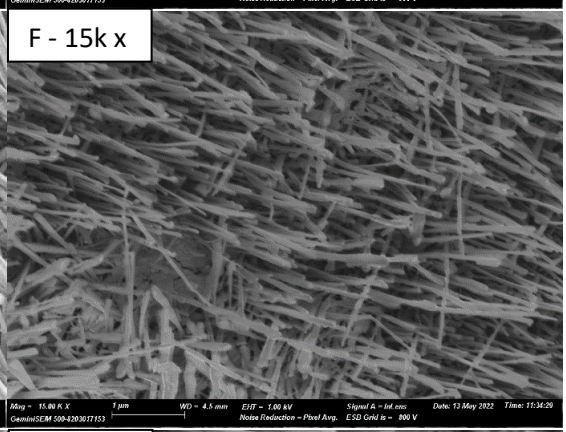

G - 35k x

H - 30k x

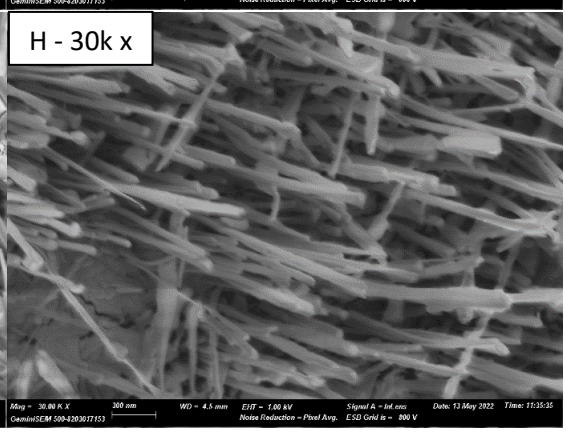

APPENDIX VI: RESULTS SEM OF TI-6AL-4V 0.5 L/MIN – BEGINNING OF THE REACTOR

Serie 1

A – 1,5kx

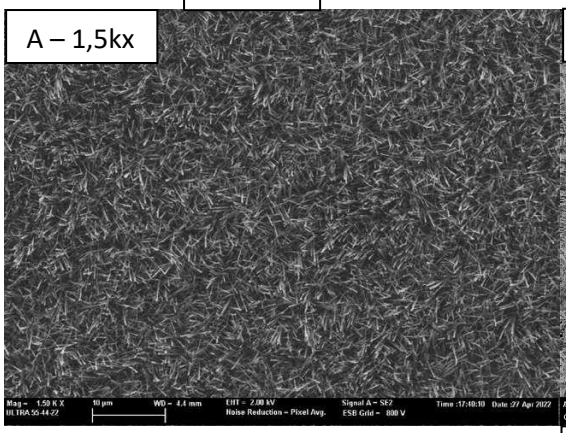

Serie 2

B - 1k x

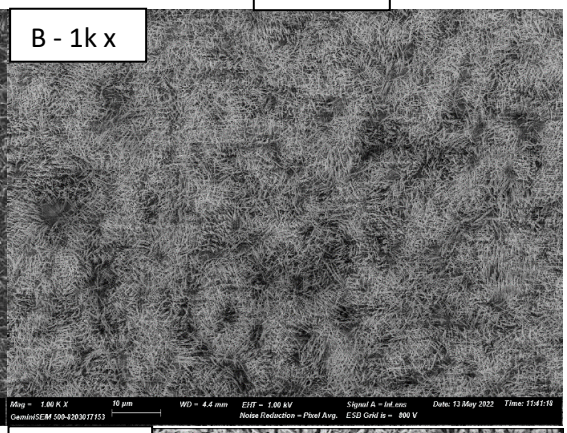

C - 5k x

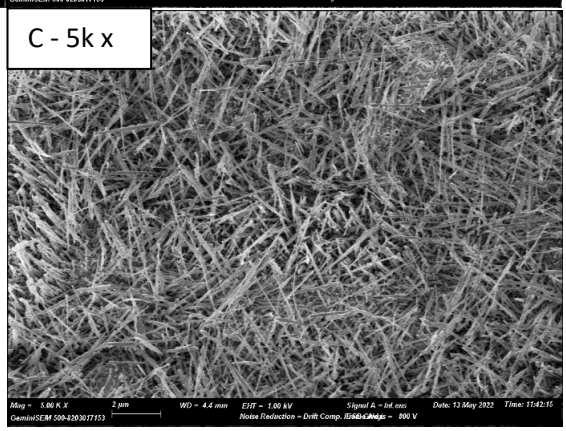

D - 15k x

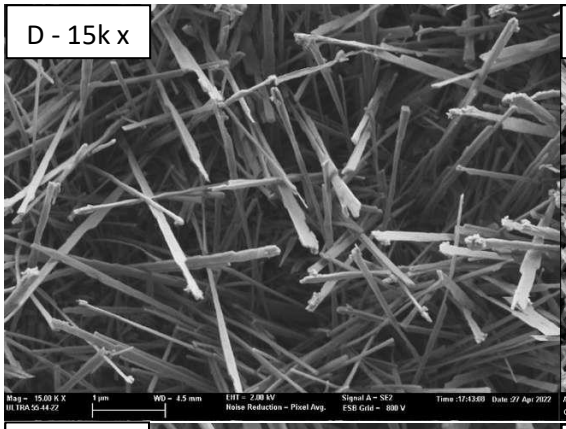

E – 15k x

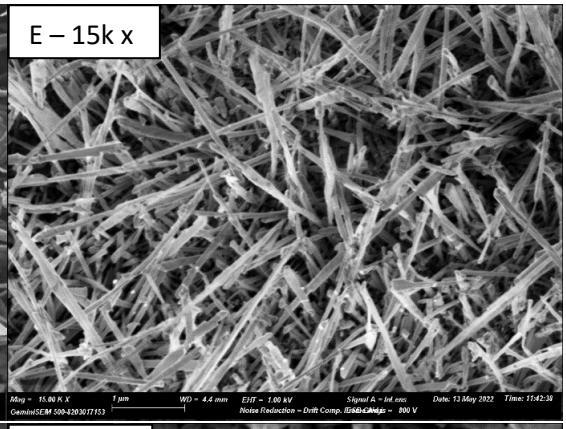

F - 30k x

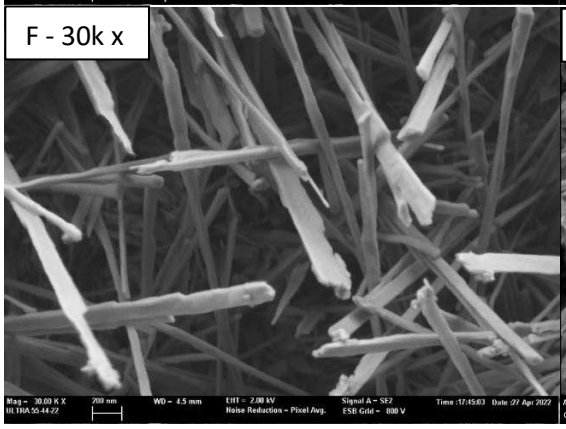

G - 30k x

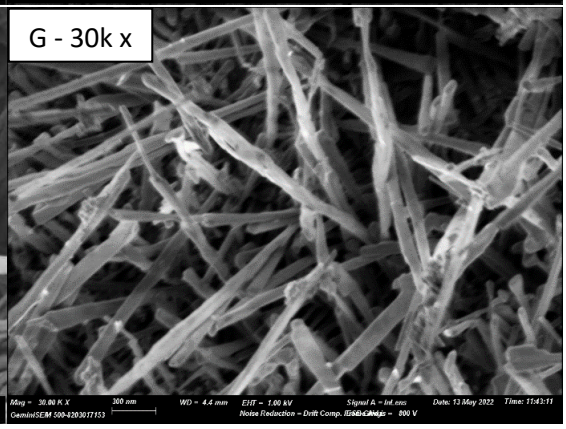

APPENDIX VII: RESULTS SEM OF TI-6AL-4V 0.5 L/MIN – END OF THE REACTOR

Serie 1

A – 1.5k

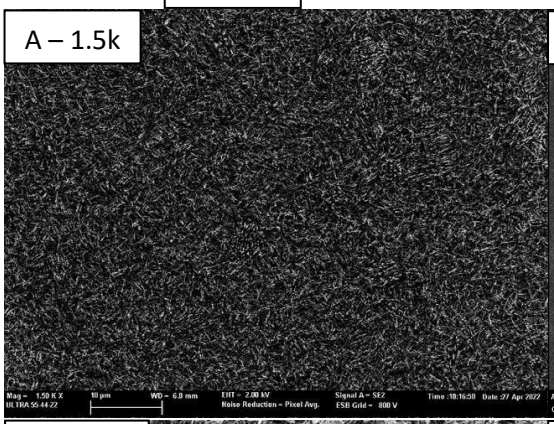

Serie 2

B - 1k

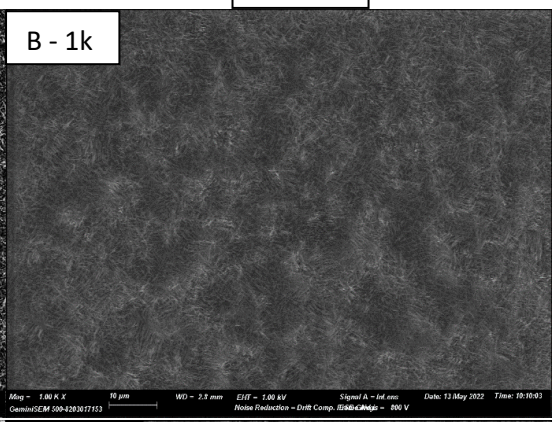

C - 3k x

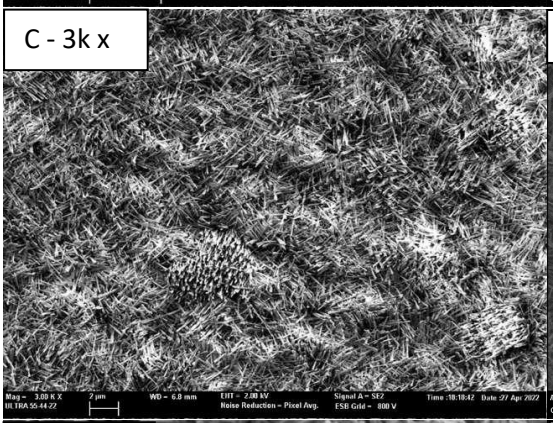

D - 5k x

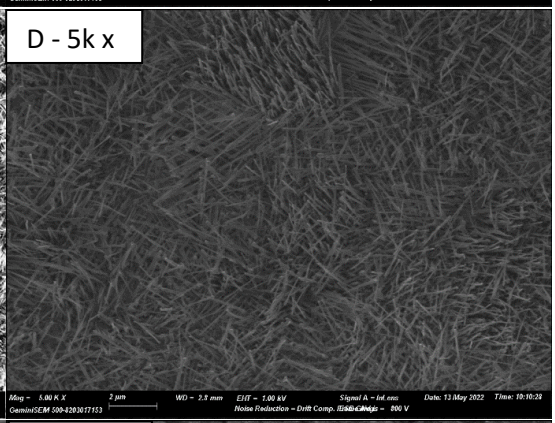

E – 25k x

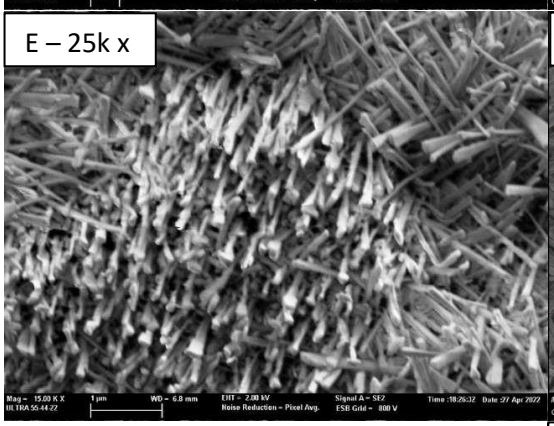

F - 15k x

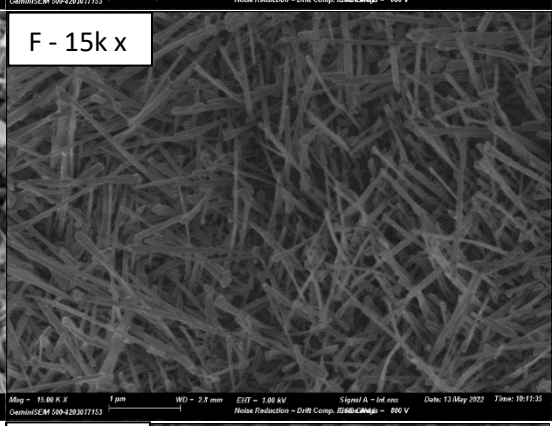

G - 35k x

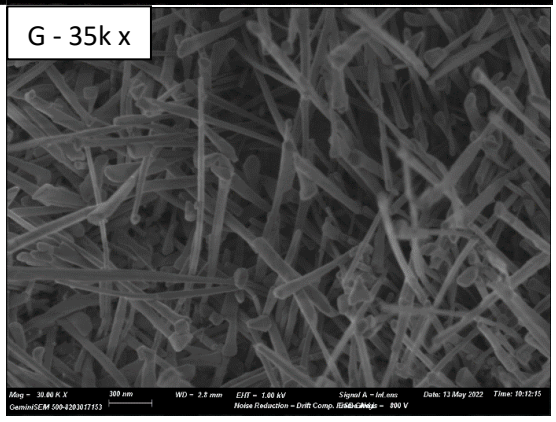

APPENDIX VIII: RESULTS SEM OF TI-6AL-4V 1.0 L/MIN – BEGINNING OF THE REACTOR

A - 1k x

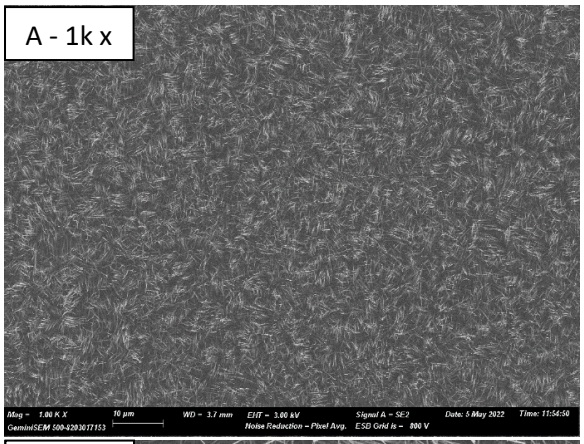

B - 5k x

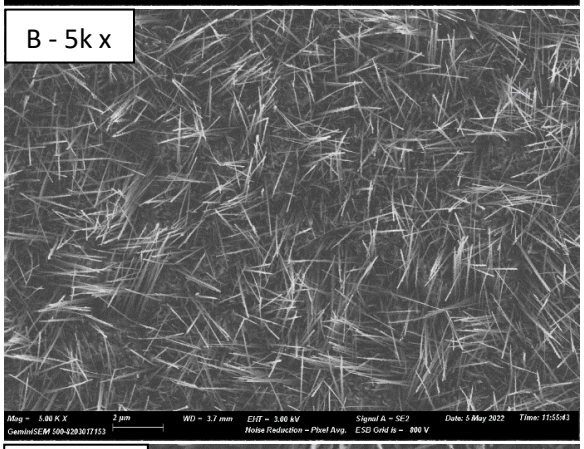

C - 15k x

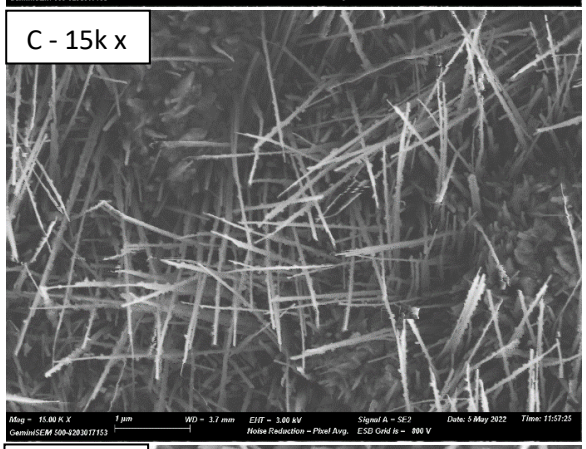

D - 30k x

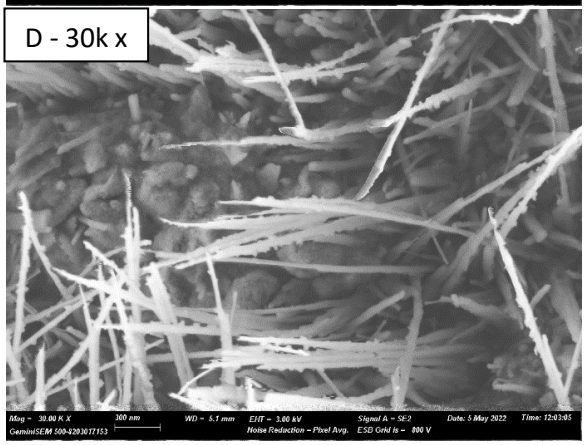

APPENDIX IX: RESULTS SEM OF TI-6AL-4V 1.0 L/MIN – MIDDLE OF THE REACTOR

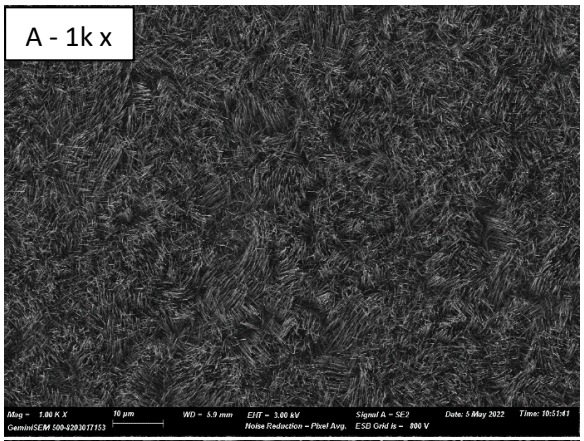

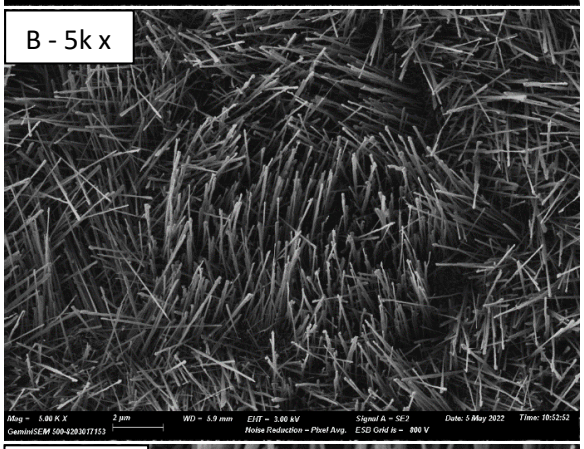

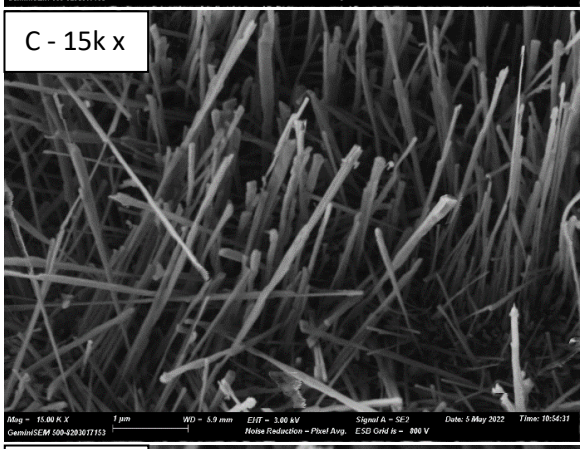

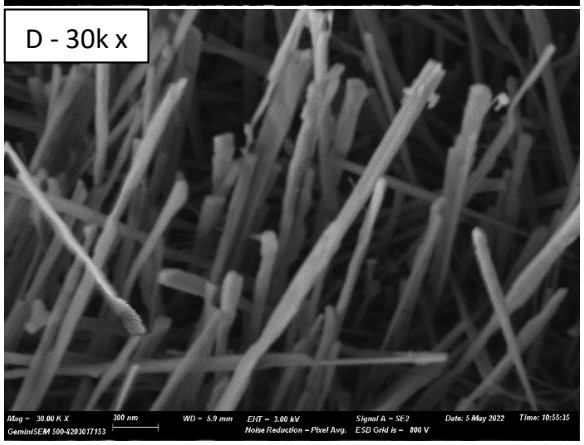

APPENDIX X: RESULTS SEM OF TI-6AL-4V 1.0 L/MIN – END OF THE REACTOR

I - 1k x

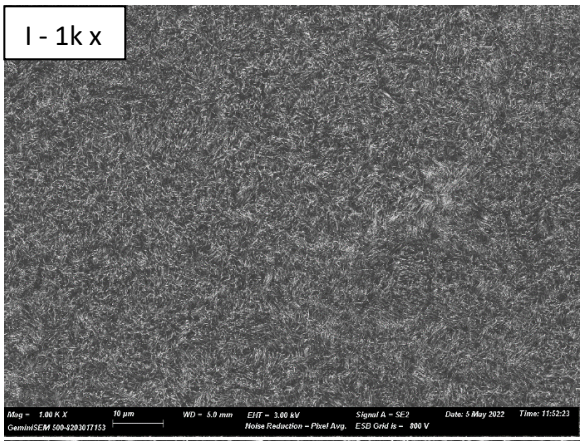

J - 5k x

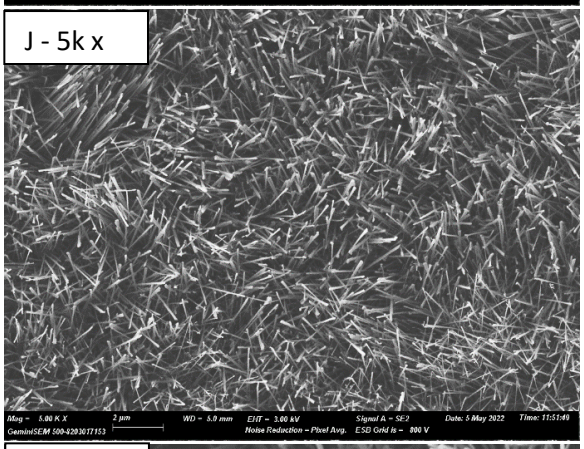

K - 15k x

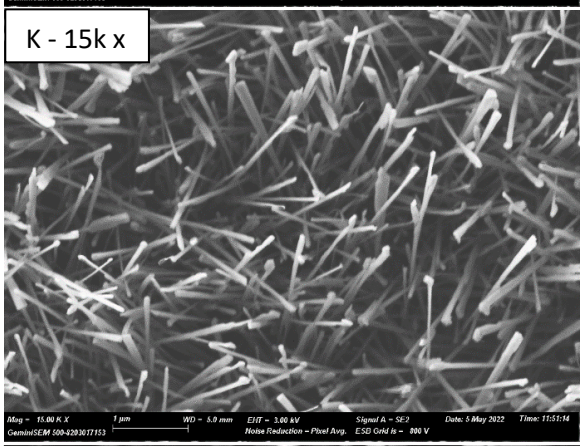

L - 35k x

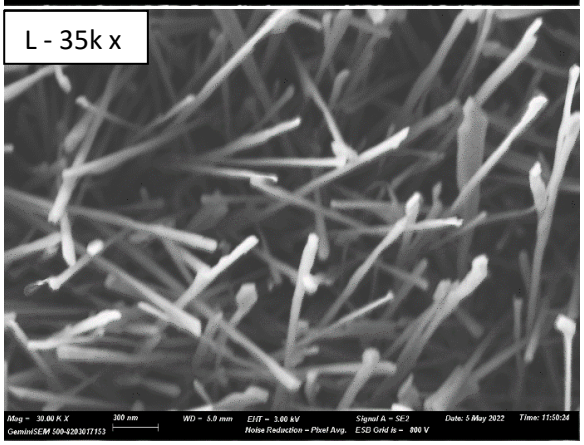

APPENDIX XI: RESULTS SEM OF TI-SN 0.3 L/MIN

Serie 1

A – 1.5x k

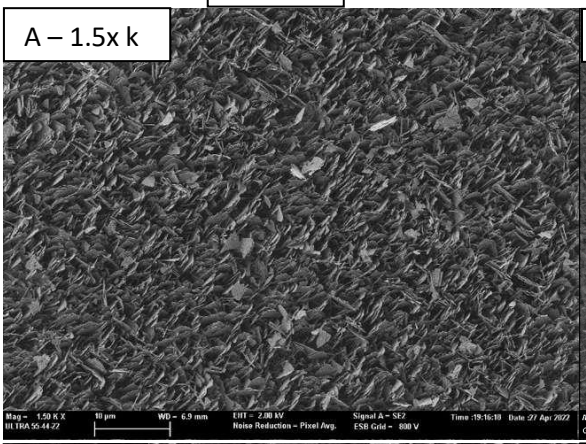

Serie 2

B - 1k x

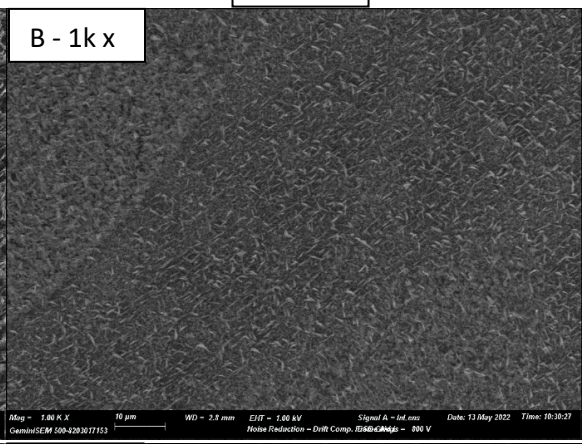

C - 5k x

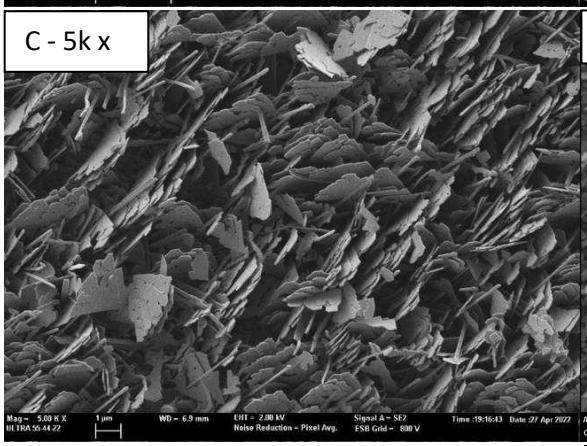

D - 5k x

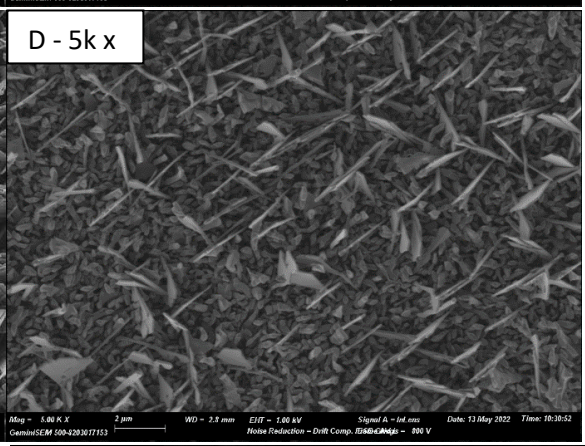

E – 15k x

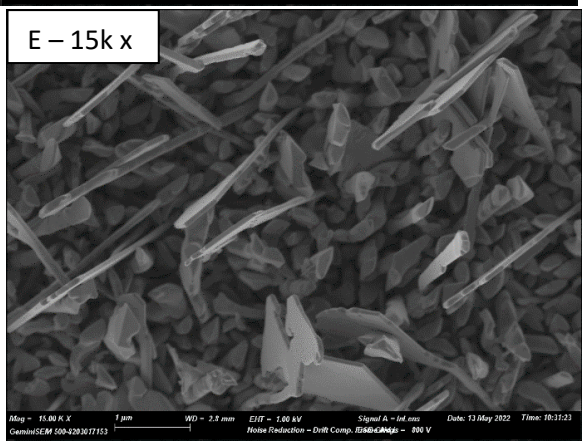

F - 25k x

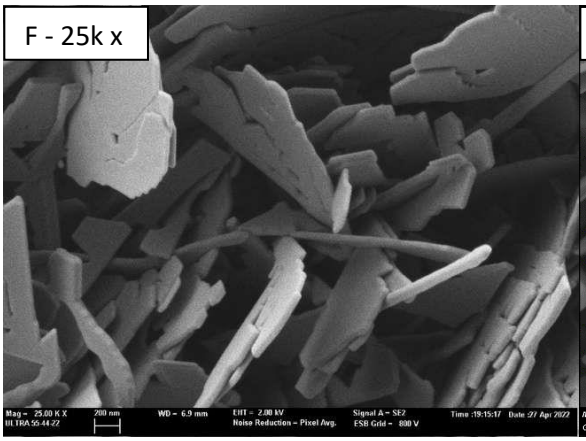

G - 35k x

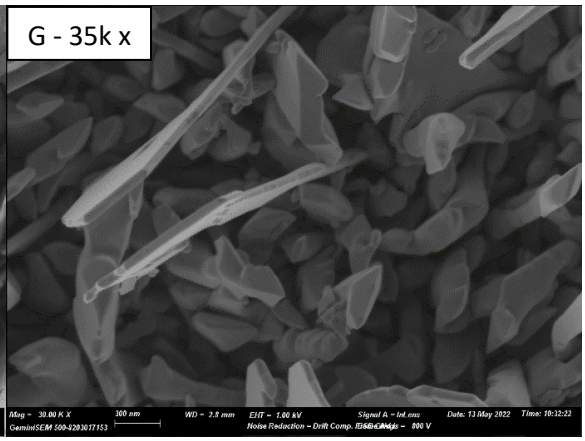

APPENDIX XII: RESULTS SEM OF TI-SN 0.5 L/MIN

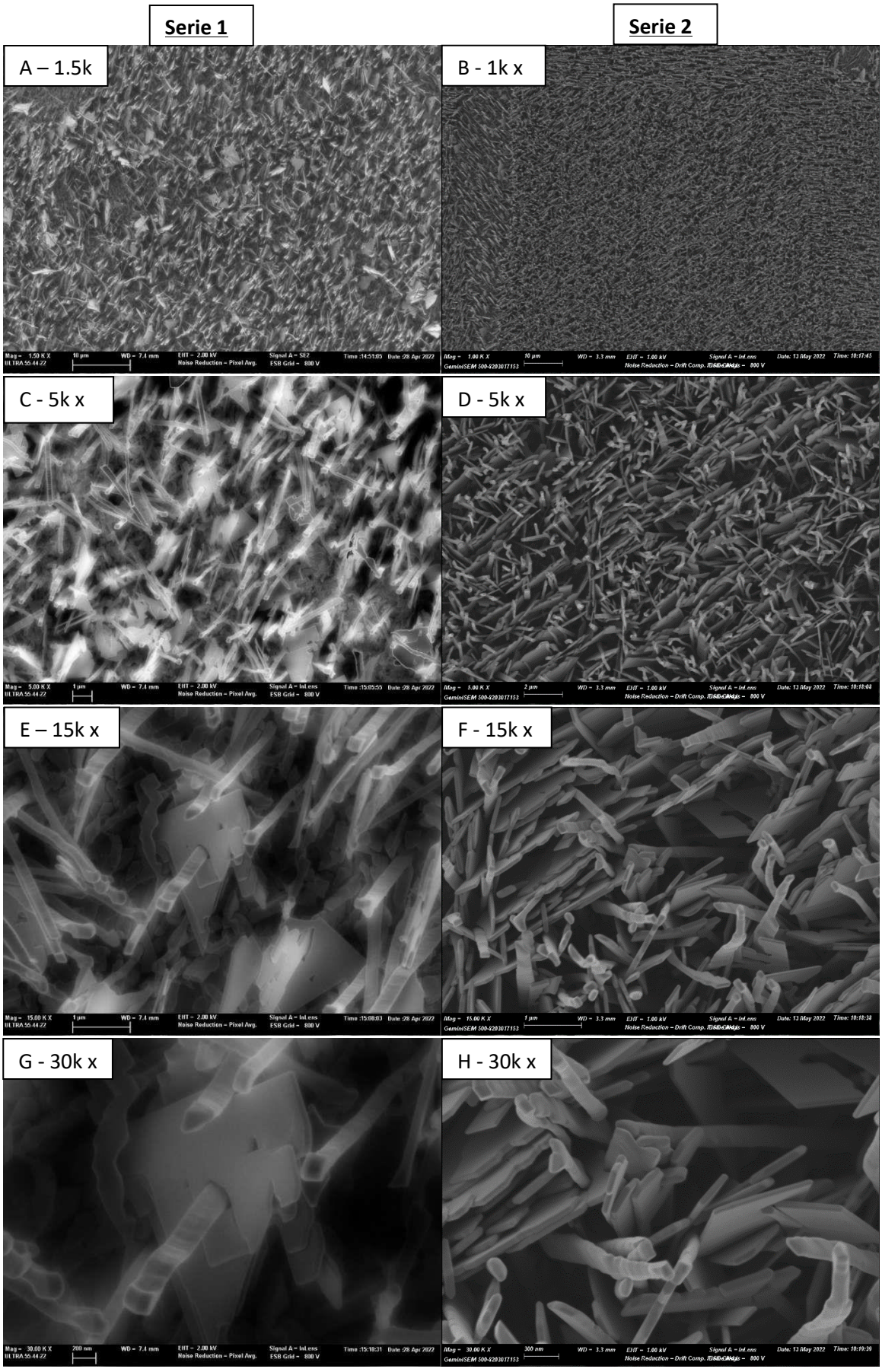

APPENDIX XIII: RESULTS SEM OF TI-CP 0.3 L/MIN

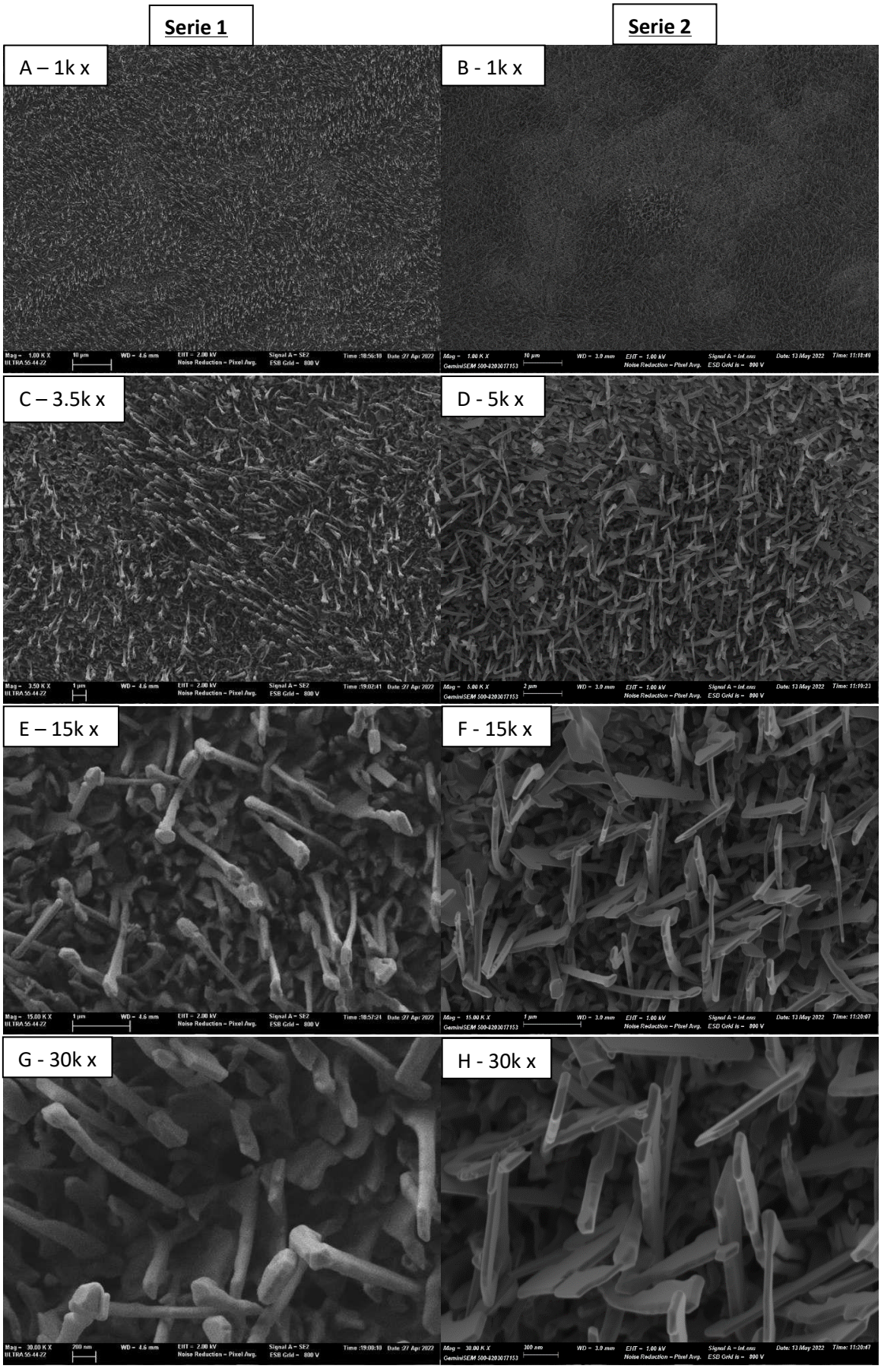

Budget cover

Table of Contents

1. PARTIAL BUDGETS

A technical-economic analysis of this TFM has been carried out in order to determine the approximate cost of the project.

The following points have been taken into account for the calculation of the budget:

- Indirect costs are costs that cannot be directly associated with the given unit of work and are therefore considered as a percentage of the direct costs. Examples of indirect costs are rent, salaries, maintenance, etc. In this work an indirect cost of 25% has been considered.
- For the calculation of the amortisation cost of the machinery, 200 working days/year, 12 hours a day, for 10 years have been considered.
- The use of the scanning electron microscope (SEM) and Transmission electron microscopy (TEM) is not an expense to be amortised. The price of these services is
  30 €/h and 25 €/h respectively including VAT.
- Overheads correspond to the costs of running an activity (gas, electricity, cleaning, water, etc.). They are usually between 9% and 16% depending on the work carried out. In this case, 13% overheads have been considered. The percentage of industrial profit will be zero as UPV has not obtained any economic benefit from this project.
- Those elements to which VAT can be applied already have it applied in the prices shown in the tables, which is why the total budget and the contract budget are the same. VAT is 21%.

It has been decided to divide the budget into three chapters: equipment, material and labour. In addition, within each chapter, the different work units have been identified as shown in Table 1.

Table 1: Budget organised in chapters

Chapter 1: Equipment	UO1: Equipment experimental part.
	UO2: Analysis and characterisation equipment.
Chapter 2: Materials	UO3: Laboratory equipment and instrumentation.
	UO4: Reagents and compounds.
Chapter 3: Manpower	UO5: Manpower

1.1 Equipment

Table 2 shows the costs for the use of the equipment in the experimental part.

Table 2: Equipment costs of the experimental part

Ref.	Description	Equipment price (€)	Unit cost (€/h)	Quantity (h)	Total (€)
E1	Struers roughing machine model LaboPol-21	23.595,79	0,98	32,5	31,85
E2	Struers polishing machine model LaboPol-5	3.056,36	0,34	10	3,4
E3	High temperature tube furnace (MTI CORPORATION) model OFT-1200X-S)	3.669,35	0,45	42	18,9
Total					54,15

Therefore, the price for the use of the equipment for the experimental part amounts to a total of 54,15 €.

Table 3 shows the costs pertaining to the use of analysis and characterisation equipment.

Table 3: Costs of analysis and characterisation equipment

Ref.	Description	Equipment price (€)	Unit cost (€/h)	Quantity (h)	Total (€)
EQ1	Scanning Electron Microscope (HRFESEM)	/	30	5	150
EQ2	AUTOLAB Potentiostat	21.175,44	0,88	100	88
EQ3	Platinum counter electrode (Metrohm)	401,72	0,02	100	2

EQ4	Ag/AgCl electrode (Metrohm)	390,83	0,02	100	2
EQ5	Transmission electron microscopy 120kV with X-ray detector (EDS)	/	25	4	100
Total					342

Therefore, the price for the use of the equipment for the analysis and characterisation amounts to a total of 342,00 €.

1.2 Materials

Table 4 shows the costs of the laboratory materials and instrumentation used to carry out this work.

Table 4: Costs of laboratory materials and instrumentation

Ref.	Description	Unit cost (€/piece)	Quantity (piece)	Total (€)
MAT1	Rubber mallet	8,31	1	8,31
MAT2	Hacksaw	4,99	1	4,99
MAT3	Chisel	1,39	1	1,39
MAT4	Glass gas wash bottle with cap 500 mL	34,26	2	68,52
MAT5	Silicone tube	0,20	2	0,4
MAT6	Rotameter (Brooks model 2520)	105,27	1	105,27
MAT7	Valve	1,98	2	3,96
MAT8	Holder with clamp and nut	48,99	3	146,97
MAT9	Porous zirconia plug	7,89	2	15,78
MAT10	Alumina	11,92	5	59,6

	support			
MAT11	Clamp	5,38	1	5,38
MAT12	Petri dish	0,20	3	0,6
MAT13	SiC sanding disc	2,50	14	35
MAT14	Screwdriver	4,69	1	4,69
Total				460,86

The price for the use of materials and instrumentation in this TFG has been valued at a total of 460,86 €.

Table 5 shows the cost of the reagents and compounds to carry out this work.

Table 5: Cost of Reagents and Compounds

Ref.	Description	Unit cost (€/l)	Quantity (l)	Total (€)
COMP1	Acetone for analysis. Purity of 99.5%	8.31	1	8,31
COMP2	Sulphuric acid. 98% purity	8.72	1	8,72
COMP3	OPS	66.00	1	66,00
COMP4	Hydrogen peroxide	140.00	1	140,00
COMP5	Ethanol	40.00	1	40,00
Total				263,03

The price for the use of reagents and compounds has been calculated at 263,03 €.

1.3 Manpower

Table 6 shows the cost of labour, in this case a chemical engineer.

It also relies on the work of tutors and laboratory technicians.

Table 6: Labour costs

Ref.	Description	Unit cost (€/h)	Quantity (h)	Total (€)
MO1	Laboratory work	15	520	7800
MO2	Bibliography	15	100	1500

	research			
MO3	Drafting the document	15	120	1800
MO4	Tutors/mentor	39	175	6825
MO5	Laboratory technicians	21,6	200	4320
Total				22.245

The estimated cost of the labour required to carry out this project totals 22.245 €.

2. BUDGET FOR MATERIAL EXECUTION

Table 7 shows a summary of the budget broken down by work units.

Table 7: Summary of work units

Unit of work	Description	Measurement (pc)	Amount (€)
UO1	Equipment of the experimental part	1	54,15
UO2	Analysis and characterisation equipment	1	342,00
UO3	Laboratory equipment and instrumentation	1	460,86
UO4	Reagents and compounds	1	263,03
UO5	Labour	1	22.245
Total			23365,04

The Material Execution Budget is obtained as the sum of the partial budgets and in which it is necessary to consider indirect costs of 25% of the total direct costs.

Sub-budget	23365,04
Indirect costs (25%)	5841,26
Total physical execution	29206,30

The budget for Material Execution amounts to the aforementioned amount of 29.206,30 €.

3. CONTRACT EXECUTION BUDGET

The Contract Execution Budget is the sum of the material execution budget and the overheads applicable to this budget (13% of the material execution budget).

Material execution budget	23.365,04
Overheads (13%)	3.037,46
Contractual implementation budget	26.402,49

Therefore, the budget for execution by contract amounts to a total of 26.402,49 €.

4. BIBLIOGRAPHY

The budget has been made by contacting different distributors and commercial houses to obtain the prices of some equipment and instruments and by consulting the Labbox (www.labbox.com/es) and Sigma-Aldrich (www.sigmaaldrich.com/spain.html) price catalogue to obtain the prices of chemical reagents and laboratory instrumentation. Prices consulted in February 2022.